UNIVERSITY OF THESSALY

POLYTECHNIC SCHOOL

DEPARTMENT OF MECHANICAL ENGINEERING

LABORATORY OF MATERIALS

Diploma Thesis

"Simulation of bainitic transformation in advanced high-strength steels under paraequilibrium Driving Forces"

By

Psyridis Konstantinos

Supervisor :

Dr. Helen Kamoutsi

Submitted for the Partial Fulfilment of the requirements for

the degree of Diploma in Mechanical Engineering

Certified by the members of the Thesis Committee:

First Examiner (Supervisor)

Dr. Helen Kamoutsi
Lab Teaching Staff,
Department of Mechanical Engineering,
University of Thessaly

Second Examiner

Dr. Nikolaos Aravas
Professor of Computational Mechanics of Structures
Department of Mechanical Engineering
University of Thessaly

Third Examiner

Dr. Alexis Kermanidis
Assistant Professor of Mechanical Behaviour of Metallic Materials
Department of Mechanical Engineering
University of Thessaly

Acknowledgements

First and foremost, I would like to express my sincere gratitude to my supervisor Dr. Helen Kamoutsi, for the continuous support of my research, for her patience, and motivation. Her guidance helped me in during the whole time of process and writing of this thesis.

Besides Dr. Helen Kamoutsi, I would like to thank also my supervisor Prof. G. Haidemenopoulos for his encouragement.

In addition I would like to thank both of them because most importantly they believed in me.

Last but not least, special recognition to my family and all my friends for their support during this study.

Abstract

TRIP steels, due to their microstructure, have great formability and ductility, which is required for the complex shapes of automotive parts. A typical microstructure contains mainly bainite, ferrite and retained austenite. This microstructure is achieved by heating in the intercritical annealing range, isothermal holding, rapid cooling to the bainitic transformation temperature, isothermal holding to the bainitic temperature and quenching. So bainite plays a major role in the microstructure and mechanical properties of this type of steels.

This study presents an overall modeling approach for the thermal process for the production of TRIP steels. This approach includes thermodynamic evaluation of the initial condition of the alloy (THERMOCALC), kinetic evaluation of the thermal process up to cooling before the bainitic transformation, thermodynamic calculations of the paraequilibrium conditions governing the bainitic transformation and finally mathematical modelling of the bainitic transformation.

The mathematical model that was used for this work is that proposed by Azuma. The initial values for that specific model were calculated by kinetic software DICTRA where the thermal treatment of steel has been simulated for the different heating and cooling rates. Azuma model takes into account and quantifies the precipitation of cementite during the bainitic transformation which allows for more realistic modelling of the bainitic transformation. This makes necessary the evaluation of the driving forces of formation for all participating phases, cementite precipitating from austenite and ferrite as well as ferrite forming from austenite. The evolution of bainite transformation is under paraequilibrium control, so the aforementioned driving forces need to be calculated under paraequilibrium conditions.

In order to calculate those driving forces a modification in thermodynamic database SSOL2 of THERMOCALC software must be done. The thermodynamic functions describing a pseudo-binary system of a fictitious element Z with carbon are incorporated into the database. Z-element accumulates all the thermodynamic functions of the substitutional elements in the initial alloy. Driving forces calculated for the phases of the pseudo-binary system of Z-C in equilibrium are driving forces of the respective phases of the initial alloy in paraequilibrium, these functions are inserted into the Azuma model and the kinetics of the bainitic transformation are modelled.

The result of this approach was validated with dilatometric measurements performed in RTHW during the collaboration for an RFCS project.

1 Introduction

The worldwide demand for a reduction in greenhouse gas emissions, better fuel economy and safety in automobiles has required the development of a variety of new alloy steels. Steel is a material with a unique, inherent capacity to absorb impact, and thus to diffuse the consequences of a crash. In addition to strength, automotive safety requires alloys with considerable ductility and formability, which is required due to the complex shapes of automotive parts. Multiphase transformation-induced plasticity (TRIP) steel is an example with great combination of these demands, due to its unique microstructure, that contains mainly bainite, ferrite, and retained austenite.

Bainite plays a major role in the microstructure and mechanical properties of TRIP steels. Optimization of the production and exploitation of bainite-involving steel grades and, more importantly, optimization of the design of new alloy compositions and/or processing routes, necessitate the clarification of the effect of chemical composition and heat-treatment conditions on the evolution of the bainitic transformation. This in turn creates a necessity for the development of appropriate models, with the highest possible degree of accuracy and applicability.

There are many empirical models dealing with bainitic transformation. The majority employs the Johnson-Mehl-Avrami-Kolmogorov (JMAK) approach, however, a few models were developed, such as the one proposed by Azuma, that more physically based. This particular model was the one employed for the specific work.

2 Literature Review

The increased demand of the automotive industry for steel grades exhibiting high strength and formability has been the main incentive for the advent of new, multi-phase steel families, such as the low-alloy DP and TRIP steels [1]. TRIP steels have a microstructure consisting of retained austenite in a ferrite matrix. Apart from retained austenite it also contains hard phases like bainite and martensite [2]. The higher silicon and carbon content of TRIP steels results in significant volume fractions of retained austenite in the final microstructure. TRIP steels use higher quantities of carbon than dual-phase steels to obtain sufficient carbon content for stabilizing the retained austenite phase to below ambient temperature. Higher contents of silicon and/or aluminium accelerate the ferrite/bainite formation. They are also added to avoid formation of carbide in the bainite region. The first practical exploitation of TRIP came from Zackay and coworkers [3], who developed steels with dramatically improved elongation, as a consequence of deformation-induced martensitic transformation. In the 1980's, the TRIP effect was demonstrated in low-alloy steels made with 0.2 C, 1-2 Mn and 1-2 Si (wt%) [4, 5].

The mechanical behaviour of TRIP steels is unique among the Fe-based alloys, since they manage to combine high strength (typical tensile strengths 600–1000 MPa) and formability (typical uniform elongations 20–25%) [6]. This excellent combination of mechanical properties of TRIP steels is largely attributed to their complex microstructure. It consists of dispersed retained austenite (γ_R) and bainite in a ferritic matrix which results in the namely TRIP effect, where the plasticity is enhanced by martensitic transformation from retained austenite during deformation.

The stress-strain curves are valuable for comparing different alloys (Figure 2.1). Any increase in strength is in general associated with a loss of ductility. The exceptions are the transformation-induced plasticity (TRIP) steels, where considerable ductility is obtained in spite of the strength. The major factor influencing the mechanical behavior of low-alloy TRIP steels is the stability of the γ_R dispersion, which in turn is affected by chemical composition, particle size and stress-state. Alloy elements have an important role in the final microstructure.

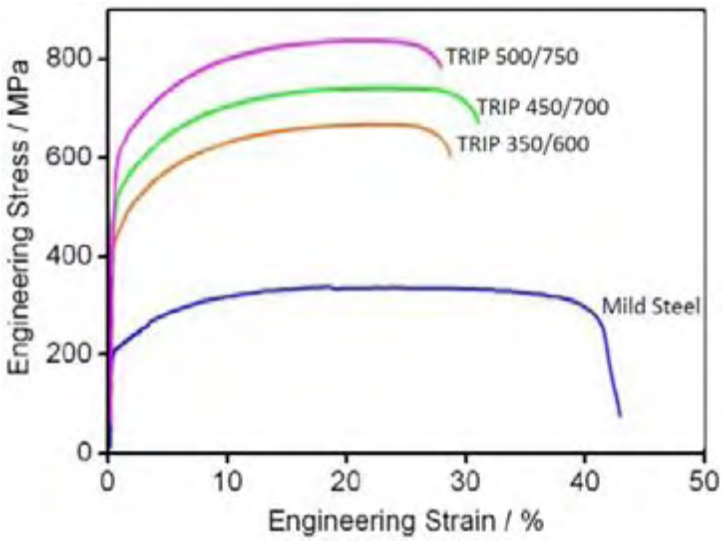

Figure 2.1 Engineering stress-strain curves for a series of TRIP steels [7]

Carbon plays a key role in the composition of TRIP-assisted steel. It strengthens austenite by interstitial solid solution hardening and enhances its stability. The carbon does diffuse and can enrich in austenite during bainitic transformation. TRIP steels use higher quantities of carbon than dual phase alloys to obtain sufficient carbon content for stabilizing the retained austenite to below ambient temperature. The stress or strain level at which retained austenite begins to transform to martensite can be controlled by adjusting the carbon content. At lower carbon levels, the retained austenite begins to transform almost immediately upon deformation, increasing the work hardening rate and formability during the stamping process. At higher carbon contents, the retained austenite is more stable and begins to transform only at strain levels beyond those produced during forming. At these carbon levels the retained austenite persists into the final part. It transforms into martensite during subsequent deformation, such as during forming or in a crash event.

Silicon is needed in TRIP steels to effectively suppress cementite formation. Increase of silicon content is beneficial for enhancing the combination of strength and ductility, and effectively retards the pearlite formation, but prolongs the bainitic transformation time required for the optimum mechanical properties [8]. Silicon levels > 0.5wt% can cause problems during the galvanizing operation and can oxidized preferentially to form SiO_2 and mixed oxide $MnSiO_4$ in manganese containing TRIP steels.

Aluminum retards cementite precipitation during bainitic transformation and hence can substitute for silicon. It is less potent in retarding the formation of cementite than silicon at the same weight concentration [9-11]**.** The aluminum bearing steels actually exhibit a remarkable TRIP effect during tensile testing because of the large amount of austenite that can be retained. Unlike silicon, aluminum doesn't cause problems during galvanizing steels.

Manganese, being an austenite stabilizer, lowers the temperature at which cementite starts to precipitate. It also lowers the activity coefficient of C in ferrite and austenite and increases the C solubility in ferrite [12]. Manganese is soluble in cementite. Higher manganese concentration requires longer holding time for bainitic transformation to achieve maximum strength-ductility balance.

Bainite plays a major role in the microstructure and mechanical properties of TRIP steels. Thus it is necessary to optimize the process for the bainitic transformation takes. There are many models dealing with the simulation of bainitic transformation, in literature and most of them employ the well-known Johnson-Mehl-Avrami-Kolmogorov (JMAK) approach for the description of the kinetics of the bainitic transformation [13]. The JMAK approach accounts for the hard impingement between growing particles, and calculates the volume fraction of the product phase as a function of time, using an expression of the general form:

$$f = 1 - exp[-k \cdot (t - t_0)^n] \quad \textbf{(1)}$$

In Eq. (1) f is the volume fraction of the product phase, to an incubation time, whereas parameters *k* and n contain all the terms depending on temperature, transformation driving force and other variables. However, information from literature has shown that the JMAK approach finds limited applicability for the case of the bainitic transformation. In particular, it has been found that the JMAK approach works satisfactorily only for a limited range of steel compositions and cooling conditions. On the other hand there exist in literature [14-16], a lot of information about courses of bainite transformations, describing the changes in the microstructures and describing the kinetic qualitatively and/or quantitatively in a numerical manner. With respect to the early stages of the bainitic transformation, i.e. the nucleation of bainitic ferrite, some fundamental concepts are reported in literature. As regards nucleation thermodynamics, it has been suggested that bainitic ferrite does not follow the classical nucleation theory based on heterogeneous thermal fluctuations, but that the activation energy for nucleation is directly proportional to the driving force of the transformation, a characteristic more consistent to

martensitic nucleation [17, 18]. The thermodynamic condition in order to obtain any detectable nucleation rate of Widmanstätten or bainitic ferrite is that the available minimum free energy, a quantity which has been determined experimentally by Ali et al. [19], must exceed the maximum Gibbs free energy change available for Para equilibrium nucleation, during which only carbon partitions between bainitic ferrite and austenite [20]. The magnitude of the maximum Gibbs free energy change available for Para equilibrium nucleation can be determined by a parallel tangent construction method described in [18]. The aforementioned approach establishes the thermodynamic perspective of the nucleation kinetics of bainitic ferrite, which is necessary for the subsequent determination of nucleation rates. With respect to this issue, some recent investigations are reported in literature. In a very recent work by Matsuda and Bhadeshia [21] two different nucleation processes are considered: the nucleation of individual bainitic ferrite plates (or ‘‘sub-units’’) on austenite grain surfaces and the subsequent autocatalytic nucleation of new sub-units on pre-existing bainitic ferrite plates. As regards nucleation on austenite grain surfaces, in their analysis the nucleation rate is considered to be dependent on the activation energy for nucleation. Subsequently, by expressing this activation energy as a linear function of the available driving force for nucleation, an expression for the nucleation rate per unit grain surface is obtained, which involves two adjustable parameters. Furthermore, the nucleation rate due to subsequent autocatalytic nucleation events is expressed in a form similar to that for grain surface nucleation, which also involves another two adjustable parameters. Values for the total of the four adjustable parameters were obtained by appropriate fitting to available experimental measurements [22, 23].

In another very recent work, Quidort and Brechet [24] adopted classical nucleation theory to describe the nucleation rate of bainitic ferrite, accounting for both the diffusional process limiting the formation of a nucleus and the activation energy for nucleation. The activation energy for nucleation in that analysis was evaluated by employing the so called ‘‘pill box’’ nucleation model proposed by Aaronson et al. [25]. The activation energy for diffusion was estimated by available experimental data and its value, compared to the activation energy for bulk diffusion of carbon in austenite, led to the conclusion that bainitic ferrite nucleation is more likely to be controlled by the austenite grain-boundary diffusion of carbon. Their analysis resulted to an expression for the nucleation rate of bainitic ferrite involving one adjustable parameter.

As regards growth kinetics, the mechanism by which individual bainitic ferrite plates grow in austenite has been the subject of significant controversy. In principal, two opposing theories for the growth of bainitic ferrite (α_B) have been suggested. According to one, individual α_B plates grow edge wisely under diffusion-control conditions, the growth rate being determined by carbon diffusion in austenite (γ), away from the advancing α_B/γ interface [26-30]. According to the other theory, α_B plates grow instantaneously in a displacive manner, their lengthening being limited by the accumulation of plastic deformation in austenite, and thus initially become fully or partially supersaturated in carbon [20, 31]. The excess carbon is subsequently rejected in a thickness-wise manner to the surrounding austenite. Therefore, as regards this later theory, the growth of individual α_B plates is overlooked, and all attention is concentrated on the nucleation process. Consequently, models describing the growth rate of bainitic ferrite plates available in literature are mostly based on the diffusion-control theory. The most important of these growth models are reviewed in the following paragraphs.

In a very early work, Hillert [26, 32], modified an equation by Zener for the diffusion-controlled edgewise growth of a plate, and suggested an expression for the growth rate of both Widmanstätten and bainitic ferrite plates. In this approach, the growth rate is given as a function of the diffusivity of carbon in austenite, of the α/γ interfacial energy and of the solute super saturation. Subsequent comparison with experimental growth-rate data assessed from steels with 0.2–1.4 % mass C showed acceptable agreement, although the experimental findings were somewhat lower than the calculated results [33, 34].

In a more complicated treatment, Trivedi developed a model for the diffusion-controlled growth of plates with geometry of a parabolic [35]. The expression suggested by Trivedi for the growth rate was a function of the curvature of the plate's tip, of the diffusivity of carbon in austenite, of solute super saturation (taking into account the Gibbs-Thomson capillarity effect [13]) and of two parameters depending on the Péclet number. In a more recent series of investigations, Quidort et al. [24, 36, 37] adopted a more simplified version of the original Trivedi model, which assumes infinite mobility at the interface and negligible capillarity effects [38]. In addition, in their treatment the thermodynamic effect of substitutional alloying elements on the ferrite-austenite equilibrium was taken into account, by employing the Thermo-Calc software and the SGTE thermodynamic database for iron alloys [39] for the necessary thermodynamic calculations. Comparison of growth rates calculated by this later model with

experimental growth-rate measurements in Fe-6%Ni-C alloys (carbon varying between 0.29–0.71%) [40], showed good qualitative but not so good quantitative agreement, with the calculations overestimating the experimental growth rates.

As already mentioned in the beginning of this section, the final goal of describing the evolution of the transformation is actually to describe the overall, macroscopic kinetics, basically in terms of determining the volume fraction of bainite as a function of transformation temperature, holding time (for isothermal treatments) or cooling rate (for continuous-cooling treatments) and alloy composition. For any practical alloy or/and process design purposes, it is also important that such kinetic approaches involve as few adjustable parameters as possible.

Models aiming to describe the overall kinetics incorporate the nucleation and growth kinetics of the transformation to a suitable integration scheme, which subsequently provides information about the macroscopic evolution of the phase transformation. Within this framework, overall kinetics models for the bainitic transformation reported in literature are based on the Johnson-Mehl-Avrami-Kolmogorov (JMAK) method or variations of it.

In a very recent work by Quidort and Brechet [24] the general JMAK equation is employed:

$$f = 1 - exp\left(-\frac{V^e}{V}\right) \quad \textbf{(2)}$$

where f is the volume fraction of bainite, V^e the ‘‘extended’’ volume of the transforming region and V the actual volume of the transforming region. By integrating with respect to transformation time, an expression for the evolution of volume fraction bainite was obtained, involving two adjustable parameters. Comparison with dilatometric measurements performed in isothermally-treated specimens showed good qualitative and quantitative agreement for the case of a 0.5% C steel, but not so for an alloyed steel. The model was also applied for continuous-cooling treatment, where an acceptable agreement to corresponding experimental measurements was observed for the lower of the cooling-rates examined [24, 36].

In another very recent investigation, Matsuda and Bhadeshia [21], in order to explicitly deal with the grain-boundary nucleation of bainitic ferrite, employed a very early idea by Cahn, who adapted the extended volume to an ‘‘extended area’’ concept [41]. According to that concept, particles of a phase that nucleate randomly on a planar grain-boundary consume some of its area. Subsequently, the extended grain-boundary area is related to the actual grain-boundary, exactly as the extended volume is related to actual volume in the classic approach. The calculation of

volumes involves the employment of a plane parallel to the grain-boundary, placed at a distance y away from the later. Particles nucleated at the boundary are assumed to intersect this plane with varying extended areas. Therefore, by integrating these extended areas with respect to distance y, it becomes possible to obtain the extended volume of the growing phase. By exploiting this idea, Matsuda and Bhadeshia developed a rather complicated numerical iterative process in order to solve for the variation of volume fraction bainite with respect to time. The model accounts for the evolution of aggregates (‘‘sheaves’’) of bainitic ferrite plates, by allowing for the repeated autocatalytic nucleation of new plates, and incorporates the effect of variables such as transformation temperature, holding time, austenite grain size and alloy composition. The model was applied for isothermal and continuous cooling treatments exhibiting fairly good agreement to corresponding experimental results.

The most integrated model has been proposed by Azuma et al. [42]. The major advantage over other existing models is that it takes into account and quantifies the precipitation of cementite during the bainitic transformation. This allows for more realistic modelling of the bainitic transformation overall and, furthermore, it widens the range of applicability of the model to practically any steel composition and heat-treatment route. Other proposed models, which neglect carbide precipitation and focus solely on the kinetics of bainitic ferrite, are inevitably limited to be best applicable to steel compositions where carbide precipitation is severely suppressed, e.g. in steels containing Si and/or Al in excess of 1 mass %. But even in these cases, cementite will eventually precipitate at prolonged holding times, which means that neglecting carbide precipitation poses limitations not only with respect to steel composition, but also with respect to heat-treatment conditions.

The model of reference [42] also manages to account for a number of significant features of the bainitic transformation. Due to its structure it can discriminate and identify the evolution of upper and lower bainite, depending on the chemistry of the steel and transformation temperature. Furthermore, it takes into account and calculates important microstructural features of bainite, such as the size of bainitic ferrite platelets and the size of cementite particles, as well as the variation of these microstructural features during the transformation (e.g. gradual refinement of bainitic ferrite platelets due to the gradual enrichment of untransformed austenite in carbon). Finally, although lacking in the form presented in reference [42], the model can be easily modified, in order to be applied for continuous-cooling transformation and to take into account

the grain-size of parent austenite, the later feature being of great interest for application in multi-phase TRIP steels.

Besides calculating vol. fractions, the model of reference [42] manages to provide quantitative information about a series of very important features, such as the average carbon content and yield-strength of untransformed austenite, the average size of cementite precipitates, the average size of ferrite platelets, etc, all as functions of temperature and time. The bainitic transformation proceeds by the nucleation and growth mechanisms. Two opposing doctrines have been proposed, regarding the controlling process of the bainitic transformation: diffusion-controlled growth and nucleation-control. According to the first approach, the rate of the transformation is determined by the growth-rate of bainitic ferrite laths in austenite, which is considered to take place under diffusion-control. The opposing approach supports the idea that the overall transformation rate is determined by the rate at which bainitic ferrite nucleates in austenite.

Published modelling approaches are based either on the diffusion-control or on the nucleation-control mechanism. Most of the models reported in Σφάλμα! Το αρχείο προέλευσης της αναφοράς δεν βρέθηκε., however, are based on the nucleation-control mechanism, which presents certain advantages over diffusion-control. In conclusion, as regards the evaluation of existing models retrieved from literature, the model of [42] is the most integrated, and presents the greatest potential for wide applicability in comparison to other published models. These empirical models are generally insufficient and only able to describe some very special aspects for a rather limited range of steel composition and only for simple cooling conditions. Beside these empirical models there exist some more physically based theories on bainite formation. They concern the nucleation kinetics, the growth kinetics or the overall transformation kinetics. Although they are somewhat controversial they seem to describe the transformation for those steel compositions and thermal cycles for which they are used in a more convincing way than JMAK approaches can do. The most reliable of these models require the evaluation of the Driving Force ΔG for formation of bainitic ferrite from austenite ($\gamma \rightarrow \alpha_B$) and the Driving Force ΔG for formation of cementite from austenite ($\gamma \rightarrow Fe_3C$). the majority of these models consider the evaluation of the required ΔG's under equilibrium. However the bainitic transformation takes place under paraequilibrium conditions. As a result an essential stepping stone in the development and application of any model describing the bainitic transformation is the evaluation of the required ΔG's under paraequilibrium.

Model and related references	**Year**	**Controlling process**	**Type of heat-treatment**	**Carbide precipit.**	**Chemical composition limitations**	**Comments**
Rees-Bhadeshia [23]	1992	Nucleation control	Isothermal	No	Si + Al > 1%*	Accounts for autocatalytic nucleation, austenite grain size, incomplete reaction phenomenon, does not provide quantitative information for M_3C
Quidort - Brechet [24, 36, 37]	2002	Diffusion control	Isothermal & continuous cooling	No	Si + Al > 1%*	Calculated α_B sub-unit growth-rates significantly higher than experimental, does not account for incomplete reaction phenomenon, does not provide quantitative information for M_3C
Matsuda - Bhadeshia [21]	2004	Nucleation control	Isothermal & continuous cooling	No	Si + Al > 1%*	Accounts for autocatalytic nucleation, austenite grain size, incomplete reaction phenomenon, does not provide quantitative information for M_3C
Azuma et al. [42]	2005	Nucleation control	Isothermal	Yes	Fundamentally none	Accounts for autocatalytic nucleation, incomplete reaction phenomenon, sub-unit refinement, calculates vol. fraction, size & distribution of carbides, identifies upper & lower bainite
Gaude-Fugarolas - Jacques [43]	2006	Nucleation control	Isothermal	No	Si + Al > 1%*	Accounts for autocatalytic nucleation, austenite grain size, incomplete reaction phenomenon, does not provide quantitative information for M_3C
Katsamaset al. [44]	2006	Nucleation control	Isothermal	No	Si + Al > 1%*	Semi-empirical model for calculation of retained austenite in multiphase TRIP steels, can calculate vol. fraction of α_B indirectly

* Since these models neglect carbide precipitation, they would be more realistically applicable in steels containing Si and/or Al in excess of 1% mass, in order for cementite precipitation to be drastically suppressed.

Table 1 Summary of most worth-noting, published models for bainite kinetics

3 Paraequilibrium Calculations

In order to apply and exploit the selected kinetic model for the bainitic transformation in the steels of interest, a series of cumbersome thermodynamic calculations have to be performed. For example, calculation of the thermodynamic driving-forces for the nucleation of the product phases (i.e. bainitic ferrite and cementite) in paraequilibrium with the respective parent phases, as functions of transformation temperature and C-content of parent austenite, is necessary, since these functions are required input to the kinetic model.

The kinetic theories of diffusional phase transformations in alloys containing both substitutional and interstitial elements are well developed [45]. An important feature of various kinetic models is the assumption of local equilibrium at the interface. Depending on the interface velocity during transformation, it is convenient to classify the kinetics into two distinct modes:
partitioning local equilibrium is characterized by low interface velocity while maintaining local equilibrium at the interface. This condition is also referred to as orthoequilibrium (OE). The overall kinetics of OE transformation is governed by the slowest diffusing specie (substitutional element). The thermodynamic condition for OE between ferrite (α) and cementite (θ) in steels is given by

$$\mu_j^{\alpha} = \mu_j^{\theta} \qquad (3)$$

where μi is the chemical potential of element i (=C, Co, Cr, Fe, Mn, Mo, Ni, Si) .
paraequilibrium (PE) is a kinetically constrained equilibrium when the diffusivity of the substitutional species is negligible compared to that of interstitial species. The kinetics of PE is governed by the fastest diffusing specie, which is either C or N in steels. Hultgren [46] argued that if carbon diffuses appreciably faster than the substitutional alloying elements, then the growing phase inherits the substitutional alloy contents. Furthermore, if the substitutional alloying elements are not allowed to partition, their individual chemical potentials have no physical relevance and thus the thermodynamic behavior of these elements can be expressed by one hypothetical element, Z. Then, PE is defined by a uniform carbon potential and a uniform site fraction of substitutional elements across the transforming interface. For example, in the case of α/θ transformation, the thermodynamic conditions for PE are given by

$$\mu_C^{\alpha} = \mu_C^{\theta} \quad (4)$$

$$y_C^{\alpha} = y_C^{\theta} \quad (5)$$

$$\mu_Z^{\alpha}\left(\equiv \sum y_j \mu_j^{\alpha}\right) = \mu_Z^{\theta}\left(\equiv \sum y_j \mu_j^{\theta}\right) \quad (6)$$

where the yj terms are the site fractions of substitutional element j (representing Co, Cr, Fe, Ni, Mo, V, and W). For a system containing both substitutional (j) and interstitial elements (C or N), the site fractions are related to the ordinary mole fractions (x) as follows.

$$y_j = \frac{x_j}{1 - x_C - x_N} \quad (7)$$

$$y_{C \text{ or } N} = \frac{p}{q} \frac{x_{C \text{ or } N}}{1 - x_C - x_N} \quad (8)$$

According to the two-sublattice model [8] used here to express substitutional alloying, p= 1 and q= 3 for ferrite, and p =q=1 for austenite.

Driving-forces under paraequilibrium are of special importance in the kinetic model and the method to calculate them has to be extended to all the major alloying elements in the steels under consideration. It is also necessary to calculate paraequilibrium concentrations between the involved phases, as well as the molar volumes of the product phases. Since there is no readily available computational thermodynamics software to implement the aforementioned calculations automatically, a methodology had to be developed towards this direction.

As the bainitic transformation in steels evolves, three simultaneous phase-transformations take place in the system (Figure 3.1):

$$\gamma \rightarrow \gamma' + \alpha B \quad (9)$$

$$\gamma' \rightarrow \gamma'' + \theta\gamma \quad (10)$$

$$\alpha B \rightarrow \alpha' B + \theta\alpha \quad (11)$$

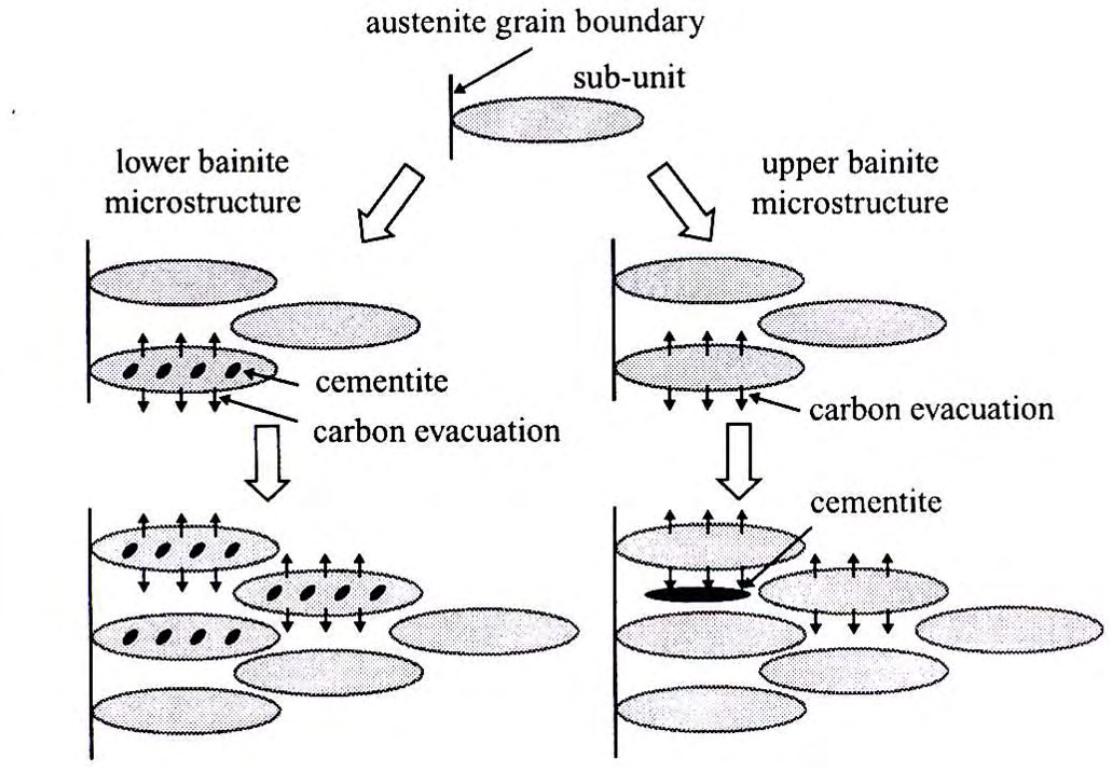

Figure 3.1 Mechanism of the bainitic transformation

In transformation (9), parent austenite (γ) of nominal C-content transforms to bainitic ferrite (αB). The untransformed fraction of austenite (γ′) is substantially enriched in C compared to parent austenite, due to the carbon rejected by bainitic ferrite.

In transformation (10), cementite (θγ) precipitates from C-rich austenite (γ′). Precipitation takes place within the austenitic grains, leading to the morphology known as upper bainite. The precipitation of cementite reduces drastically the C-content of austenite, so that the remaining austenite (γ′′) contains substantially lower amounts of carbon.

In transformation (11), cementite (θα) precipitates in bainitic ferrite, leading to the morphology known as lower bainite. As in the case of austenite, cementite draws carbon from bainitic ferrite, leaving the later with even lower C-content (α′B).

During the bainitic transformation, the aforementioned phase-transformations take place under paraequilibrium conditions. Calculation of paraequilibrium driving-forces (Figure 3.2, Figure 3.3) for the nucleation of the product phases is not a straightforward task and cannot be performed directly in Thermo-Calc software. In order to perform these calculations a

modification was necessary, by intervening in the Gibbs Energy System (GES) module of Thermo-Calc software.

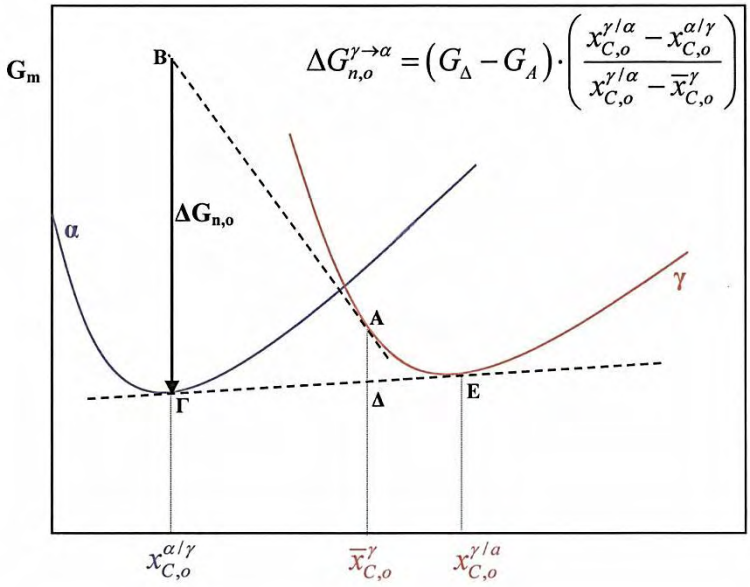

Figure 3.2 The driving force for nucleation of (α) in para-equilibrium with austenite (γ) is determined (Thermo-Calc).

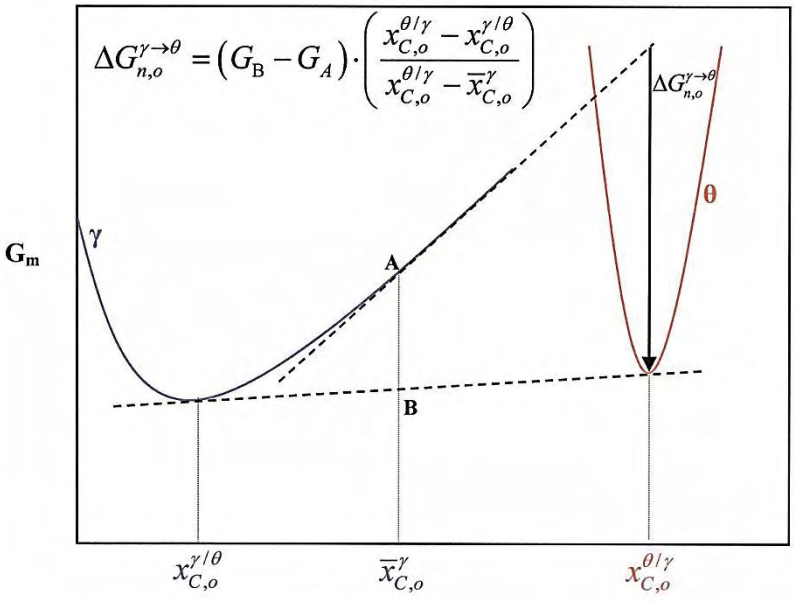

Figure 3.3 The driving force for nucleation of (θ) in para-equilibrium with austenite (γ) is determined (problem with Thermo-Calc!).

Haidemenopoulos et al. [47] and Olson et al. [39, 45, 48] established a technique, by which paraequilibrium thermodynamic calculations can be performed in multicomponent steels,

containing various substitutional alloying elements. The fundamental idea behind this technique is that in a multicomponent steel Fe-C-M1-M2-…-Mn, where Mi represent the substitutional alloying elements of the steel, all substitutional elements (including Fe) can be replaced by a fictitious element, Z, so that the alloy reduces to a pseudo-binary Z-C system.

The thermodynamic conditions for two multi-component solid phases, α1 and α2, to exist in paraequilibrium are the following:

$$\mu_C^{\alpha 1} = \mu_C^{\alpha 2} \qquad (12)$$

$$y_j^{\alpha 1} = \mu y_j^{\alpha 2} \qquad (13)$$

In order for these two phases to exist in paraequilibrium, the chemical potential of C (μ_C) has to be the same in the two phases, and the site-fractions of each substitutional element (yj) have to be the same in the two phases.

The site-fraction of a substitutional element j, yj, is defined by:

$$y_j = \frac{x_j}{1 - x_C} \qquad (14)$$

In Eq. (14) x_j and x_C are the usual mole-fractions of substitutional element j and of carbon, respectively.

The chemical potential of the fictitious element Z, which replaces all substitutional elements of the steel, is defined by:

$$\mu_Z^{\alpha 1} = \sum y_j \mu_j^{\alpha 1} \qquad (15)$$

$$\mu_Z^{\alpha 2} = \sum y_j \mu_j^{\alpha 2} \qquad (16)$$

Now, paraequilibrium conditions for the actual steel reduce to the corresponding orthoequilibrium condition for the pseudo-binary Z-C system:

$$\mu_C^{\alpha 1} = \mu_C^{\alpha 2} \qquad (17)$$

$$\mu_Z^{\alpha 1} = \mu_Z^{\alpha 2} \qquad (18)$$

The molar Gibbs free energy of a phase (α) in the pseudo-binary Z-C system is given by the following expression:

$$G_m^a = y_C \sum y_j \cdot G_{j:C}^{0,a} + y_{Va} \sum y_j \cdot G_{j:Va}^{0,a}$$

$$+R \cdot T\left(\sum y_j \ln y_j \cdot + 3y_C \ln y_C + 3y_{Va} \ln y_{Va}\right)$$

$$+G_m^{xs,a} + G_m^{mag,a} \qquad (19)$$

In Eq. (19), yj, yC and yVa represent the site-fractions of substitutional elements, carbon and vacancies, respectively, $G_{j:C}^{o,\alpha}$ and $G_{j:Va}^{o,\alpha}$ are the lattice-stability parameters of substitutional element j with carbon atoms and vacancies, respectively, $G_m^{xs,\alpha}$ is the term representing the excess Gibbs energy of mixing and $G_m^{mag,\alpha}$ is the magnetic ordering energy contribution term. In the CALPHAD method, the excess Gibbs energy of mixing term ($G_m^{xs,\alpha}$) is approximated by a Redlich-Kister-Muggianu polynomial expansion [39]. The expanded form of the molar Gibbs free energy of phase (α), after introducing the Redlich-Kister-Muggianu polynomial approximation for $G_m^{xs,\alpha}$, has the following form:

$$
\begin{aligned}
G_m^a = y_C \Bigg(& \sum y_j \cdot G_{j:C}^{0,a} \\
& + RT \sum y_j \ln y_j + \sum_{j \neq k} \sum y_j y_k \left(L_{j,k:C}^{0,a} + (y_j - y_k) L_{j,k:C}^{1,a} + \cdots \right) \\
& + \sum_{j \neq k \neq 1} \sum \sum y_j y_k y_1 L_{j,k,1:C}^{0,a} \Bigg) \\
& + y_{Va} \Bigg(\sum y_j \cdot G_{j:Va}^{0,a} \\
& + RT \sum y_j \ln y_j + \sum_{j \neq k} \sum y_j y_k \left(L_{j,k:Va}^{0,a} + (y_j - y_k) L_{j,k:Va}^{1,a} + \cdots \right) \\
& + \sum_{j \neq k \neq 1} \sum \sum y_j y_k y_1 L_{j,k,1:Va}^{0,a} \Bigg) \\
& + y_C y_{Va} \left(\sum y_j \cdot G_{j:C,Va}^{0,a} + \sum_{j \neq k} \sum y_j y_k L_{j,k:C,Va}^{0,a} + \cdots \right) \\
& + y_C y_{Va} (y_C - y_{Va}) \left(\sum y_j \cdot L_{j:C,Va}^{1,a} + \sum_{j \neq k} \sum y_j y_k (y_j - y_k) L_{j,k:C,Va}^{1,a} + \cdots \right) \\
& + 3R \cdot T (y_C \ln y_C + y_{Va} \ln y_{Va}) + G_m^{mag,a}
\end{aligned}
\tag{20}
$$

In Eq. (20) L's represent the interaction parameters of the corresponding substitutional elements with carbon atoms and vacancies. The various lattice stabilities and interaction parameters are functions of temperature and pressure, which are contained in special thermodynamic databases included in Thermo-Calc software.

The energy contributed to the system by magnetic ordering effects ($G_m^{mag,\alpha}$) is determined by the following expression:

$$
G_m^{mag,\alpha} = RT \ln(\beta^\alpha + 1) f\left(\frac{T}{T_C^\alpha}\right) \tag{21}
$$

In Eq.(21), T_C^{α} is the critical Curie temperature and βα the average Bohr magneton of the phase. Both these quantities are also approximated by a Redlich-Kister-Muggianu polynomial expansion.as follows:

$$
\begin{aligned}
\mathrm{T_c^a} = \mathrm{y_C}\Bigg(& \sum \mathrm{y_j}\, \mathrm{T}^{0,a}_{\mathrm{c_j:C}} + \sum\sum \mathrm{y_j y_k}\left(\mathrm{T}^{0,a}_{\mathrm{c_j,k:C}} + (\mathrm{y_j}-\mathrm{y_k})\mathrm{T}^{1,a}_{\mathrm{c_j,k:C}} + \cdots\right) \\
& + \sum_{\mathrm{j\neq k\neq 1}} \sum\sum \mathrm{y_j y_k y_1}\, \mathrm{T}^{0,a}_{\mathrm{c_j,k,1:C}} \Bigg) \\
& + \mathrm{y_{Va}}\Bigg(\sum \mathrm{y_{c_j}}\, \mathrm{T}^{0,a}_{\mathrm{c_j:Va}} + \sum_{\mathrm{j\neq k}} \sum \mathrm{y_j y_k}\left(\mathrm{T}^{0,a}_{\mathrm{c_j,k:Va}} + (\mathrm{y_j}-\mathrm{y_k})\mathrm{T}^{1,a}_{\mathrm{c_j,k:Va}} + \cdots\right) \\
& + \sum_{\mathrm{j\neq k\neq 1}} \sum\sum \mathrm{y_j y_k y_1}\, \mathrm{T}^{0,a}_{\mathrm{c_j,k,1:Va}} \Bigg) \\
& + \mathrm{y_C y_{Va}}\Bigg(\sum \mathrm{y_j}\cdot \mathrm{T}^{0,a}_{\mathrm{c_j:C,Va}} + \sum_{\mathrm{j\neq k}} \sum \mathrm{y_j y_k T} + \cdots \Bigg) \\
& + \mathrm{y_C y_{Va}}(\mathrm{y_C}-\mathrm{y_{Va}})\Bigg(\sum \mathrm{y_j}\cdot \mathrm{T}^{1,a}_{\mathrm{c_j:C,Va}} \\
& + \sum_{\mathrm{j\neq k}} \sum \mathrm{y_j y_k}(\mathrm{y_j}-\mathrm{y_k})\, \mathrm{T}^{1,a}_{\mathrm{c_j,k:C,Va}} + \cdots \Bigg)
\end{aligned}
\tag{22}
$$

$$\beta^{a} = y_C\left(\sum y_j\,\beta^{0,a}_{j:C} + \sum_{j\neq k}\sum y_j y_k\left(\beta^{0,a}_{j,k:C} + (y_j - y_k)\beta^{1,a}_{j,k:C} + \cdots\right)\right.$$
$$+ \sum\sum y_j y_k y_l\left(\beta^{0,a}_{c_j,k:C} + (y_j - y_k)T^{1,a}_{c_j,k:C} + \cdots\right)$$
$$\left. + \sum_{j\neq k\neq 1}\sum\sum y_j y_k y_1 \beta^{0,a}_{j,k,1:C}\right)$$
$$+ y_{Va}\left(\sum y_j\,\beta^{0,a}_{j_j:Va} + \sum_{j\neq k}\sum y_j y_k\left(\beta^{0,a}_{j_j,k:Va} + (y_j - y_k)\beta^{1,a}_{j,k:Va} + \cdots\right)\right.$$
$$\left. + \sum_{j\neq k\neq 1}\sum\sum y_j y_k y_1 \beta^{0,a}_{j,k,1:Va}\right)$$
$$+ y_C y_{Va}\left(\sum y_j \cdot \beta^{0,a}_{j:C,Va} + \sum_{j\neq k}\sum y_j y_k \beta^{0,a}_{j,k:C,Va} + \cdots\right)$$
$$+ y_C y_{Va}(y_C - y_{Va})\left(\sum y_j \cdot \beta^{1,a}_{j:C,Va} + \sum_{j\neq k}\sum y_j y_k (y_j - y_k)\beta^{1,a}_{j,k:C,Va} + \cdots\right) \quad (23)$$

In a similar manner, the molar Gibbs free energy of a phase (α) in the fictitious binary Z-C system is given by:

$$G_m^{PE-a} = y_C G^{0,PE-a}_{Z:C} + y_{Va} G^{0,PE-a}_{Z:Va} + y_C y_{Va} L^{0,PE-a}_{Z:C,Va} + y_C y_{Va}(y_C - y_{Va}) L^{1,PE-a}_{Z:C,Va}$$
$$+ 3RT(y_C \ln y_C + y_{Va} \ln y_{Va}) + G_m^{mag,PE-a} \quad (24)$$

Cross-examining Eqs (19), and (24), it is evident that there is a one-to-one correspondence between parameters in the molar Gibbs free energy descriptions of the phases of the actual steel and of the binary Z-C system.

Thus, all parameters of the Z-C system (i.e. lattice stabilities, interaction parameters, Bohr magnetons and critical Curie temperatures) can be determined by the corresponding parameters of the actual steel.

For example, assume a multicomponent steel represented by the alloy system Fe-C-Mn-Cr-Si-Nb, which is typical of e.g. a dual-phase steel. In this case, all the substitutional elements of the system (Fe, Mn, Cr, Si and Nb) are substituted by a fictitious element Z. Thus, the multicomponent system reduces a binary Z-C system, as mentioned previously.
Subsequently ,in order to determine the thermodynamic description of every phase in the Z-C system, the lattice stabilities, interaction parameters, critical Curie temperatures and average Bohr magnetons of each phase have to be determined, as functions of the corresponding parameters of the phases of the actual multicomponent system.

All the conversion equations are introduced into Thermo-Calc, in order to thermodynamically describe the Z-C system in the software. This is performed through intervention to the Gibbs Energy System (GES) module of Thermo-Calc. After the description has been appropriately introduced there, then the driving-force for the nucleation of a phase in the Z-C system can be calculated under orthoequilibrium conditions. These calculated driving-forces for nucleation represent the corresponding driving-forces for the nucleation of the same phase in the actual multicomponent steel, but for paraequilibrium conditions.
By employing the methodology described above, the driving-forces for nucleation of the involved product phases under paraequilibrium conditions have been calculated, as functions of temperature and C-content of the parent phases, for many of the steel grades examined in the project. These results are of great value, since such research work is very scarce in literature.

4 Methodology

4.1 Material and Microstructure

Two different steel grades were selected with compositions in the range of current industrial interest. The chemical composition of the alloys, under investigation is presented in Table 2. The material was provided by Voest-Alpine.

Table 2 Chemical composition of TRIP and DP steels

Steel	C	Al	Mn	Cr	Si
TRIP-Al steel	0.219	1.35	1.6	0.033	0.122
DP-steel	0.146	-	2.39	0.77	0.13

A typical microstructure of TRIP steel is depicted in Figure 4.1. Three distinct regions of the participating phases are observed, retained austenite (white color), ferrite (light grey), and bainite (black).

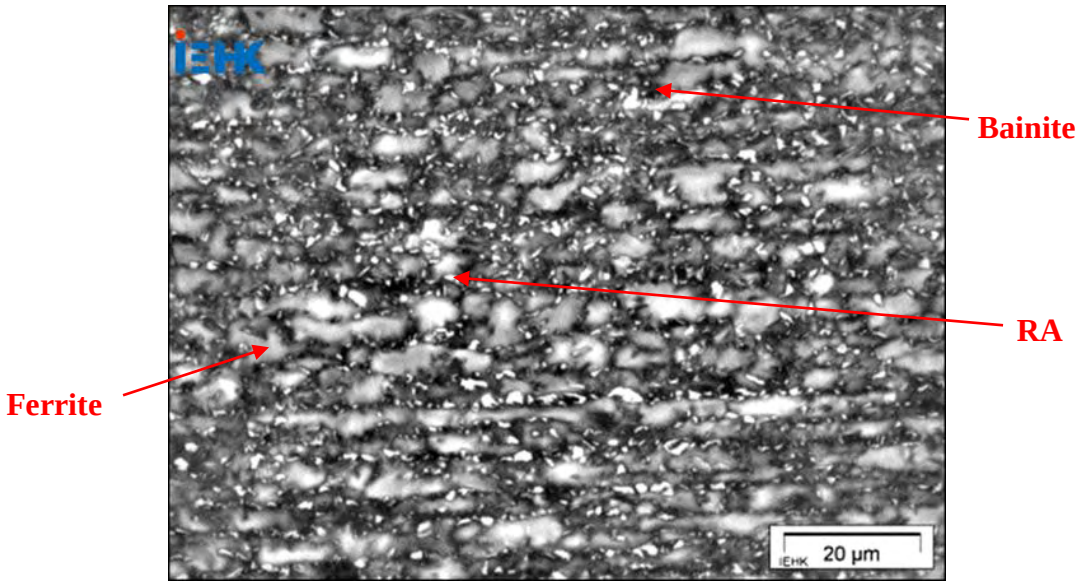

Figure 4.1 Typical microstructure of TRIP steel

4.2 Heat Treatment

In order to develop the desired microstructure both alloys were subjected to a thermal cycle depicted in Figure 4.2. The thermal cycle consists of heating, up to a temperature in the intercritical annealing range, isothermal holding for 300 seconds with subsequent cooling to the bainitic transformation temperature (350-500^{o}C), isothermal holding at the proposed temperature for 600sec and final cooling to room temperature.

Intercritical annealing temperature for the case of TRIP steel was 830^{o}C. This temperature is evaluated as the temperature where the thermodynamic calculations predict 50% austenite and 50% of ferrite. During cooling austenite is the only phase that transforms into ferrite, and as the process continues at the isothermal section it will continue transforming to bainite. The aim is a microstructure of 50% ferrite, 35% - 45 % bainite, and 5% to 15% austenite. A final cooling section takes place where the austenite from the previous process remains as retained austenite or in some cases a combination of retained austenite and martensite.

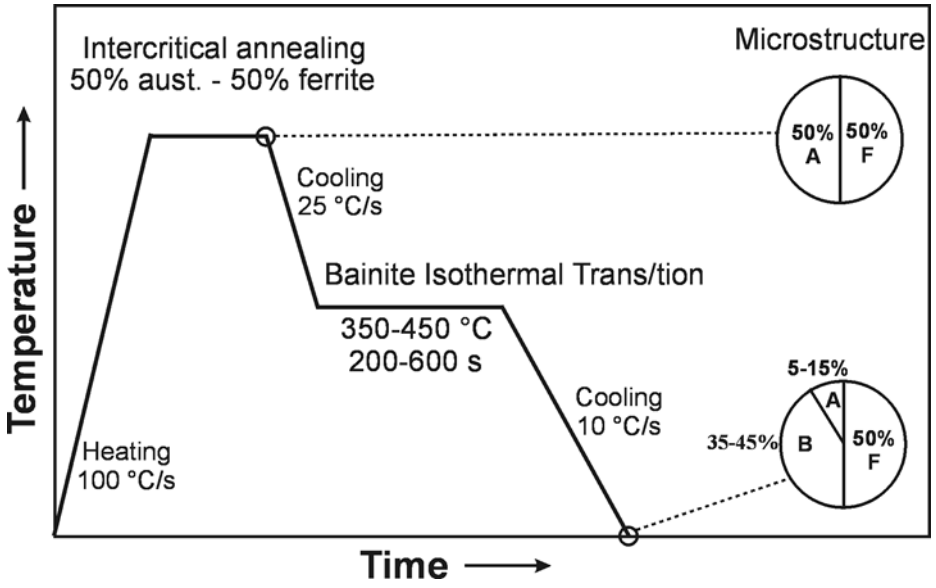

Figure 4.2 Thermal process for TRIP steel production

4.3 Thermodynamic Calculations

The thermodynamic calculations were performed using the commercially available THERMOCALC software and the TCFe-6 database for steels. Thermodynamic simulations were performed for the identification of cementite dissolution temperature. The composition of each phase was calculated for this case.

4.4 Kinetic Calculations under orthoequilibrium

Kinetic calculations where performed in order to simulate the heating, intercritical annealing and cooling part of the heat treatment. DICTRA software was used in combination with MOBFE2 mobility database. It is well established, that austenite formation during heating of ferrite/pearlite mixtures proceeds in two kinetically distinct steps. The first step is very fast and involves the formation of austenite from pearlite. The second step is much slower and involves the formation of austenite from proeutectoid ferrite, in the model presented here, the assumption is therefore that pearlite transformation to austenite is completed in a negligible amount of time. The conditions at the end of the first step are considered as initial conditions for the second step. The model is one-dimensional and a planar geometry is assumed. Thus, the initial widths of the two regions, Lα and Lγ, can be directly related to the volume fractions of the two phases, ferrite and austenite calculated at a temperature T which corresponds to the temperature where all pearlite has been dissolved and only γ and proeutectoid α remain in the system (Figure 4.3):

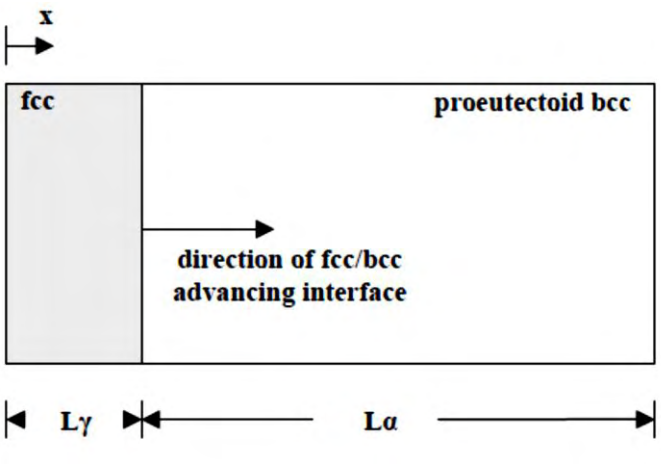

Figure 4.3 Geometrical model for austenite formation

4.4.1 Procedure for Calculation of Paraequilibrium Driving Forces

Calculation of paraequilibrium driving-forces for the nucleation of the product phases is not a straightforward task and cannot be performed directly in Thermo-Calc software. In order to perform these calculations a modification was necessary, by intervening in the Gibbs Energy System (GES) module of Thermo-Calc software.

As soon as the procedure mentioned above was implemented, the driving forces for paraequilibrium nucleation of the phases of interest were determined, as functions of temperature and carbon-content of parent phases. These calculations were performed and were necessary for the application of the bainite kinetic model under both isothermal and continuous-cooling conditions.

Following the establishment of a step-by-step procedure for the exploitation of the kinetic model in isothermal conditions, the selected kinetic model was appropriately adapted in order to be used for bainitic transformations under continuous-cooling conditions. The corresponding step-by-step procedure was established and the calculation of the driving force for formation of the phases under paraequilibrium condition will be descripted in this chapter. The calculation of driving forces of formation will be demonstrated for any steel containing the following elements: Fe, Mn, Cr, Si, Nb, Al, C. The paraequilibrium calculations consist of several steps described in detail below. All the corresponding equations can be found in the appendix.

1st STEP: Definition of phase parameters

The expanded form of the molar Gibbs free energy of the three phases under paraequilibrium G_m^{PE-a} from equation (24) is obtained for the alloy in and the have the following form, where PHASE or φ stand for either austenite, ferrite and cementite. For example, the lattice stability of a phase φ containing atoms of the fictitious element Z and of carbon is given by the expression shown in Eq. (39), as a function of thermodynamic parameters of the actual multicomponent system. Eqs (40) to (50) give the corresponding modification functions for all the thermodynamic parameters needed for the description of the Z-C system. It should be noted that the general format of Eqs. (39) to (50) could be used for the modification of any alloy system containing five substitutional and one interstitial element.

2nd STEP: Acquisition of GES phase description for THERMOCALC

Input of the alloys chemical composition into the therodynamical calculation software THERMO-CALC and acquiring the GES files of the phases participating in the thermodynamic equilibrium. The thermodynamic database used throughout this work is SSOL2 Database.

3rd STEP: Para-equilibrium composition of the alloy

The third step is to acquire the new modified composition of the alloy under para-equilibrium conditions; this is achieved by calculating equilibrium in Thermo-calm software for the alloy after suspending the phases of cementite and austenite. The code inserted into the Thermocalc software is described in the Appendix.

The result of the calculation is the alloy's composition xFe, xMn, xCr, xSi, xNb, xAl and xC valuesunder paraequilibrium conditions..

4th STEP: Calculation of site fractions

From Eq. (14) the yj (element site fractions) values are calculated. The required site fractions are listed in Table 3 where x_j are the mole fractions of the elements participating in the alloy calculated under paraequilibrium conditions in the previous step. Also all the y_j combinations required in the expanded form of the molar Gibbs free energy of the three phases under paraequilibrium are calculated Table 3.

Table 3: Site fractions.

Element	**xj**	**$y_j^{(fcc)}$**	**$y_j^{(bcc)}$**	**$y_j^{(M3C)}$**	
Fe	xFe	$yFe^{(fcc)}$	$yFe^{(bcc)}$	$yFe^{(M3C)}$	Y1
Mn	xMn	$yMn^{(fcc)}$	$yMn^{(bcc)}$	$yMn^{(M3C)}$	Y2
Cr	xCr	$yCr^{(fcc)}$	$yCr *^{(bcc)}$	$yCr *^{(M3C)}$	Y3
Si	xSi	$ySi^{(fcc)}$	$ySi^{(bcc)}$	$ySi^{(M3C)}$	Y4
Nb	xNb	$yNb^{(fcc)}$	$yNb^{(bcc)}$	$yNb^{(M3C)}$	Y5
Al	*xAl	$yAl^{(fcc)}$	$yAl^{(bcc)}$	$yAl^{(M3C)}$	Y6
C	*xCl	$yC^{(fcc)}$	$yC^{(bcc)}$	$yC^{(M3C)}$	

5th STEP: Definition of phase parameter in SSOL2

In this step it is essential to compare the excess model REDLICH-KISTER_MUGGIANU in the SSOL2 database of thermocalc with all the functions participating in the expanded form of the molar Gibbs free energy of the three phases under paraequilibrium G_m^{PE-a} from equation (24). The SSOL2 database contains only some of the functions, so a comparison is made and only the participating functions are considered for the construction of the Z file.

The resulting functions, where PHASE or φ stand, for either austenite, ferrite and cementite are described in the Appendix.

6th STEP: Modification of SSOL2

The modified participating functions are then inserted into the thermocalc database SSOL2 and thereafter the database is modified to perform equilibrium calculations for a binary Z-C which is actually paraequilibrium calculations for the initial alloy.

This method has to be performed every time the composition of the alloy changes.

4.5 Azuma model description

The purpose of the analytical selected in the second chapter this work was to enable a complete quantitative treatment of the bainitic transformation in steels, by taking into consideration the majority of metallurgical processes that occur during it. For example - and in contrast with most other relevant models – the Azuma model takes into account and quantifies the precipitation of cementite during the transformation. This enables more realistic modelling of the transformation and widens the range of applicability of the model to practically any steel composition. Other published models, which focus solely on the kinetics of bainitic ferrite, are inevitably limited to cases where carbide precipitation is severely suppressed, e.g. in steels containing Si and/or Al in excess of mass %. Furthermore, the model proposed for a number of significant aspects of the bainitic transformation. Due to its structure it identifies the formation of upper or lower bainite, depending on the chemistry of the steel and transformation temperature. It also calculates important microstructural features of bainite, such as the size of bainitic ferrite platelets and cementite particles, as well as the variation of these features during the transformation (e.g. gradual refinement of α_B platelets due to the gradual enrichment of untransformed austenite in carbon). Finally, the model can be appropriately modified to take into account the grain-size of parent austenite, the later feature being of great interest in multi-phase TRIP steels.

A typical calculation procedure with the model begins by setting the time to t=0. The transformation temperature, T, can be considered as either constant (i.e. isothermal treatment), or a function of time (i.e. continuous-cooling treatment).

A brief description of the mathematical formulation of the model begins with the initial (i.e. at t=0) overall (i.e. primary and autocatalytic) nucleation-rate density of bainitic ferrite (α_B) platelets:

$$I_o^{\alpha_B} = (1+\beta \cdot f_o^{\alpha_B}) \cdot I_{o,pr}^{\alpha_B} \qquad (in \;\; m^{-3}\sec^{-1}) \qquad \textbf{(25)}$$

$f^{\alpha B}$ is the vol. fraction and $I_{\alpha B,pr}$ the *primary* nucleation-rate density of bainitic ferrite, both functions of time. β is a constant accounting for the contribution of *autocatalytic* nucleation during the transformation.

The initial primary nucleation-rate density is given by nucleation theory:

$$I_{o,pr}^{\alpha_B} = N_o \cdot \frac{kT}{h} \cdot \exp\left(-\frac{Q_C^{\gamma}}{RT}\right) \cdot \exp\left(-\frac{\Delta G_{\gamma\to\alpha_B,o}^{*}}{RT}\right) \quad (in \ \ m^{-3}\sec^{-1}) \tag{26}$$

where $Q_{C,\gamma}$ represents the activation energy for carbon diffusion in austenite, ΔG^* the activation energy for ferrite nucleation *in paraequilibrium* with parent austenite and N_o the initial nucleation-site density for ferrite. Constants k, h and R have their usual meanings.

The activation energy, ΔG^*, is a function of thermodynamic driving-force and surface energy:

$$\Delta G_{\gamma\to\alpha_B,o}^{*} = \frac{16\pi \cdot (\sigma^{\alpha/\gamma})^3}{3\left(\Delta G_{v,o}^{\gamma\to\alpha}\right)^2} \cdot N_A - \left[3.637 \cdot (T - 273.18) - 2540\right] \qquad (in \ \ J/mol) \tag{27}$$

In eq. **(27)**, N_A is the Avogadro number, $\sigma^{\alpha/\gamma}$ the ferrite/austenite interfacial energy and ΔG_v the initial thermodynamic driving-force, per unit volume, for the nucleation of ferrite in paraequilibrium with austenite. The latter parameter is a strong function of chemical composition and, thus, will decrease with time, as parent austenite becomes gradually enriched in carbon during the transformation.

By definition, ΔG_v is given by dividing the molar thermodynamic driving-force for ferrite nucleation in paraequilibrium with austenite, ΔG_n, by the molar volume of the product phase (i.e. ferrite), $V_{m,\alpha}$:

$$\Delta G_{v,o}^{\gamma\to\alpha} = \frac{\Delta G_{n,o}^{\gamma\to\alpha}}{V_m^{\alpha}} \tag{28}$$

A schematic depiction of ΔG_n is given in the G-x diagram of Figure 3.2, showing the thermodynamic driving-force necessary for the nucleation of ferrite of *paraequilibrium composition* with respect to parent austenite.

Calculation of the thermodynamic driving-forces under paraequilibrium conditions has been implemented, through appropriate modification of the related thermodynamic databases integrated in Thermo-Calc software.

The vol. fraction of bainitic ferrite is calculated at the end of each time increment, by first determining the number of platelets that nucleated within this time interval. This is done by employing eq. **(25)** to **(28)**. Each individual platelet is considered to have a volume:

$$v_{\alpha_B,1} = L_{\alpha_B,1} \cdot W_{\alpha_B,1} \cdot s_{\alpha_B,1} \tag{29}$$

with L, W and s being the length, width and thickness of each platelet, respectively. The spatial dimensions of each individual platelet will vary with time, since they depend on the mechanical strength of surrounding austenite, within which they grow. The yield strength of austenite increases during the transformation, mainly due to carbon enrichment, and can be calculated by the following empirical expression:

$$S_{\gamma,o} = [1 - 0.26\times10^{-2}\cdot(T-298) + 0.47\times10^{-5}\cdot(T-298)^2 - \\ - 0.326\times10^{-8}\cdot(T-298)^3]\cdot 15.4\cdot(3.6 + 23\bar{w}^{\gamma}_{C,o} + 1.3w_{Si} + 0.65w_{Mn}) \quad (in\ MPa) \tag{30}$$

The dimensions of the platelets can subsequently be calculated by the following empirical equations:

$$W_{\alpha_B,o} = \left[0.478 + 1.2\times10^{-4}T + 1.25\times10^{-4}\left(T - \Delta G^{\gamma\to a}_{n,o}\right) - 2.2\times10^{-3}S_{\gamma,o}\right]\cdot10^{-6} \quad (in\ m)$$
$$L_{\alpha_B,o} = 6W_{\alpha_B,o}$$
$$s_{\alpha_B,o} = 0.12W_{\alpha_B,o} \tag{31}$$

Once the nucleation-rate density (i.e. the number of platelets formed per unit time and volume) and the volume each individual platelet have been calculated for the running time increment, the *extended* vol. fraction increment of bainitic ferrite, which formed within this time increment, is given by:

$$\Delta f^{\alpha_B,ext}_{0-1} = I^{\alpha_B}_o \cdot v_{\alpha_B,o}\cdot\Delta t \tag{32}$$

Subsequently, the corresponding *real* vol. fraction increment of bainitic ferrite is calculated:

$$\Delta f^{\alpha_B}_{0-1} = \Delta f^{\alpha_B,ext}_{0-1}\cdot\left(1 - f^{\alpha_B}_o - f^{\theta/\gamma}_o - f^{\theta/\alpha}_o\right) \tag{33}$$

where the f's denote the vol. fractions of the respective phases that had already formed until that moment.

The new value of the vol. fraction of bainitic ferrite is then given by:

$$f^{\alpha_B}_1 = f^{\alpha_B}_o + \Delta f^{\alpha_B}_{0-1} \tag{34}$$

A similar approach is used for the calculation of the vol. fraction of cementite, which may precipitate either within ferrite or in austenite during the transformation. For example, the nucleation-rate density of cementite in austenite, under paraequilibrium conditions, is given by:

$$I_o^{\theta/\gamma} = N_o^{\theta/\gamma} \cdot \frac{kT}{h} \cdot \exp\left(-\frac{Q_C^{\gamma}}{RT}\right) \cdot \exp\left(-\frac{\Delta G^{*}_{\gamma\to\theta,o}}{RT}\right) \quad (in\ \ m^{-3}\sec^{-1}) \qquad \textbf{(35)}$$

Similarly to eq. **(26)**, $Q_{C,\gamma}$ in eq. **(35)** represents the activation energy for carbon diffusion in austenite, ΔG^* the activation energy for cementite nucleation *in paraequilibrium* with parent austenite and $N_{o,\theta/\gamma}$ the initial nucleation-site density for cementite.

The *extended* vol. fraction increment of cementite precipitated in austenite, which formed within the time increment under consideration, is then given by:

$$\Delta f_{0-1}^{\theta/\gamma,ext} = \frac{25\pi}{4} I_o^{\theta/\gamma} \cdot \Delta t \cdot \left[\frac{\left(\bar{x}_{C,o}^{\gamma} - x_{C,o}^{\gamma/\theta}\right)^2 \cdot D_C^{\gamma} \cdot \Delta t}{\left(x_{C,o}^{\theta/\gamma} - \bar{x}_{C,o}^{\gamma}\right) \cdot \left(x_{C,o}^{\theta/\gamma} - x_{C,o}^{\gamma/\theta}\right)}\right]^{3/2} \qquad \textbf{(36)}$$

In eq. **(36)** $x^{\gamma/\theta}$ and $x^{\theta/\gamma}$ stand for the paraequilibrium carbon concentrations between cementite and austenite, x^{γ} is the average carbon concentration in parent austenite and D_C the diffusivity of carbon in austenite.

The corresponding *real* vol. fraction increment of cementite in austenite is calculated by:

$$\Delta f_{0-1}^{\theta/\gamma} = \Delta f_{0-1}^{\theta/\gamma,ext} \cdot \left(1 - f_o^{\alpha_B} - f_o^{\theta/\gamma} - f_o^{\theta/\alpha}\right) \qquad \textbf{(37)}$$

and, the overall vol. fraction, up to that moment, is equal to:

$$f_1^{\theta/\gamma} = f_o^{\theta/\gamma} + \Delta f_{0-1}^{\theta/\gamma} \qquad \textbf{(38)}$$

A corresponding set of equations is used for the calculation of cementite precipitation in ferrite.

Through the above described calculational process, which is repeated with updated parameter values for every new time increment, the vol. fractions of the involved phases are calculated with respect to time. This way the kinetics of the bainitic transformation is quantitatively determined. In addition, results are obtained regarding the evolution of the chemical composition of the phases and the microstructural features of ferrite platelets and cementite particles.

4.5.1 Calculation Procedure

The major steps of the algorithm are listed below:

1. Transformation temperature (T) and time-step (Δt) for the calculations are set.
2. The C-contents of ferrite ($x_{C,o}^{\alpha/\gamma}$) and austenite ($x_{C,o}^{\gamma/\alpha}$) in paraequilibrium are calculated.
3. The thermodynamic driving-force for nucleation of ferrite ($\Delta G_{n,o}^{\gamma\to\alpha}$) in paraequilibrium with austenite is calculated.
4. Values are set for the ferrite/austenite ($\sigma^{\alpha/\gamma}$), cementite/austenite ($\sigma^{\theta/\gamma}$) and cementite/ferrite ($\sigma^{\theta/\alpha}$) interfacial energies and the corresponding nucleation-site densities (N_o, $N_o^{\theta/\gamma}$, $N_o^{\theta/\alpha}$).
5. The activation energy for paraequilibrium nucleation of ferrite in austenite is calculated:

$$\Delta G^{*}_{\gamma\to\alpha_B,o} = \frac{16\pi\cdot(\sigma^{\alpha/\gamma})^3}{3\left(\Delta G_{v,o}^{\gamma\to\alpha}\right)^2}\cdot N_A - \left[3.637\cdot\left(T-273.18\right)-2540\right]$$

6. The initial primary nucleation-rate density of ferrite is calculated: $I_{o,pr}^{\alpha_B} = N_o\cdot\frac{kT}{h}\cdot\exp\left(-\frac{Q_C^{\gamma}}{RT}\right)\cdot\exp\left(-\frac{\Delta G^{*}_{\gamma\to\alpha_B,o}}{RT}\right)$ The initial overall nucleation-rate density of ferrite is calculated: $I_o^{\alpha_B} = (1+\beta\cdot f_o^{\alpha_B})\cdot I_{o,pr}^{\alpha_B}$
8. The initial yield-stress of austenite is calculated:

$$S_{\gamma,o} = [1-0.26\times10^{-2}\cdot(T-298)+0.47\times10^{-5}\cdot(T-298)^2 - \\ -0.326\times10^{-8}\cdot(T-298)^3]\cdot15.4\cdot(3.6+23\overline{w}_{C,o}^{\gamma}+1.3w_{Si}+0.65w_{Mn})$$

9. The size of the bainitic ferrite platelet is calculated: $W_{\alpha_B,o} = \left[0.478+1.2\times10^{-4}T+1.25\times10^{-4}\left(T-\Delta G_{n,o}^{\gamma\to a}\right)-2.2\times10^{-3}S_{\gamma,o}\right]\cdot10^{-6}$
10. The C-contents of cementite ($x_{C,o}^{\theta/\gamma}$) and austenite ($x_{C,o}^{\gamma/\theta}$) in para-equilibrium are calculated.
11. The thermodynamic driving-force for nucleation of cementite ($\Delta G_{n,o}^{\gamma\to\theta}$) in paraequilibrium with austenite is calculated.

12. The activation energy for paraequilibrium nucleation of cementite in austenite is calculated: $\Delta G^{*}_{\gamma\to\theta,o} = \dfrac{16\pi\cdot(\sigma^{\theta/\gamma})^{3}}{3\left(\Delta G^{\gamma\to\theta}_{v,o}\right)^{2}}\cdot N_{A}$
13. The initial nucleation-rate density of cementite in austenite is calculated: $I^{\theta/\gamma}_{o} = N^{\theta/\gamma}_{o}\cdot\dfrac{kT}{h}\cdot\exp\left(-\dfrac{Q^{\gamma}_{C}}{RT}\right)\cdot\exp\left(-\dfrac{\Delta G^{*}_{\gamma\to\theta,o}}{RT}\right)$
14. The C-contents of cementite ($x^{\theta/\alpha}_{C,o}$) and ferrite ($x^{\alpha/\theta}_{C,o}$) in paraequilibrium are calculated.
15. The thermodynamic driving-force for nucleation of cementite ($\Delta G^{\alpha\to\theta}_{n,o}$) in paraequilibrium with ferrite is calculated.
16. The activation energy for paraequilibrium nucleation of cementite in ferrite is calculated: $\Delta G^{*}_{\alpha\to\theta,o} = \dfrac{16\pi\cdot(\sigma^{\theta/\alpha})^{3}}{3\left(\Delta G^{\alpha\to\theta}_{v,o}\right)^{2}}\cdot N_{A}$
17. The initial nucleation-rate density of cementite in ferrite is calculated: $I^{\theta/\alpha}_{o} = N^{\theta/\alpha}_{o}\cdot\dfrac{kT}{h}\cdot\exp\left(-\dfrac{Q^{\alpha}_{C}}{RT}\right)\cdot\exp\left(-\dfrac{\Delta G^{*}_{\alpha\to\theta,o}}{RT}\right)$
18. Time is increased by Δt.
19. The extended vol. fraction increment of bainitic ferrite is calculated: $\Delta f^{\alpha_B,ext}_{0-1} = I^{\alpha_B}_{o}\cdot v_{\alpha_B,o}\cdot\Delta t$
20. The real vol. fraction increment of bainitic ferrite is calculated: $\Delta f^{\alpha_B}_{0-1} = \Delta f^{\alpha_B,ext}_{0-1}\cdot\left(1-f^{\alpha_B}_{o}-f^{\theta/\gamma}_{o}-f^{\theta/\alpha}_{o}\right)$
21. The vol. fraction of bainitic ferrite at time t_1 is calculated: $f^{\alpha_B}_{1} = f^{\alpha_B}_{o}+\Delta f^{\alpha_B}_{0-1}$
22. The extended vol. fraction increment of cementite in austenite is calculated: $\Delta f^{\theta/\gamma,ext}_{0-1} = \dfrac{25\pi}{4}I^{\theta/\gamma}_{o}\cdot\Delta t\cdot\left[\dfrac{\left(\overline{x}^{\gamma}_{C,o}-x^{\gamma/\theta}_{C,o}\right)^{2}\cdot D^{\gamma}_{C}\cdot\Delta t}{\left(x^{\theta/\gamma}_{C,o}-\overline{x}^{\gamma}_{C,o}\right)\cdot\left(x^{\theta/\gamma}_{C,o}-x^{\gamma/\theta}_{C,o}\right)}\right]^{3/2}$
23. The real vol. fraction increment of cementite in austenite is calculated: $\Delta f^{\theta/\gamma}_{0-1} = \Delta f^{\theta/\gamma,ext}_{0-1}\cdot\left(1-f^{\alpha_B}_{o}-f^{\theta/\gamma}_{o}-f^{\theta/\alpha}_{o}\right)$
24. The vol. fraction of cementite in austenite at time t_1 is calculated: $f^{\theta/\gamma}_{1} = f^{\theta/\gamma}_{o}+\Delta f^{\theta/\gamma}_{0-1}$

25. The extended vol. fraction increment of cementite in ferrite is calculated:

$$\Delta f_{0-1}^{\theta/\alpha,ext} = \frac{25\pi}{4} I_o^{\theta/\alpha} \cdot \Delta t \cdot \left[\frac{\left(\overline{x}_{C,o}^{\alpha} - x_{C,o}^{\alpha/\theta} \right)^2 \cdot D_C^{\alpha} \cdot \Delta t}{\left(x_{C,o}^{\theta/\alpha} - \overline{x}_{C,o}^{\alpha} \right) \cdot \left(x_{C,o}^{\theta/\alpha} - x_{C,o}^{\alpha/\theta} \right)} \right]^{3/2}$$

26. The real vol. fraction increment of cementite in ferrite is calculated:

$$\Delta f_{0-1}^{\theta/\alpha} = \Delta f_{0-1}^{\theta/\alpha,ext} \cdot \left(1 - f_o^{\alpha_B} - f_o^{\theta/\gamma} - f_o^{\theta/\alpha} \right)$$

27. The vol. fraction of cementite in ferrite at time t_1 is calculated: $f_1^{\theta/\alpha} = f_o^{\theta/\alpha} + \Delta f_{0-1}^{\theta/\alpha}$

Important notice: As the transformation proceeds in time, new cementite particles will nucleate and grow during every time-step, but also already existing (i.e. formed in previous timesteps) cementite particles will continue to grow. In order to take these processes simultaneously into account, it can be shown that the vol. fraction of cementite at time t_n is given by:

$$f_n^{\theta/\gamma} = f_{n-1}^{\theta/\gamma} + \frac{25\pi}{4} \cdot \sum_{i=0}^{n} \left(I_i^{\theta/\gamma} \cdot \Delta t_i \right) \cdot \left[\frac{\left(\overline{x}_{C,n-1}^{\gamma} - x_{C,n-1}^{\gamma/\theta} \right)^2 \cdot D_C^{\gamma} \cdot \Delta t_{n-1}}{\left(x_{C,n-1}^{\theta/\gamma} - \overline{x}_{C,n-1}^{\gamma} \right) \cdot \left(x_{C,n-1}^{\theta/\gamma} - x_{C,n-1}^{\gamma/\theta} \right)} \right]^{3/2} \cdot \left(1 - f_{n-1}^{\alpha_B} - f_{n-1}^{\theta/\gamma} - f_{n-1}^{\theta/\alpha} \right)$$

for cementite in austenite, and by:

$$f_n^{\theta/\alpha} = f_{n-1}^{\theta/\alpha} + \frac{25\pi}{4} \cdot \sum_{i=0}^{n} \left(I_i^{\theta/\alpha} \cdot \Delta t_i \right) \cdot \left[\frac{\left(\overline{x}_{C,n-1}^{\alpha} - x_{C,n-1}^{\alpha/\theta} \right)^2 \cdot D_C^{\alpha} \cdot \Delta t_{n-1}}{\left(x_{C,n-1}^{\theta/\alpha} - \overline{x}_{C,n-1}^{\alpha} \right) \cdot \left(x_{C,n-1}^{\theta/\alpha} - x_{C,n-1}^{\alpha/\theta} \right)} \right]^{3/2} \cdot \left(1 - f_{n-1}^{\alpha_B} - f_{n-1}^{\theta/\gamma} - f_{n-1}^{\theta/\alpha} \right)$$

for cementite in ferrite.

28. The average mole-fraction of C in austenite is updated: $\overline{x}_{C,1}^{\gamma} = \frac{\overline{x}_{C,o}^{\gamma} - \left(f_1^{\alpha_B} \cdot x_{C,o}^{\alpha/\gamma} + f_1^{\theta/\gamma} \cdot x_{C,o}^{\theta/\gamma} \right)}{1 - f_1^{\alpha_B} - f_1^{\theta/\gamma}}$

29. The average mole-fraction of C in ferrite is updated: $\overline{x}_{C,1}^{\alpha} = \frac{\overline{x}_{C,o}^{\alpha} - f_1^{\alpha/\gamma} \cdot x_{C,o}^{\theta/\alpha}}{1 - f_1^{\theta/\alpha}}$

30. The new values of activation energies for paraequilibrium nucleation are calculated.

31. The procedure is repeated for the next timestep.

5 Results

In the following chapter the results of this thesis will be presented.

5.1 Thermodynamic results

Thermodynamic calculations were performed using THERMOCALC software and the TCFe-6 thermodynamic database. In Figure 5.1 the phase diagrams of TRIP-Al steel, is presented. The two phase region of austenite and ferrite for the intercritical annealing process is evident and denoted as α+γ. Thermodynamic simulations were performed for intercritical annealing at 830^{o}C and 850^{o}C and the results are presented in Table. 2. In the case of TRIP-Al it was estimated that 50% γ will form at 830^{o}C and 56% γ will form at 850^{o}C. Element compositions of γ is also presented in Table. 2.

Thermodynamic calculations were also performed for the temperatures at which preexisting perlite dissolves into austenite, these values were used as an input for the kinetic calculations in DICRTA and are presented in Table 3.

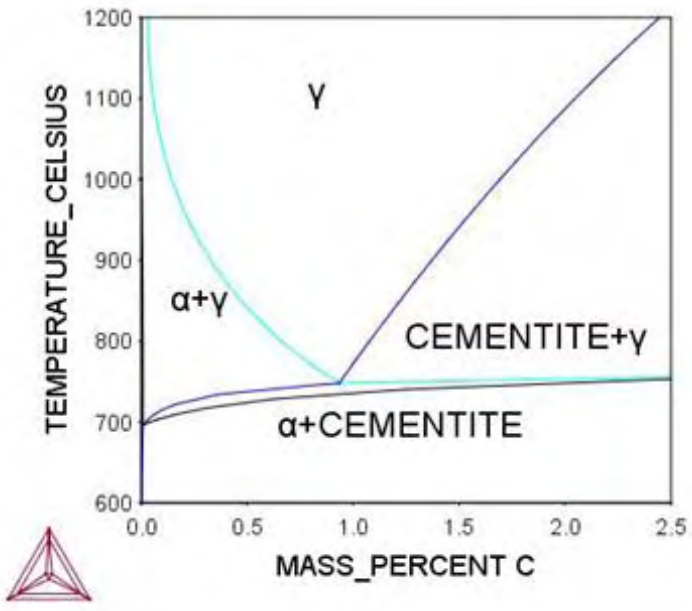

Figure 5.1 Phase diagrams of (a) Al containing TRIP steel and (b) DP steel

Table 4 Thermodynamic calculations with THERMOCALC for intercritical annealing temperature at 830°C.

Steel	Intercritical Annealing Temp	Austenite (%)	C wt%	Mn wt%	Al wt%	Si Wt%
TRIP-Al	830 °C	50	0.42	2.19	1.7	0.11
	850 °C	56.8	0.37	2.05	1.1	0.12

Table 5 Thermodynamic calculations at temperature were perlite dissolves.

Steel	Calc. Temp	Austenite (%)	C Wt%	Mn Wt%	Al Wt%	Si Wt%
TRIP-Al	726.30°C	26.3	0.8	3.47	0.91	0.1

5.2 Kinetic results

The volume fraction of austenite versus temperature is represented in Figure 5.2 (a), while the volume fraction of austenite versus time in Figure 5.2 (b). The axis of time in the second case is on logarithmic scale. The calculations were performed for the same heating and cooling rate of 1 Kelvin/sec. The starting temperature of the heating process is at 730°C. The heating treatment until the intercritical temperature of the 830°C is reached, takes place in 100 sec. It is clearly noticeable that there is a rapid development of austenite at the beginning of the heating process. Just in the first second, around 20% of austenite has formed. This is due to the partitioning of carbon, as it is the most easily diffusionable element of the system (Non Partitioning Local Equilibrium). At the end of heating 42% of austenite is formed. Afterwards, the isothermal treatment takes place at 830°C and for 300 sec and austenite forms at the expense of ferrite, reaching the total volume fraction of 56%. From the onset of cooling the amount of austenite decreases and the region shrinks as the temperature drops further.

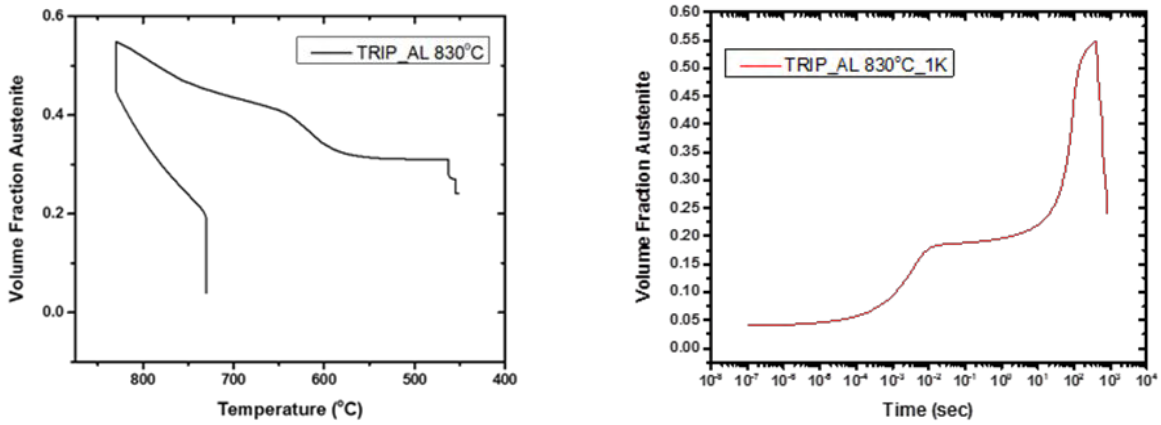

(a) (b)

Figure 5.2 Volume fraction of austenite (a) versus temperature and (b) versus time

5.2.1 Carbon partitioning

The diagrams below represent the weight percent of carbon with respect to distance. On the first two diagrams (Figure 5.3 (a) and (b)) the carbon profile during heating and the isothermal process is depicted, respectively. Each line on the graphs represents a different time during the treatment. In Figure 5.3 (a) the black profile represents the initial composition of the material as this is calculated from THERMOCALC. As the heating process begins carbon instantly, diffuses from ferrite into austenite, causing the enrichment of the austenite region. From that point on, as the process evolves the austenite region increases. At the end of the isothermal process a slice of austenite forms and it is more depleted in carbon with respect to the preexisting austenite. Partitioning of C during the cooling section of the treatment is presented in Figure 5.3c versus temperature. From the on start of cooling the amount of austenite decreases, while the carbon maintains the same profile acquired at the termination of intercritical annealing step, with the exception of a small region near the interface which gets enriched. As the cooling proceeds to lower temperatures the austenite region shrinks further and the slice near the interface becomes thinner and more enriched in C.

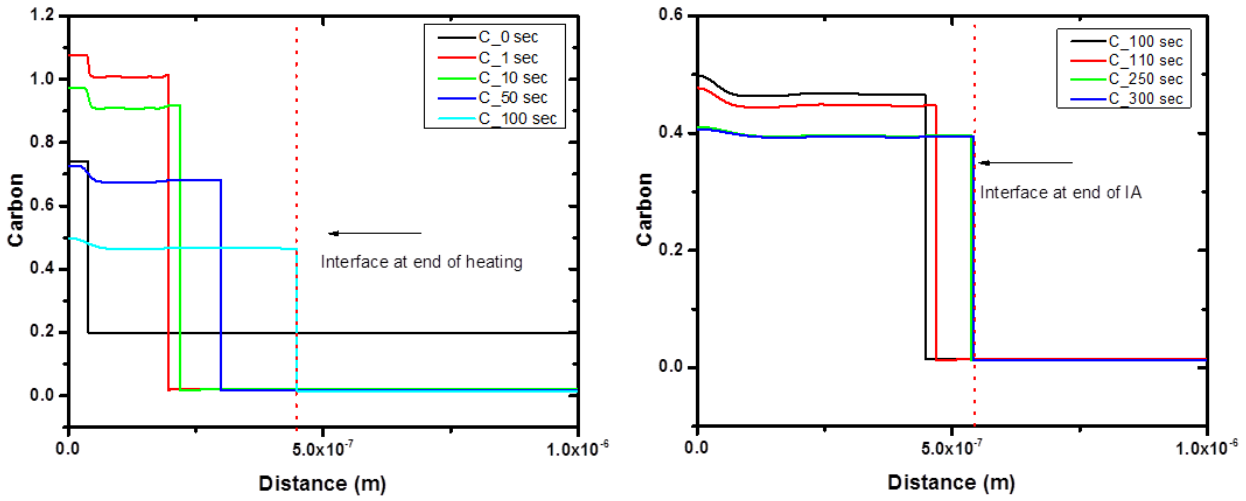

(a) (b)

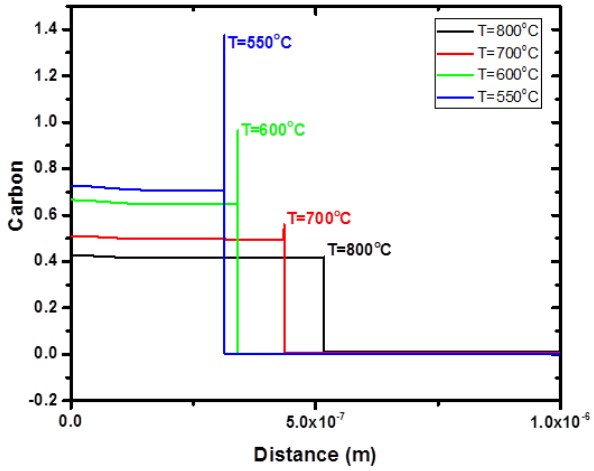

(c)

Figure 5.3 Partitioning of C during (a) heating, (b) isothermal , (c) cooling process

5.2.2 Manganese partition

Partitioning of Mn is presented in Figure 5.4. The interface of austenite at the end of heating in Figure 5.4 (a) and at the end of isothermal on Figure 5.4 (b) is indicated by a dotted red line and arrow. The new austenite formed is very poor in Mn as it inherits the Mn composition from preexisting ferrite. In the intercritical section the austenite region continues to increases and the Mn composition along it is getting smoother. Partitioning of Mn during the cooling process is

presented in Figure 5.4 (c) for several cooling temperatures. Mn maintains the same profile acquired at the termination of intercritical annealing, but due to the low diffusivity a small region inside austenite at the interface gets enriched in Mn.

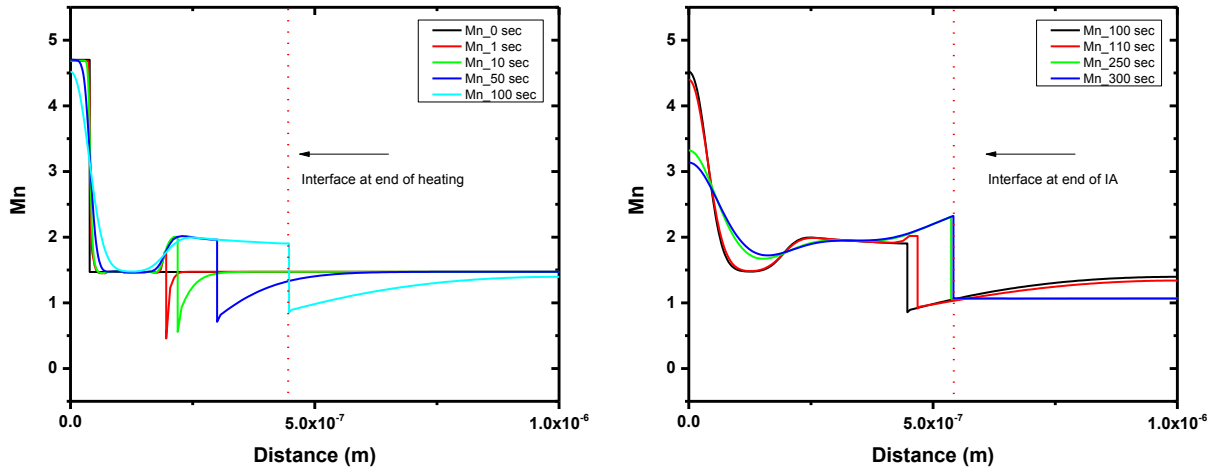

(a) (b)

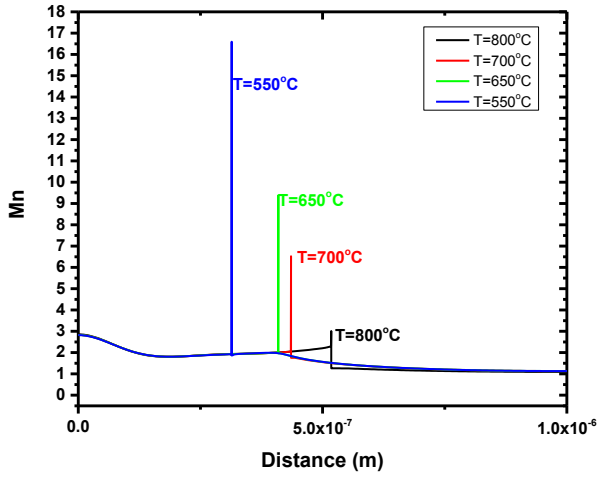

(c)

Figure 5.4 Partitioning of Mn during (a) heating, (b) isothermal, (c) cooling process

5.2.3 Aluminum partitioning

Partitioning of Al is presented in Figure 5.5. Heating and isothermal treatment versus time is presented in graphs Figure 5.5 (a) and (b) respectively. The interface of austenite at the end of heating and isothermal is indicated by a red dotted line and arrow. The new austenite formed on these cases is enriched in Al as it inherits the Al composition from preexisting ferrite. From the graphs below it is evident that Al tends to enrich the ferrite region. Partitioning of Al during the cooling section of the process is presented in Figure 5.5 c for several cooling temperatures. Al maintains the same profile acquired at the termination of intercritical annealing, with the exception a small region at the interface which gets depleted of Al.

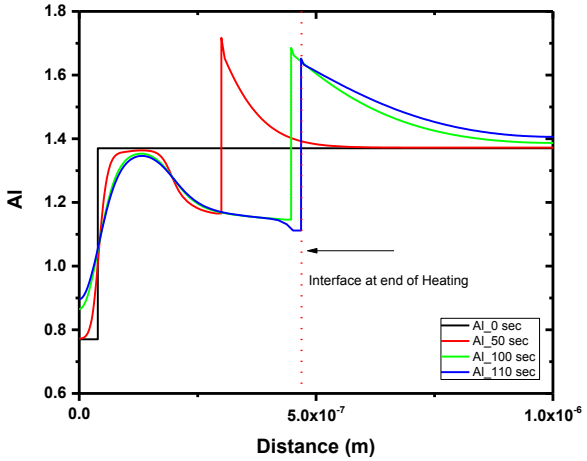

(a)

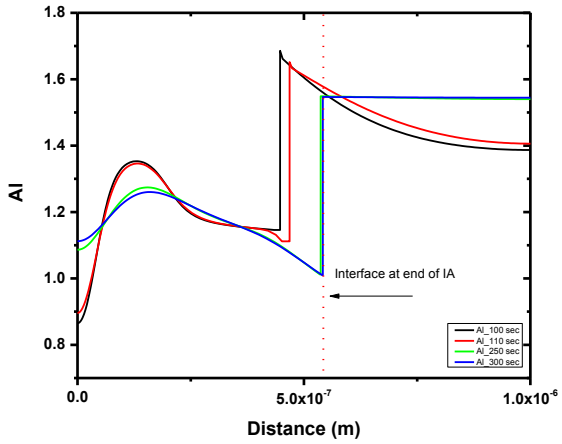

(b)

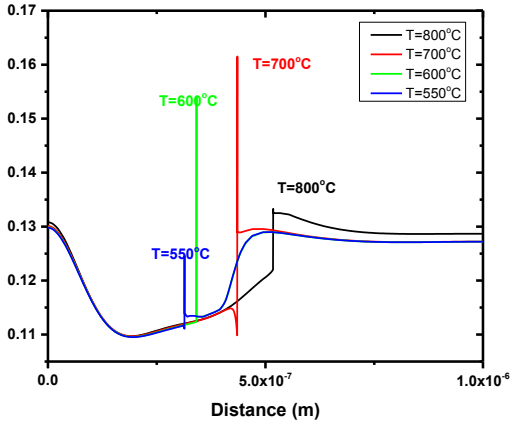

(c)

Figure 5.5 Partitioning of Al during (a) heating, (b) isothermal , (c) cooling process

5.3 Effect of different heating and cooling

In Figure 5.6 the volume fraction of austenite for different rates of heating and cooling, is depicted. Table 6 below presents the corresponding times for every section of the process.

Every different colored line represents a different rate. The faster the rate is, the less austenite is formed during the heating process, this is because it takes less time to reach the intercritical annealing temperature (830^{o}C). Meanwhile, even though, in every case the isothermal process duration is same (300 sec), the percentage of austenite that is formed is not the same. From Figure 5.6 below it is observed that the faster the rate is, the more austenite forms, in the isothermal section of the treatment. Even though the amount of austenite during the heating process, for the faster rate, is less than the others, it appears that at the end of the isothermal that situation has reversed. Below (Table 7) the amount of austenite formed at the end of heating and isothermal is provided, as well as the total amount of austenite for every different rate.

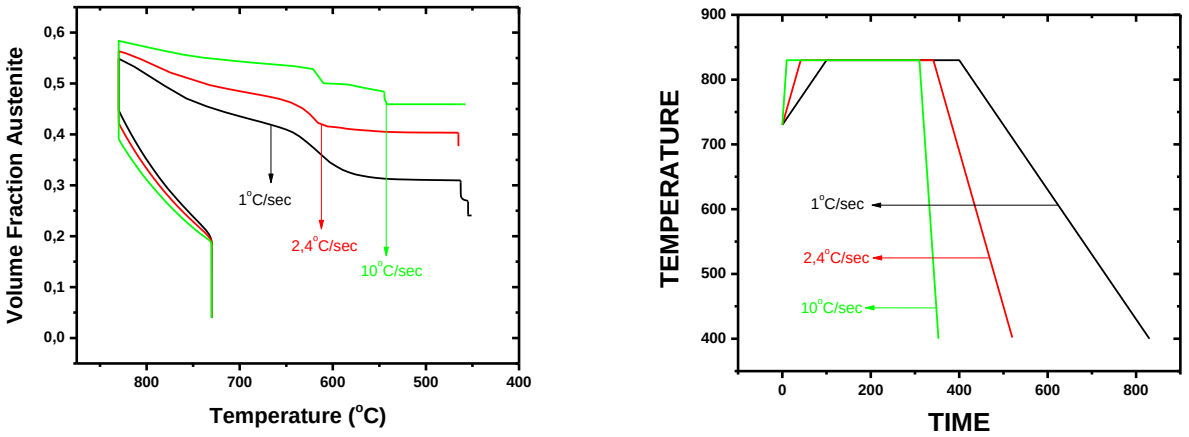

(a) (b)

Figure 5.6 Volume fraction of austenite (a) versus temperature for different rates, and (b) thermal process

Table 6 Time boundaries for different rates heating and cooling rates

	TIMES BOUNDARIES (seconds)						
Heating Rate (K/sec)	HEATING		ISOTHERMAL		COOLING		
	start	end	start	end	start	end	cooling constant (β)
0.001	0	100000	100000	100300	100300	930300	1203.45
1	0	100	100	400	400	1230	1503.15
2.4	0	41.66667	41.666667	341.6667	341.6667	687.5	1923.15
5	0	20	20	320	320	486	2703.15
10	0	10	10	310	310	393	4203.15
100	0	1	1	301	301	309.3	31203.15

Table 7 Percentage of austenite at the end of heating and isothermal process for different rate

Rates	End of Heating	End of Isothermal
1 (K/sec)	44.74%	54.88%
2.4 (K/sec)	43.34%	56.32%
10 (K/sec)	39.14%	58.36%

After the isothermal process ends the cooling section takes place, where the austenite region shrinks as the temperature drops. On the next chapter we will discuss about the effect of the different rates on the partitioning of elements, and compare them with each other for two different cooling temperatures.

5.3.1 Partitioning of elements at 800°C

Figure 5.7 represents the partitioning of carbon, manganese and aluminum respectively. The temperature which the calculations were performed, is 800 °C, this is right after intercritical annealing at 830°C. As it is noticeable from the charts that the amount of austenite produced is higher as the rate of heating increases. The interface between austenite and ferrite is the sharp vertical line. On the left side of that line is the austenite region and on the right ferrite. The carbon has smooth composition all over austenite. As mentioned before, Mn tends to enrich

austenite and Al ferrite. These profiles will be compared with the corresponding ones at a lower temperature.

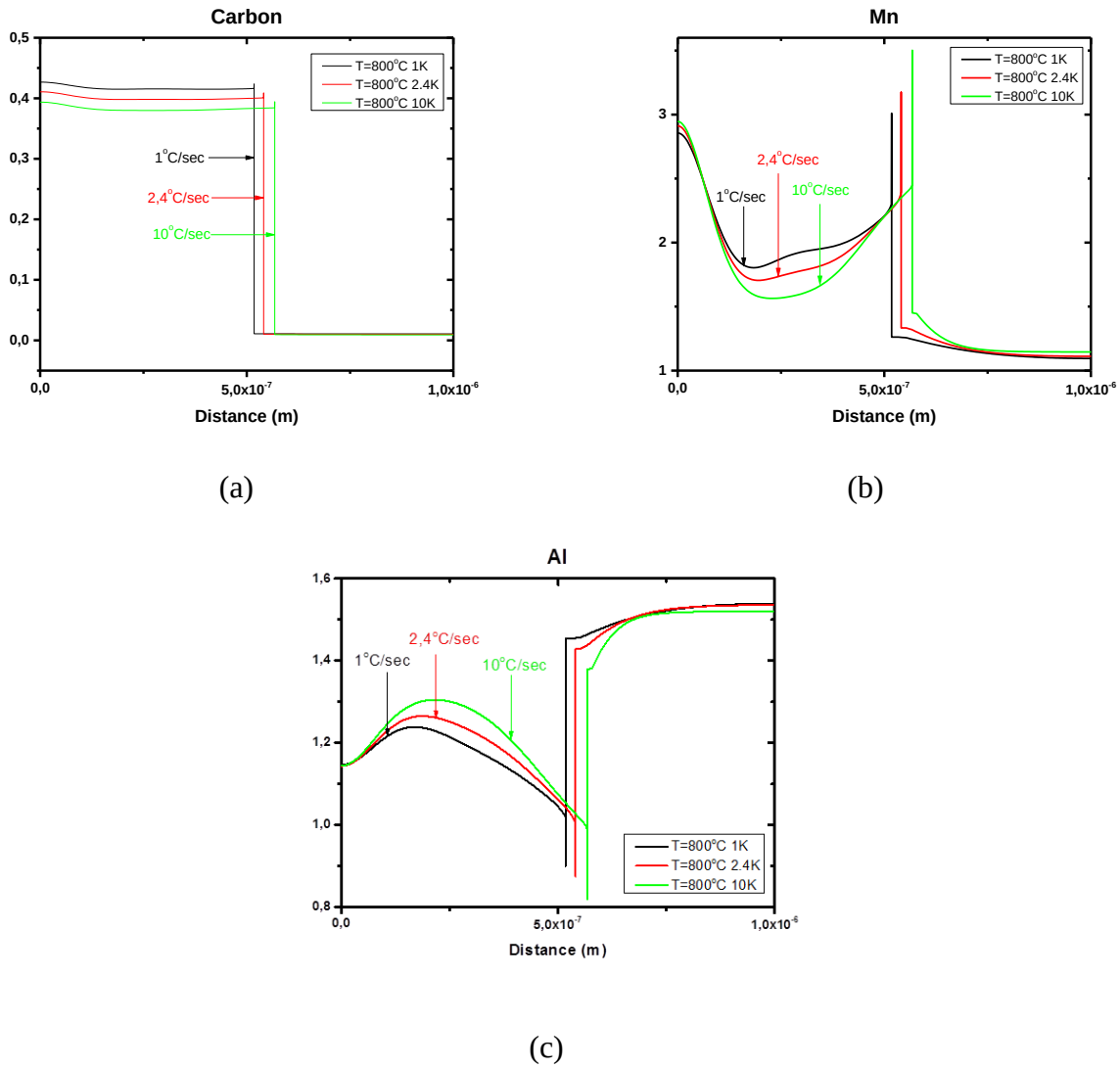

Figure 5.7 Partitioning of elements at 800°C (a) carbon, (b) manganese, (c) aluminum

5.3.2 Partitioning of elements at 500°C

Figure 5.8 shows the partitioning of carbon, manganese and aluminum respectively at 500°C. The reduction of the austenite region is readily detected in all three figures (Figure 5.8 a,b,c). The profiles of the partitioning elements remain similar as at 800°C as the temperature drops. Nevertheless, due to the low diffusivity of Mn and Al there is enrichment of these elements in the

austenite region at the interface. Sharp spikes are observed at the interface, which can reach values up to 20wt % for Mn.

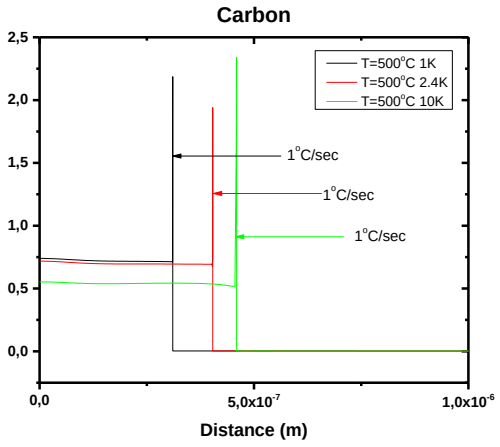

(a)

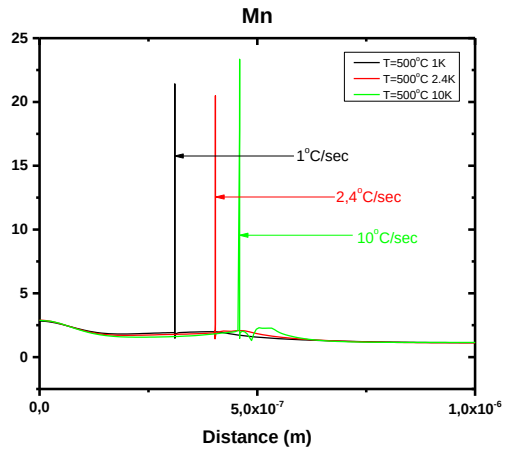

(b)

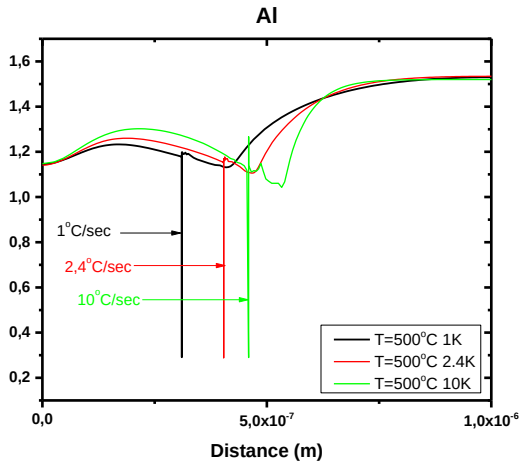

(c)

Figure 5.8 Partitioning of elements at 500°C (a) carbon, (b) manganese and (c) aluminum

5.4 Paraequilibrium results

5.4.1 Zones description

In order to continue into the calculation of the paraequilibrium driving forces, one specific heating rate was chosen, in our case this is 10 Kelvin/sec. Figure 5.9, represents the partitioning

of all the elements for the 10 Kelvin/sec rate. The axis scale was changed in order for the variation in composition at the austenite zone to be clearly observed. Due to Mn partitioning, the austenite region was separated into four smaller zones. Every one of them has different length represented in Figure 5.10. The average value of each zone and each partitioning element was calculated. The results are listed at the Table 8.

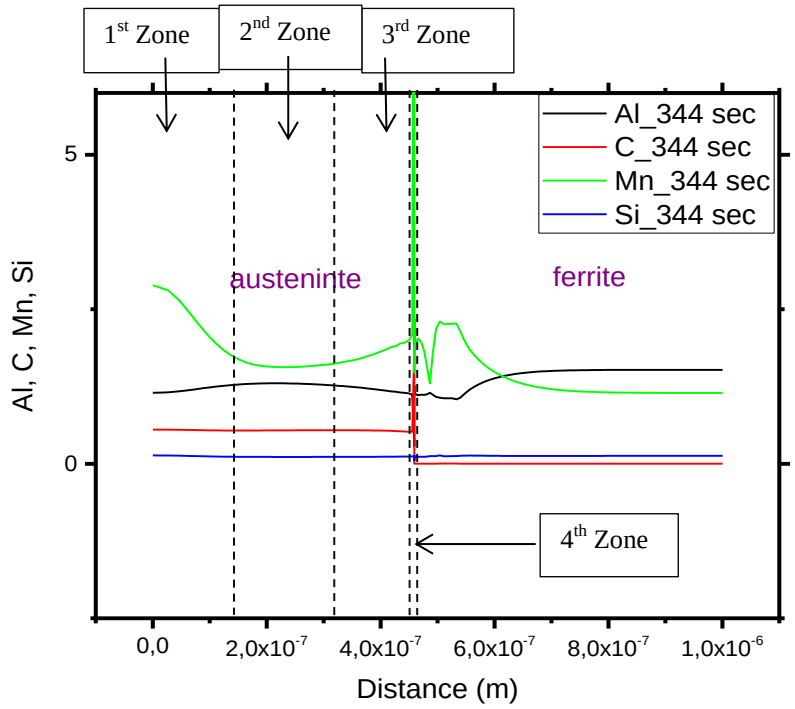

Figure 5.9 Partitioning of elements at 500°C, separation in zones (zoom-in)

1ST ZONE 30.3%	2ND ZONE 42.6%	3RD ZONE 26.4%	4TH ZONE 0.7%

Figure 5.10 Percentage of every zone of austenite region

Each zone has a different composition and range. Each zone was treated as an individual material and calculations performed for each zone independently.

Table 8 Chemical composition of each zone (in % mass)

TRIP Al	C	AI	Mn	Si	Cr	Nb
1st zone	0.5451	1.2062	2.3359	0.1248	0.035	0.001
2nd zone	0.5405	1.2898	1.5959	0.1112	0.035	0.001
3rd zone	0.5322	1.1853	1.8493	0.1144	0.035	0.001
4th zone	2.0987	0.3007	20.57	0.0913	0.035	0.001

5.4.2 Calculation of Driving Forces (ΔG) under paraequilibrium

After the modification of the database the driving forces of the alloy under paraequilibrium conditions were calculated. Examples of the aforementioned thermodynamic calculations are shown in Figure 5.11, which depicts calculated driving-forces for nucleation of bainitic ferrite on paraequilibrium with austenite for TRIP-AL of the 1st Zone, as function of transformation temperature and average carbon-content in austenite.

As shown, the driving-force for nucleation becomes more negative (i.e. the nucleation of ferrite is energetically favored) as the temperature of the transformation decreases. In contrast, as the C-content of austenite increases, the driving-force for paraequilibrium nucleation of ferrite decreases. Thus, during the course of the bainitic transformation, as austenite becomes richer in carbon the tendency of bainitic ferrite to form is gradually reduced. Unless a transformation that will draw carbon out of solid-solution in austenite acts (i.e. cementite precipitation), then the bainitic transformation will cease (‘‘transformation stasis’’) due to the lack of driving-force for the nucleation of more ferrite.

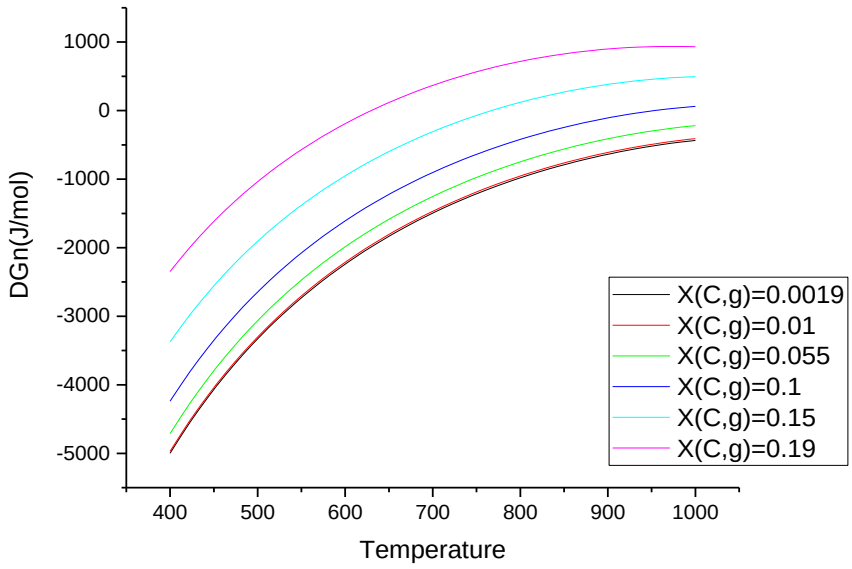

Figure 5.11 Calculated driving-forces for the nucleation of bainitic ferrite in paraequilibrium with austenite for TRIP-Al

The same procedure is followed for the determination of the driving-force for paraequilibrium nucleation of cementite in austenite and ferrite. Figure 5.12 depicts the driving force for the nucleation of cementite in austenite under paraequilibrium conditions, with as function of temperature and C-content of austenite. As shown, the driving force for nucleation decreases with temperature. Furthermore, as the C-content of austenite increases, the driving-force for paraequilibrium nucleation of cementite decreases. During the course of the bainitic transformation and as austenite becomes enriched in carbon the tendency of cementite to precipitate in austenite gradually increases. Increased cementite precipitation draws carbon out of solid-solution from austenite, which in turn favors the formation of more ferrite.

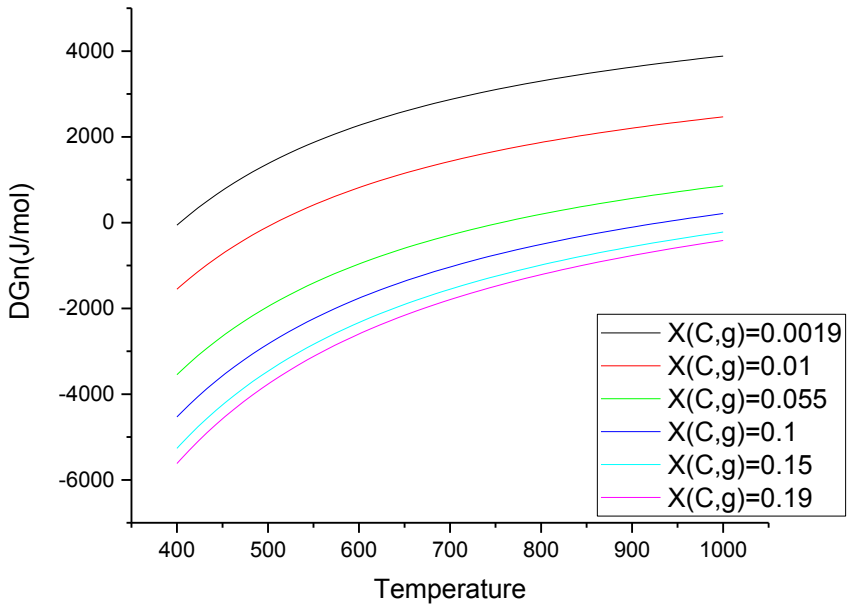

Figure 5.12 Calculated driving-forces for the nucleation of cementite in paraequilibrium with austenite for TRIP steel Al

Σφάλμα! Το αρχείο προέλευσης της αναφοράς δεν βρέθηκε. depicts the driving-force for the nucleation of cementite in ferrite under paraequilibrium conditions, as a function of temperature and C-content of ferrite. As shown, the driving-force for nucleation decreases with temperature. Furthermore, as the C-content of ferrite increases, the driving-force for paraequilibrium nucleation of cementite becomes more negative.

The aforementioned methodology was also applied in order to calculate the C-content of phases in paraequilibrium between them as well as the molar volumes of the product phases, which are also necessary input to the kinetic model.

Figure 5.13 represents the calculated molar volume for the nucleation of ferrite in paraequilibrium with austenite. As the C-contents increases, molar volume for the same value of temperature decreases.

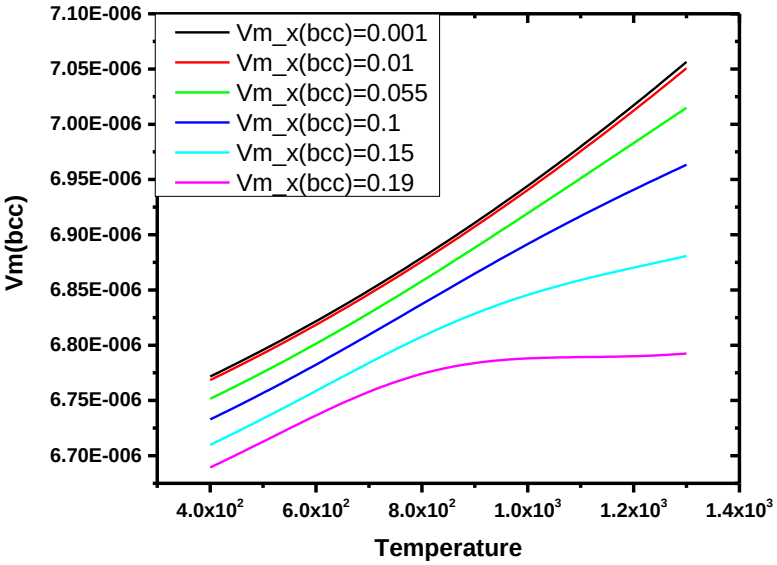

Figure 5.13 Calculated molar volumes for the nucleation of ferrite in paraequilibrium with austenite for TRIP-Al

Figure 5.14 depicts the molar volume for nucleation of cementite in paraequilibrium with ferrite.

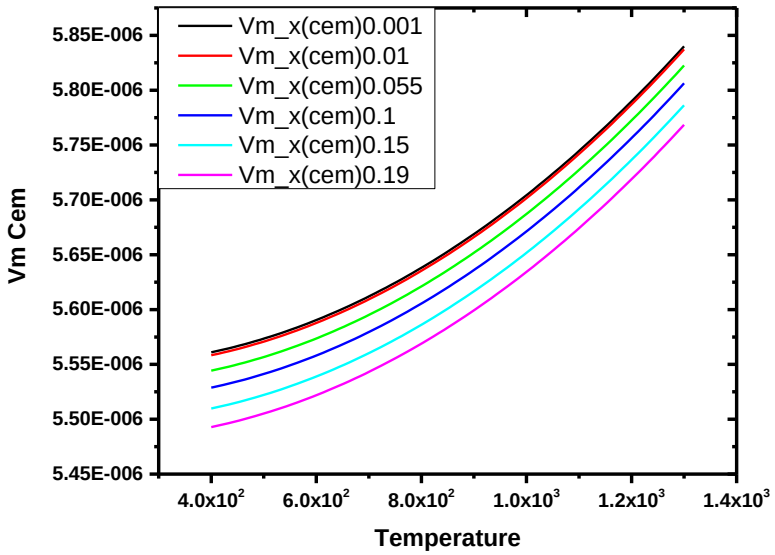

Figure 5.14 Calculated molar volumes for nucleation of cementite in paraequilibrium with ferrite for TRIP-Al

Figure 5.15 represents Carbon content of ferrite in paraequilibrium with cementite.

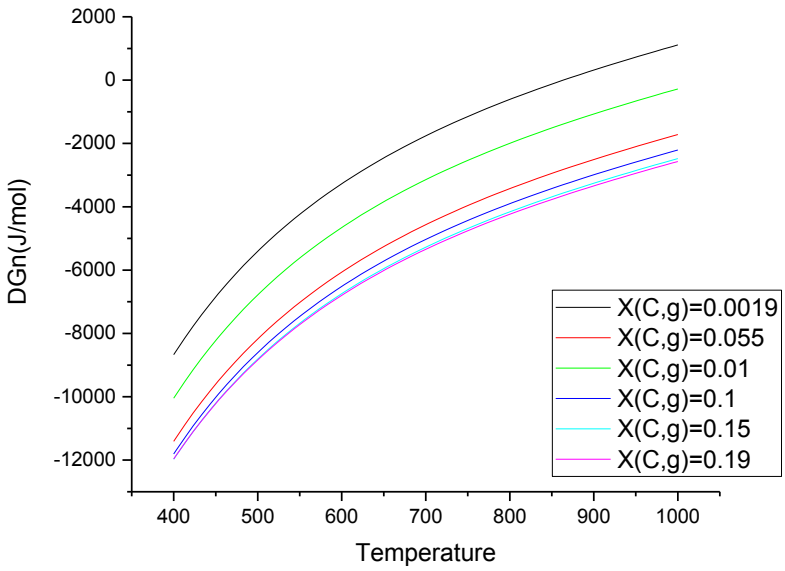

Figure 5.15 Calculated driving-forces for the nucleation of cementite in paraequilibrium with ferrite for TRIP – Al

Figure 5.16 depicts Carbon content of ferrite in paraequillibrium with austenite and Figure 5.17 depicts Carbon content of austenite in paraequilibrium with ferrite for the same amount of carbon moles

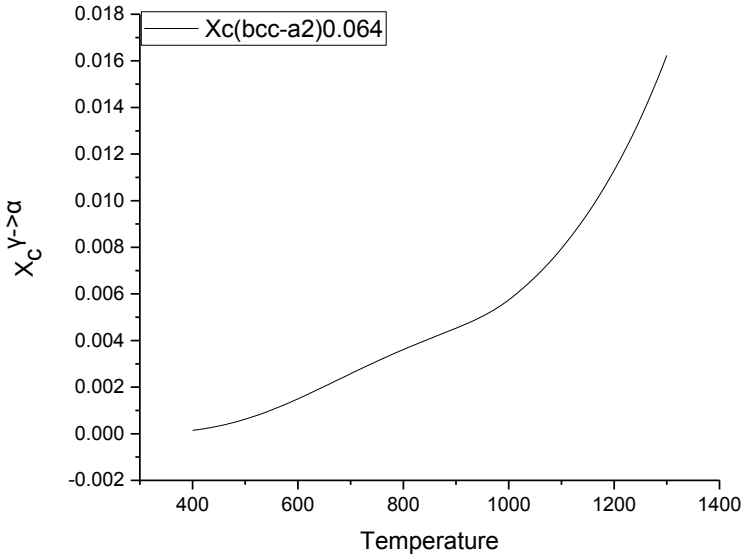

Figure 5.16 Calculated Carbon-content of ferrite in paraequilibrim with austenite for TRIP steel Al

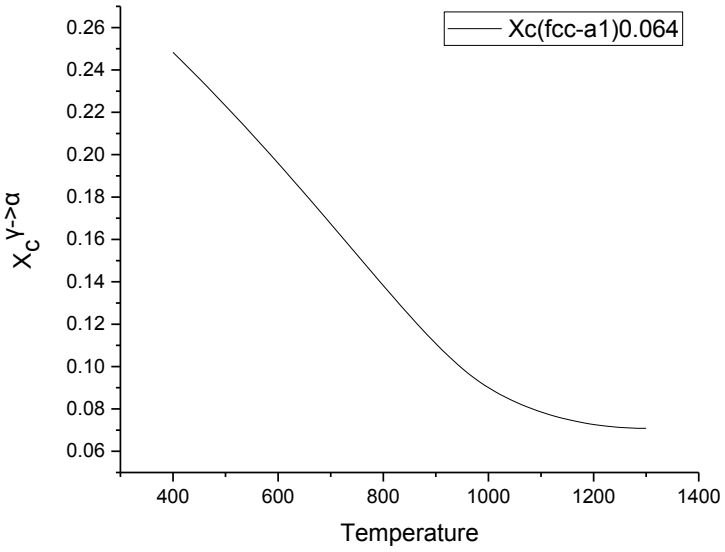

Figure 5.17 Calculated Carbon-content of austenite in paraequilibrim with ferrite for TRIP steel Al

5.4.3 Calculated functions for driving forces

In order to incorporate the calculated paraequilibrium values into the kinetic model they have to be transformed into functions of temperature and C-content, of the form $Z = f(X_C, T)$, where $Z = \Delta G_n^{\gamma\to\theta}$ or $Z = \Delta G_n^{a\to\theta}$ or $Z = \Delta G_n^{\gamma\to\alpha}$.The corresponding functions were evaluated by performing nonlinear curve fitting on the 3D surface (Figure 5.18) created by the calculated data. The paraequilibrium driving-forces for the nucleation of ferrite and cementite in austenite as well as cementeite in ferrite for the case of the TRIP steel Al can be expressed as functions of temperature and C-content by the following equation :

$$\Delta Gn = \frac{Z01 + A01 * T + B01 * (\overline{X_c}) + B02 * (\overline{X_c})^2 + B03 * (\overline{X_c})^3}{1 + A1 * T + A2 * T^2 + A3 * T^3 + B1 * (\overline{X_c}) + B2 * (\overline{X_c})^2}$$

The constants above calculated with the Rational 2D method for every zone at austenite region. Those values depicted at the matrix below.

Table 9 Constants of Driving-forces fitting equations

	1ST ZONE			2ND ZONE			3RD ZONE		
	ΔGn (γ->α)	ΔGn (γ->θ)	ΔGn (α->θ)	ΔGn (γ->α)	ΔGn (γ->θ)	ΔGn (α->θ)	ΔGn (γ->α)	ΔGn (γ->θ)	ΔGn (α->θ)
Z0=	-1.35E+12	1.63E+43	-25217.99506	-1.03E+12	4.28E+43	-1.27E+06	-1.22E+12	2.44E+43	-25439.379
A01=	5.84E+12	-2.36E+44	-6367.33531	3.47E+12	-6.09E+44	-1.98E+06	4.76E+12	-3.52E+44	-6375.4469
B01=	-3.39E+09	-9.93E+40	76.7616	-1.45E+09	-2.59E+41	2110.8247	-2.45E+09	-1.47E+41	77.25538
B02=	8.49E+06	1.69E+38	-0.08213	4.46E+06	4.39E+38	-1.05213	6.57E+06	2.48E+38	-0.08255
B03=	-4211.9344	-5.19E+34	3.06E-05	-2288.0731	-1.37E+35	2.29E-04	-3288.222	-7.70E+34	3.08E-05
A1=	-1.28E+09	1.03E+41	-4.38889	-7.13E+08	2.63E+41	-419.5529	-1.02E+09	1.42E+41	-4.37624
A2=	2.59E+09	-6.53E+41	43.88488	1.09E+09	-1.67E+42	5472.2863	2.06E+09	-8.59E+41	43.76485
A3=	4.02E+09	2.08E+42	-116.50942	5.30E+09	5.35E+42	-14566.229	3.78E+09	2.72E+42	-116.52717
B1=	745869.7096	-6.73E+36	-0.00108	480007.13	-1.74E+37	0.21441	625695.4	-9.80E+36	-0.00107
B2=	234.28412	1.87E+34	5.03E-07	90.597	4.83E+34	-1.26E-04	166.50048	2.75E+34	4.93E-07

For examples, $\Delta G_n^{\gamma\to\alpha_B}$ stands for the nucleation of bainitic ferrite in paraequilibrium with austenite, $\Delta G_n^{\gamma\to\theta}$ for the nucleation of cementite in paraequilibrium with austenite and $\Delta G_n^{\alpha_B\to\theta}$ for the nucleation of cementite in paraequilibrium with bainitic ferrite (all in J/mol). $\overline{X}_C^{\gamma}$ is the average C-content in austenite, $\overline{X}_C^{\alpha}$ the average C-content in bainitic ferrite (both expressed as mole-fractions) and T the absolute transformation temperature (in degrees K).

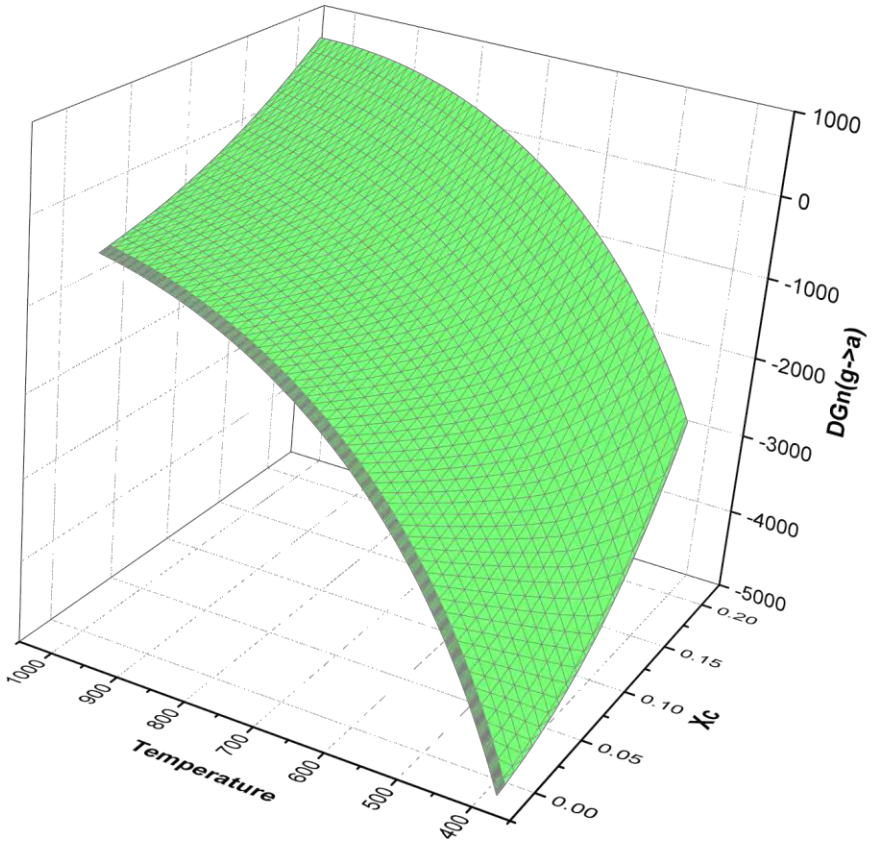

Figure 5.18 3D representation of $\Delta G_n^{\gamma->a}$ of 2nd Zone

5.5 Application of the Bainite Model

The kinetic model of Azuma was applied to three different zones in the austenite region as was mentioned above. The chemical compositions these zones are presented in Table 8. The heat treatment conditions of the experimental procedure are shown in Figure 5.19. The model was employed in order to calculate the respective kinetics of the transformation and a direct comparison between experimental and calculated results was performed. Calculations using the model were performed for a TRIP-Al steel (% mass) steel for the ‘‘isothermal’’ part of the thermal-cycle.

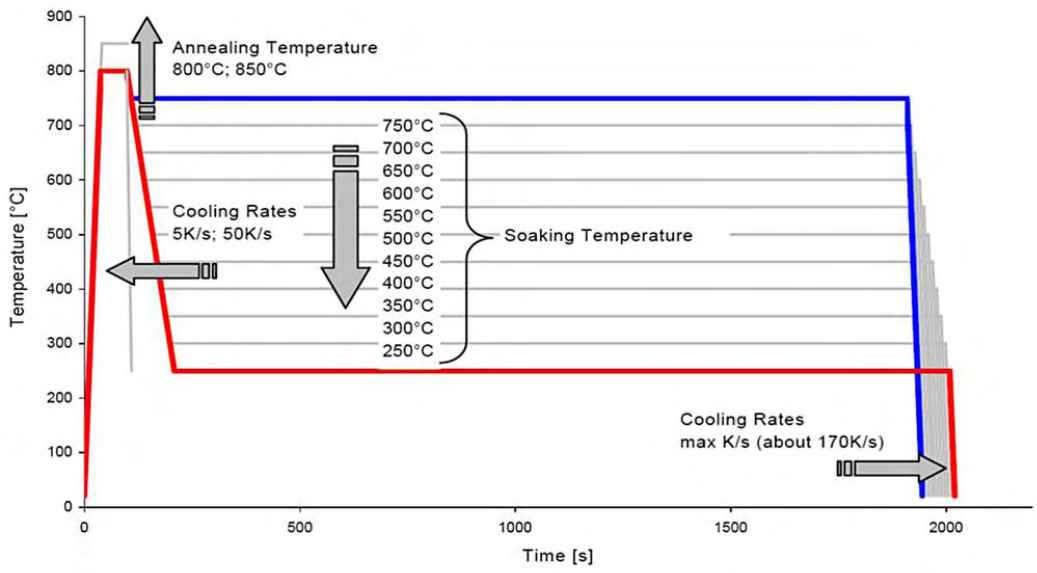

Figure 5.19 Heating Cycles for Isothermal Investigations (Simulation of Isothermal Transformation)

The Azuma model needs several parameters as input to compute the kinetics of the bainitic transformation. Some of them are already available through thermodynamic calculations such as the driving forces (ΔG) for the formation of ferrite, cementite in austenite and cementite in ferrite. The others like the autocatalytic nucleation factor β are generally treated as fix parameters. The remaining parameters, namely the interfacial energies (σα/γ, σα/cem, σγ/cem) and the nucleation densities (Nα/γ, Nα/cem, Nγ/cem), are treated in the original paper as fitting parameters to adjust the model on the experimental dilation curves. In other words, these parameters do not follow any physical rules. But a physical based model should have as least

fitting parameters as possible. Although there are some theoretical nucleation models, the nucleation density is not easy to predict properly at the moment.

During an RFCS project, RWTH went on to calculate interfacial energies by using the commercial software MatCalc. This software is able to describe the formation and growth of precipitates within a given matrix as a function of time and temperature. In this software is integrated also a model for calculating interfacial energies. The generalized nearest-neighbor broken-bond model by B. Sonderegger and E. Kozeschnik employed in the program is an extension of the classical nearest neighbor broken-bond model [49] and gives good estimation for the interfacial energies. The interfacial energies for TRIP-Al were calculated as a function of carbon content and temperature over a wide range. The interfacial energies were calculated in the temperature range between 350°C and 600°C as this is the region of major interest concerning the bainitic transformation. The carbon enrichment of the retained austenite during the transformation was taken into account by calculating the interfacial energy as a function of carbon content ranging from the initial carbon content of the respective steel until 1.5 wt.-% carbon. In Figure 5.20, Figure 5.21 and Figure 5.22 the interfacial energies are shown exemplary for the TRIP-Al steel. These values were implemented in the Azuma model

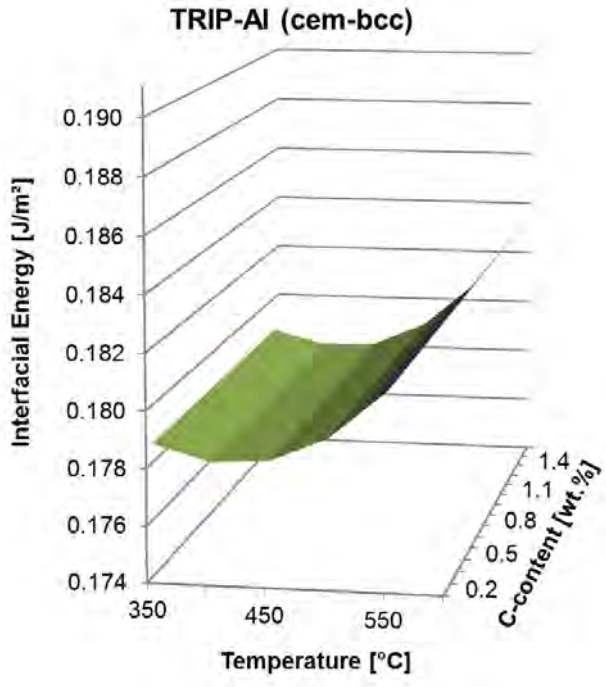

Figure 5.20 Calculated interfacial energy $\sigma_{\alpha/cem}$ as a function of carbon content and temperature for TRIP-Al steel.

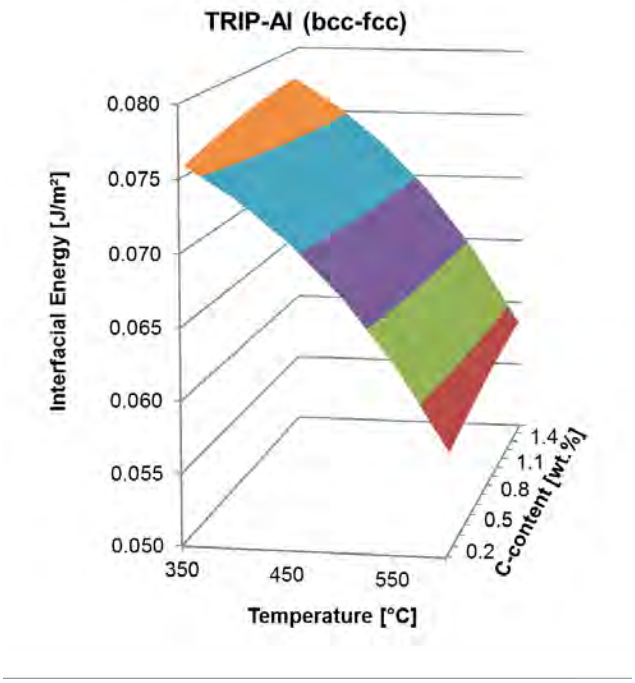

Figure 5.21 Calculated interfacial energy $\sigma_{\omega/\gamma}$ as a function of carbon content and temperature for TRIP-Al steel.

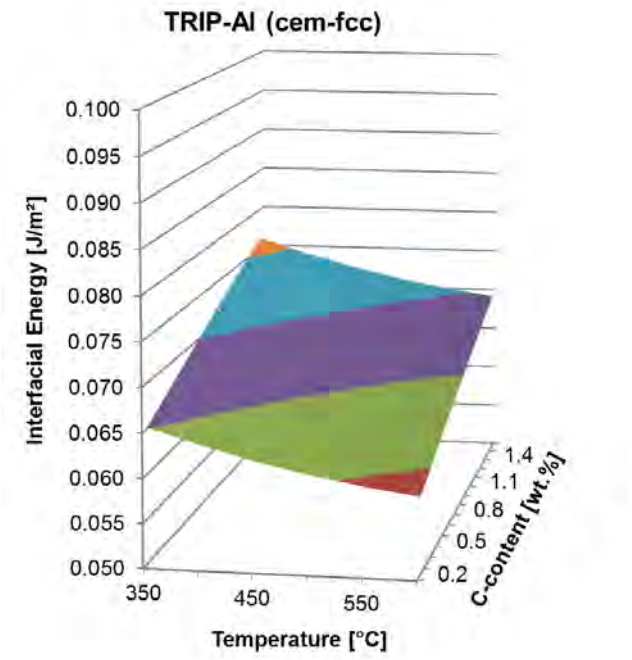

Figure 5.22 Calculated interfacial energy $\sigma_{cem/\gamma}$ as a function of carbon content and temperature for TRIP-Al steel.

Calculations are depicted in Figure 5.23 through Figure 5.25 for holding temperature 400^{o}C. Figure 5.23 depicts the vol. fraction of bainitic ferrite formed as a function of time for the 3 composition zones.

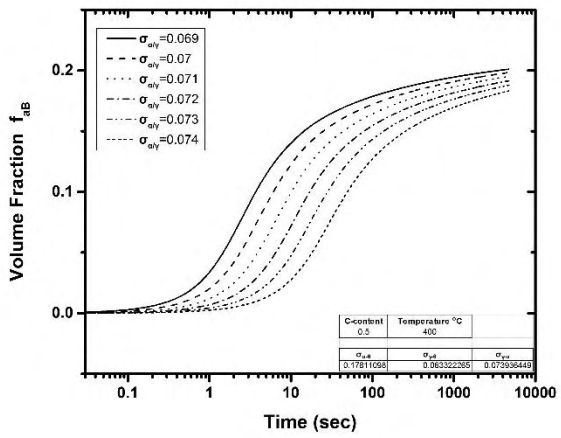

(a)

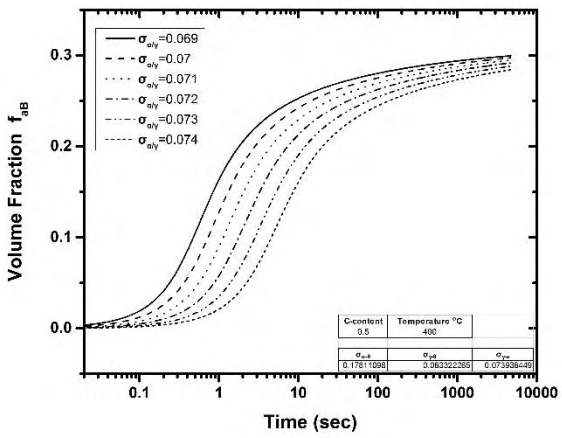

(b)

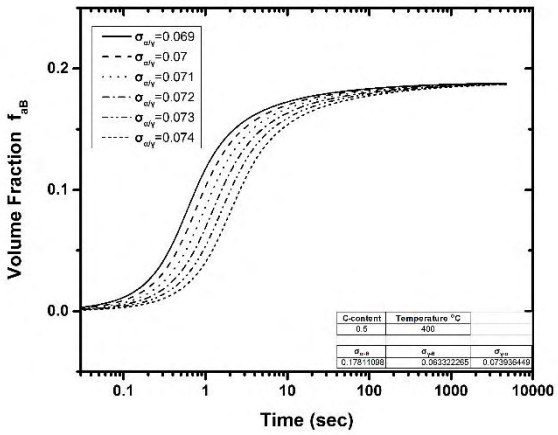

(c)

Figure 5.23 Volume fraction of ferrite versus holding time for each zone (a) 1st zone , (b) 2nd zone, (c) 3rd zone after isothermal holding during bainitic transformation at 400oC.

It is observed that the volume fraction of bainitic ferrite formed is different for each zone. This is attributed to composition as well as zone width.

Specimens of this steel had been subjected to isothermal bainitic treatment and the kinetics of bainitic ferrite formation had been experimentally recorded by dilatometric measurements by RWTH. The dilatometric results along with the volume fraction of ferrite versus holding time for all three zones combined is depicted in Figure 5.24. They are in good agreement.

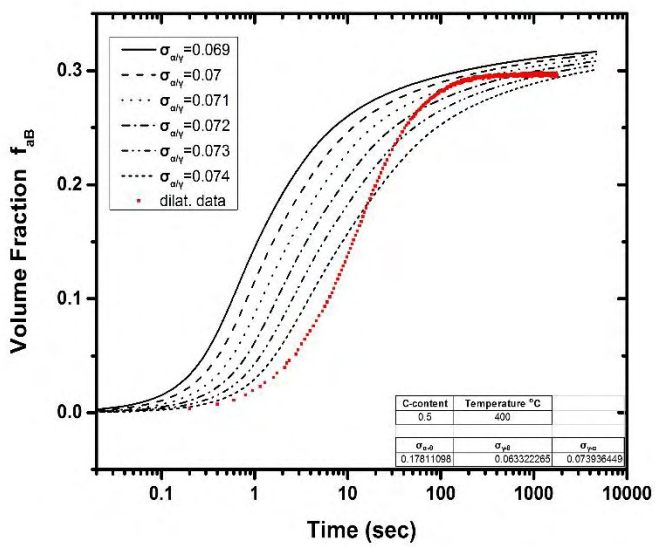

Figure 5.24 Dilatometric results along with the volume fraction of ferrite versus holding time for all three zones combined (400°C).

Figure 5.25 presents the volume fraction of austenite remaining after the bainitic transformation, versus holding time for all three zones along with its carbon contain. The longer the alloy remains in isothermal holding less austenite remains after the transformation but it is more enriched in carbon.

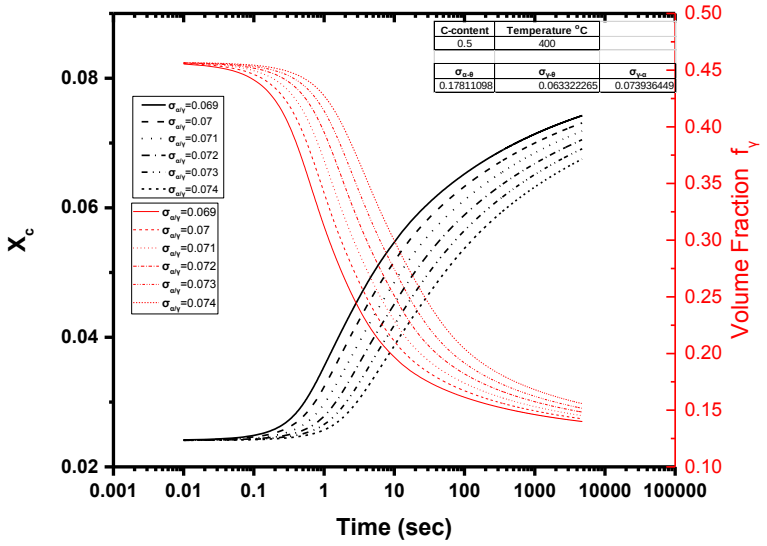

Figure 5.25 Volume fraction of austenite remaining after the bainitic transformation, versus holding time for all three zones and corresponding carbon contain (400°C).

Similar curves were derived for different bainitic isothermal holding temperatures. Figure 5.26 depicts the vol. fraction of bainitic ferrite formed as a function of time for the 3 composition zones after isothermal holding during bainitic transformation at 350^{o}C.

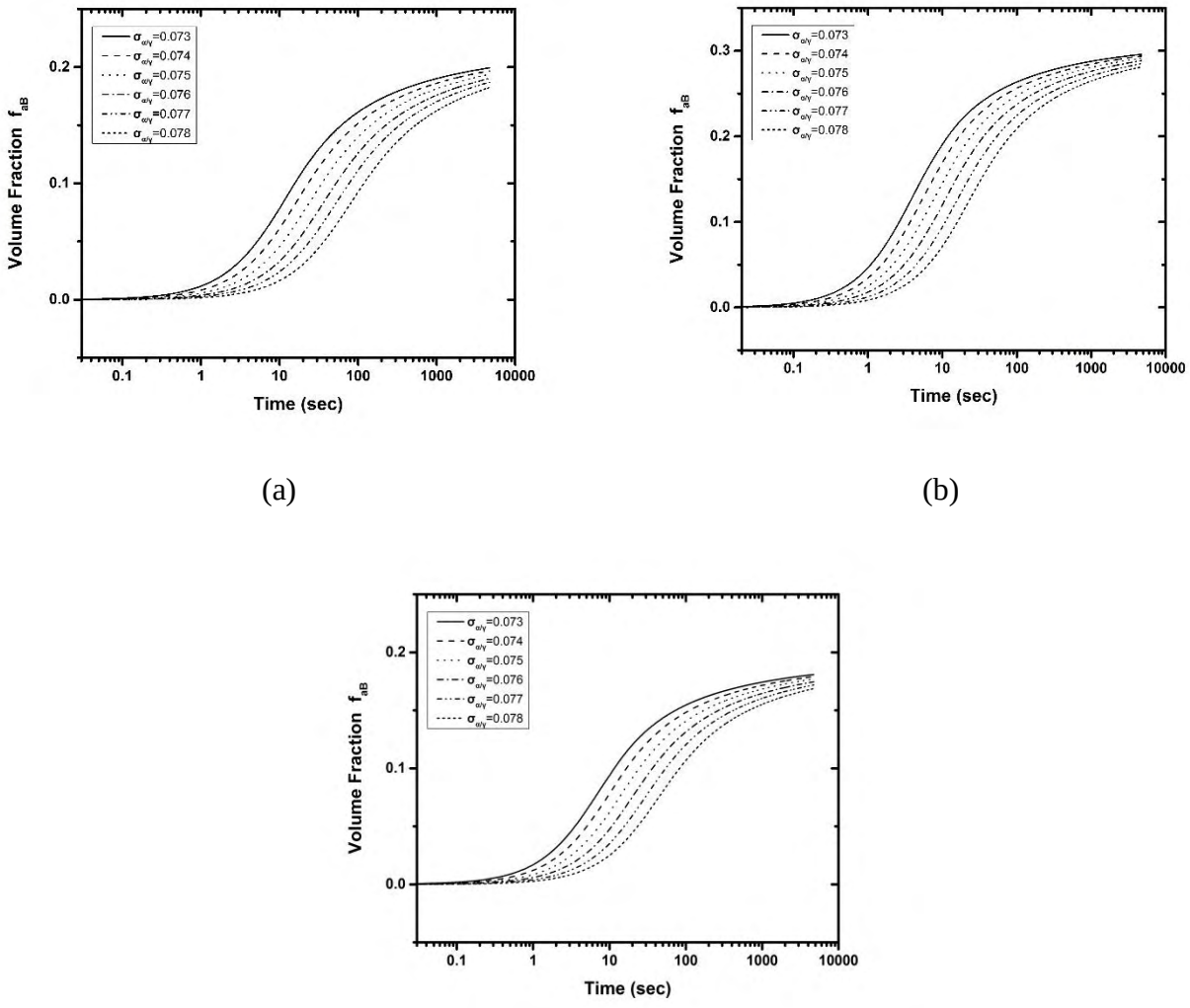

Figure 5.26 Volume fraction of ferrite versus holding time for each zone (a) 1st zone , (b) 2nd zone, (c) 3rd zone after isothermal holding during bainitic transformation at 350^{o}C.

The dilatometric results along with the volume fraction of ferrite versus holding time for all three zones combined zones, after isothermal holding during bainitic transformation at 350^{o}C. is depicted in Figure 5.27. They are in good agreement.

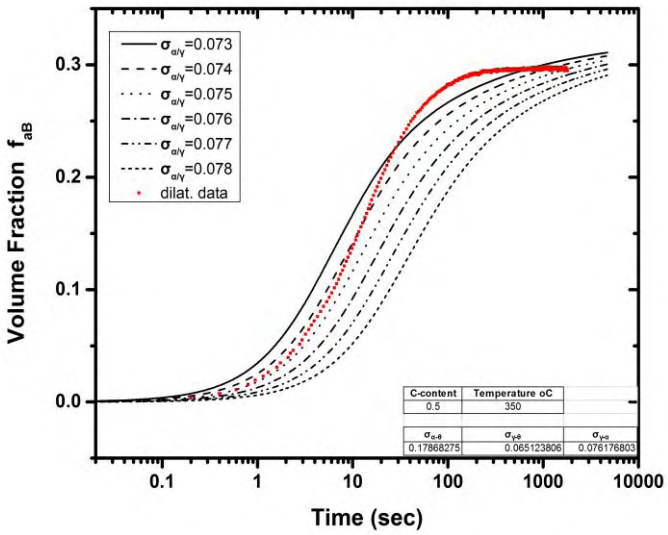

Figure 5.27 Dilatometric results along with the volume fraction of ferrite versus holding time for all three zones combined (350^{o}C).

Figure 5.28 presents the volume fraction of austenite remaining after the bainitic transformation, versus holding time for all three zones along with its carbon contain.

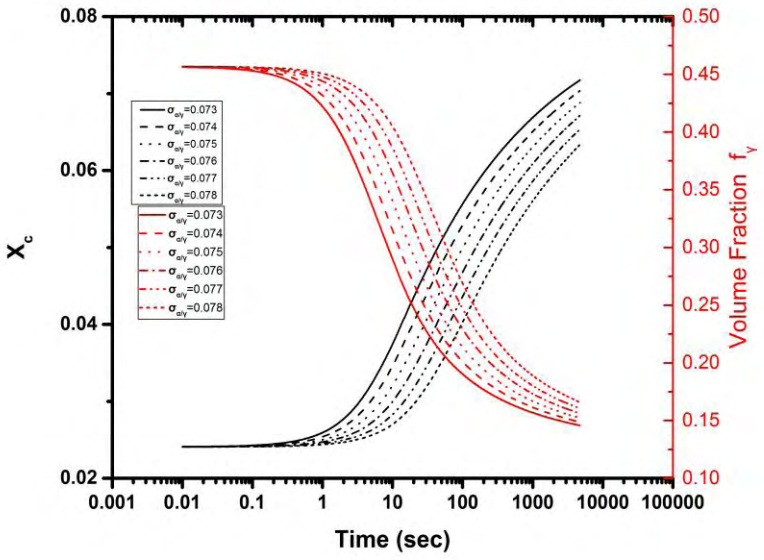

Figure 5.28 Volume fraction of austenite remaining after the bainitic transformation, versus holding time for all three zones and corresponding carbon contain (350^{o}C).

Figure 5.29 depicts the vol. fraction of bainitic ferrite formed as a function of time for the 3 composition zones after isothermal holding during bainitic transformation at 300^{o}C.

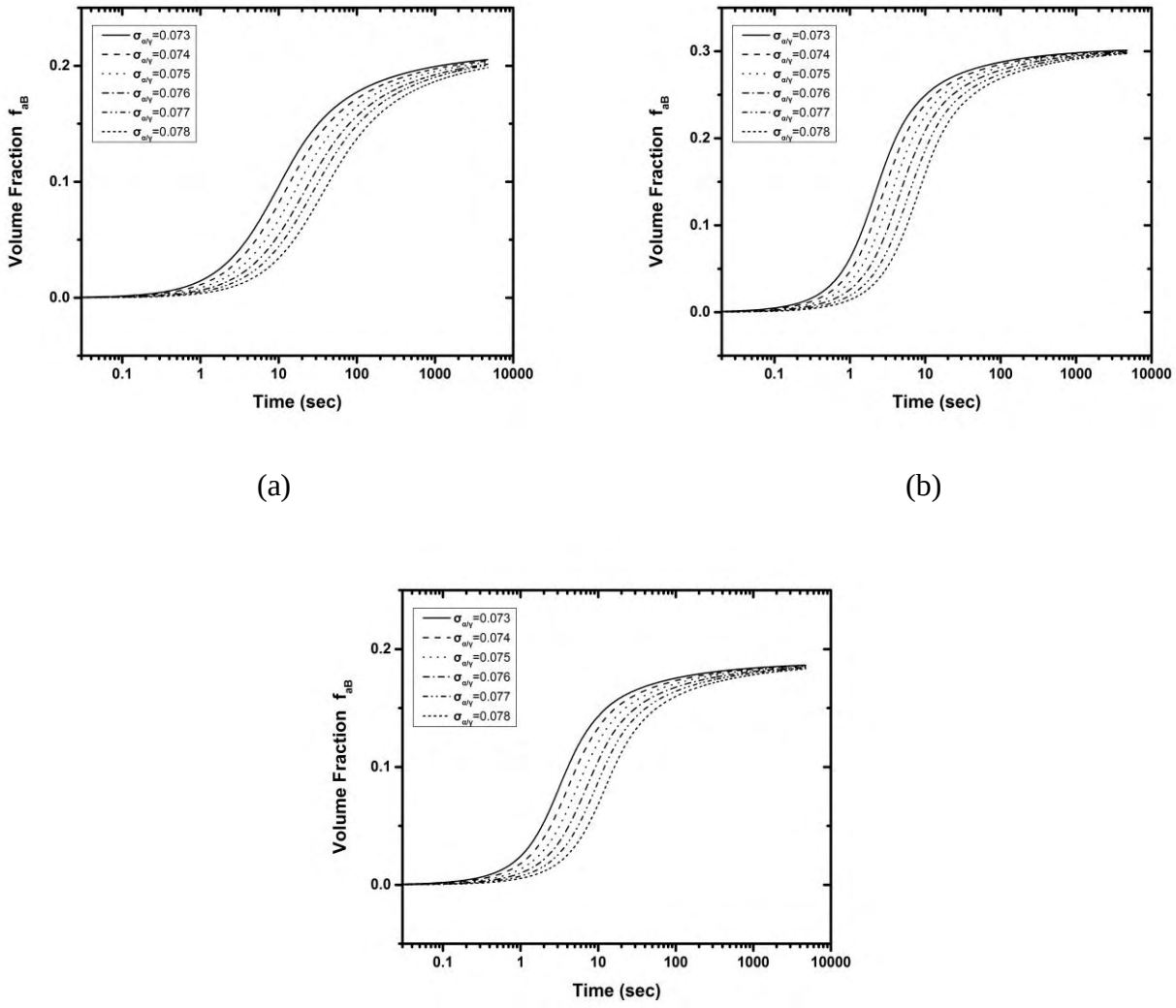

Figure 5.29 Volume fraction of ferrite versus holding time for each zone (a) 1st zone , (b) 2nd zone, (c) 3rd zone after isothermal holding during bainitic transformation at 300^{o}C.

The dilatometric results along with the volume fraction of ferrite versus holding time for all three zones combined zones, after isothermal holding during bainitic transformation at 300^{o}C, is depicted in Figure 5.30. They are in good agreement.

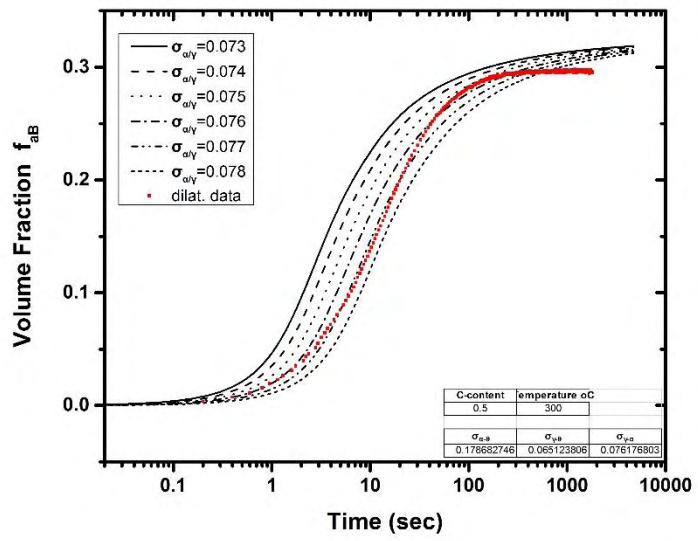

Figure 5.30 Dilatometric results along with the volume fraction of ferrite versus holding time for all three zones combined (300^{o}C).

Figure 5.31 presents the volume fraction of austenite remaining after the bainitic transformation, versus holding time for all three zones along with its carbon contain.

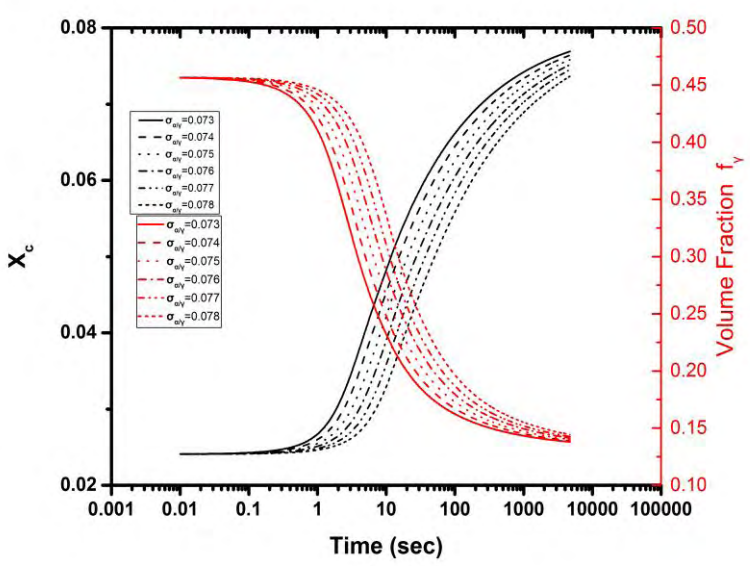

Figure 5.31 Volume fraction of austenite remaining after the bainitic transformation, versus holding time for all three zones and corresponding carbon contain (300^{o}C).

6 Results and discussion

Incorporating kinetic simulations for the intercritical annealing treatment of TRIP steels leads to the conclusions that the austenite formed at the end of the heating process is significantly less than the amount calculated by assuming equilibrium.

The austenite formed consists of three distinct regions. The first region is rapidly formed by the dissolution of perlite and is rich in C and Mn and depleted from Al and Si, while the second region is formed at the expense of ferrite and inherits its composition, being depleted of C and Mn and rich in Al and Si. The third section is formed during the cooling part of the heat treatment, during which the austenite region is suppressed and thus is enriched in C and Mn.

Heating and cooling rate have a significant effect on austenite volume fraction. Increasing the heating rate raises the austenite volume fraction during the intercritical annealing process.

Alloying elements C, Mn and Al form composition zones in austenite at the end of intercritical annealing, which are further intensified during the cooling processes to the bainitic temperature. These composition zones affect the volume fraction and composition of the remaining austenite, after the bainitic transformation. This was confirmed by dilatometric results.

7 Future work

Further work could be focus on the final step of the heating treatment quenching. During this stage depending on the composition of austenite part of it is transformed into martensite, thus leaving the remainder, retained austenite (RA) to provide the TRIP effect in this type of steels.

Another useful step would be the introduction of actual composition profiles instead of mean values in the current method, as well as mapping of RA fraction and composition as a function of annealing parameters.

8 References

1. Vasilakos, A.N., *Transformation-Induced Plasticity of Retained Austenite in Low-Alloy Steels*, in *Dept. of Mechanical & Industrial Engineering*. 2000, University of Thessaly: Volos, Greece.
2. *http://www.worldautosteel.org/steel-basics/steel-types/transformation-induced-plasticity-trip-steel/*.
3. Zackay, V.F., et al., *The enhancement of ductility in high-strength steels.* Trans. ASM 1967. **60**: p. 252–59.
4. Matsumura, O., Y. Sakuma, and H. Takechi, *Trip and its kinetic aspects in austempered 0.4C-1.5Si-0.8Mn steel.* Scripta Metallurgica, 1987. **21**(10): p. 1301-1306.
5. Matsumura, O., Y. Sakuma, and H. Takechi, *Enhancement of elongation by retained austenite in intercritical annealed 0.4C-1.5Si-0.8Mn steel.* Transactions of the Iron and Steel Institute of Japan, 1987. **27**(7): p. 570-579.
6. Öhlert, J., *Einfluss von chemischer Zusammensetzung und Herstellungsverlauf auf Mikrostruktur und mechanische Eigenschaften von TRIP-Stählen,,*, in *Institute of Ferrous Metallurgy*. 2002, RWTH: Aachen, Germany.
7. Yi, H., *δ-TRIP Steel* in *Department of Ferrous Technology*. 2010, Pohang University of Science and Technology, : Korea.
8. Sakuma, Y., O. Matsumura, and H. Takechi, *Mechanical properties and retained austenite in intercritically heat-treated bainite-transformed steel and their variation with Si and Mn additions.* Metallurgical Transactions A, 1991. **22**(2): p. 489-498.
9. Girault, E., et al., *Comparison of the effects of silicon and aluminium on the tensile behaviour of multiphase TRIP-assisted steels.* Scripta Materialia, 2001. **44**(6): p. 885-892.
10. Jacques, P.J., et al., *The Developments of Cold-rolled TRIP-assisted Multiphase Steels. Al-alloyed TRIP-assisted Multiphase Steels.* ISIJ International, 2001. **41**(9): p. 1068-1074.
11. Jacques, P.J., et al., *The Developments of Cold-rolled TRIP-assisted Multiphase Steels. Low Silicon TRIP-assisted Multiphase Steels.* ISIJ International, 2001. **41**(9): p. 1061-1067.
12. De Cooman, B.C., *Structure–properties relationship in TRIP steels containing carbide-free bainite.* Current Opinion in Solid State and Materials Science, 2004. **8**(3-4): p. 285-303.
13. Christian, J.W., *The theory of transformations in metals and alloys : an advanced textbook in physical metallurgy*. 2d ed. International series on materials science and technology. 1975, Oxford ; New York: Pergamon Press. v.
14. Bhadeshia, H.K.D.H., *Bainite in steels transformations, microstructure and properties*, in *Book 735*. 2001, IOM Communications: London. p. xxiv, 454 p.
15. De Meyer, M., J. Mahieu, and B.C. De Cooman, *Empirical microstructure prediction method for combined intercritical annealing and bainitic transformation of TRIP steel.* Materials Science and Technology, 2002. **18**(10): p. 1121-1132.
16. Honeycombe, R.W.K. and H.K.D.H. Bhadeshia, *Steels : microstructure and properties*. 2nd ed. Metallurgy and materials science series. 1996, London,New York: Arnold; Halsted Press. viii, 324 p.
17. Bhadeshia, H.K.D.H., *A rationalisation of shear transformations in steels.* Acta Metallurgica, 1981. **29**(6): p. 1117-1130.

18. Bhadeshia, H.K.D.H., *A Thermodynamic Analysis of Isothermal Transformation Diagrams.* Metallurgical Science, 1982. **16**: p. 159-165.
19. Ali, A. and H.K.D.H. Bhadeshia, *Aspects of the Nucleation of Widmanstatten Ferrite.* Materials Science and Technology, 1990. **6**: p. 781-784.
20. Bhadeshia, H.K.D.H., *Bainite in steels : transformations, microstructure and properties*. 2nd ed ed. Book. 2001, London: IOM Communications. xxiv, 454 p.
21. Matsuda, H. and H.K.D.H. Bhadeshia, *Kinetics of the bainite transformation.* Proceedings of the Royal Society A: Mathematical, Physical and Engineering Sciences, 2004. **460**(2046): p. 1707-1722.
22. Bhadeshia, H.K.D.H., *Bainite: Overall Transformation Kinetics.* Journal de Physique C, 1982. **43**(12): p. 443-448.
23. Rees, G.I. and H.K.D.H. Bhadeshia, *Bainite transformation kinetics. Part 1. Modified model.* Materials Science and Technology, 1992. **8**(11): p. 985-993.
24. Quidort, D. and Y.J.M. Brechet, *A Model of Isothermal and Non Isothermal Transformation Kinetics of Bainite in 0.5% C Steels.* ISIJ International, 2002. **42**(9): p. 1010-1017.
25. Lange, W., M. Enomoto, and H. Aaronson, *The kinetics of ferrite nucleation at austenite grain boundaries in Fe-C alloys.* Metallurgical and Materials Transactions A, 1988. **19**(3): p. 427-440.
26. Hillert, M., *Diffusion in growth of bainite.* Metallurgical and Materials Transactions A, 1994. **25**(9): p. 1957-1966.
27. Purdy, G.R. and M. Hillert, *Overview no. 38: On the nature of the bainite transformation in steels.* Acta Metallurgica, 1984. **32**(6): p. 823-828.
28. Aaronson, H., et al., *Bainite viewed three different ways.* Metallurgical and Materials Transactions A, 1990. **21**(6): p. 1343-1380.
29. Ohmori, Y. and T. Maki, Mater. Trans. JIM, 1991. **32**(8): p. 631.
30. Hillert, M., *The nature of Bainite.* ISIJ International, 1995. **35**: p. 1134.
31. Mujahid, S.A. and H.K.D.H. Bhadeshia, *Partitioning of carbon from supersaturated ferrite plates.* Acta Metallurgica et Materialia, 1992. **40**(2): p. 389-396.
32. Hillert, M., Jernkont. Ann., 1957. **141**: p. 757.
33. Hillert, M., *The growth of ferrite, bainite and martensite*. 1960, Swedish Institute for Metal Research, Stockholm, Sweden.: internal report.
34. Kaufman, L., S. Radcliffe, and M. Cohen, *The decomposition of austenite by diffusional processes*. Interscience. 1962, NY,USA.
35. Triverdi, R., Metallurgical Transactions 1970. **1**: p. 921.
36. Quidort, D. and Y. Bréchet, *The role of carbon on the kinetics of bainite transformation in steels.* Scripta Materialia, 2002. **47**(3): p. 151-156.
37. Quidort, D. and Y.J.M. Brechet, *Isothermal growth kinetics of bainite in 0.5% C steels.* Acta Materialia, 2001. **49**(20): p. 4161-4170.
38. Bosze, W.P. and R. Triverdi, Metallurgical Transactions, 1974. **5**: p. 511.
39. Sundman, B., B. Jansson, and J.-O. Andersson, *The Thermo-Calc databank system.* Calphad, 1985. **9**(2): p. 153-190.
40. Yada, H. and T. Ooka, J. Japan. Inst. Met., 1967. **31**: p. 766.
41. Cahn, J.W., *The kinetics of grain boundary nucleated reactions.* Acta Metallurgica, 1956. **4**(5): p. 449-459.
42. Azuma, M., et al., *Modelling Upper and Lower Bainite Trasformation in Steels.* ISIJ International, 2005. **45**(2): p. 221-228.

43. Gaude-Fugarolas, D. and P.J. Jacques, *A New Physical Model for the Kinetics of the Bainite Transformation.* ISIJ International, 2006. **46**(5): p. 712-717.
44. Katsamas, A.I. and G.N. Haidemenopoulos, *A semi-empirical model for the evolution of retained austenite via bainitic transformation in multiphase TRIP steels.* Steel Research International, 2008. **79**(11): p. 875-884.
45. Ghosh, G. and G.B. Olson, *Precipitation of paraequilibrium cementite: Experiments, and thermodynamic and kinetic modeling.* Acta Materialia, 2002. **50**(8): p. 2099-2119.
46. Hultgren, A., *Isothermal transformation of austenite.* Transactions of the American Society for Metals, 1947. **39**: p. 915-1005.
47. Grujicic, M. and G.N. Haidemenopoulos, *A treatment of paraequilibrium thermodynamics in AF1410 steel using the thermocalc software and database.* Calphad, 1988. **12**(3): p. 219-224.
48. Ghosh, G. and G. Olson, *Simulation of paraequilibrium growth in multicomponent systems.* Metallurgical and Materials Transactions A, 2001. **32**(3): p. 455-467.
49. Sonderegger, B. and E. Kozeschnik, *Generalized Nearest-Neighbor Broken-Bond Analysis of Randomly Oriented Coherent Interfaces in Multicomponent Fcc and Bcc Structures.* Metallurgical and Materials Transactions A, 2009. **40**(3): p. 499-510.

9 Appendix – Function for the calculation of paraequilibrium driving forces

9.1 1st STEP: DEFINITION OF PHASE PARAMETERs

DEFINITION OF PARAMETER: G(PHASE,Z:C; (39)

$$G_{Z:C}^{0,\Phi}=y_{Fe}\cdot G_{Fe:C}^{0,\Phi}+y_{Mn}\cdot G_{Mn:C}^{0,\Phi}+y_{Cr}\cdot G_{Cr:C}^{0,\Phi}+y_{Si}\cdot G_{Si:C}^{0,\Phi}+y_{Nb}\cdot G_{Nb:C}^{0,\Phi}+y_{Al}\cdot G_{Al:C}^{0,\Phi}+$$

$$R\cdot T(y_{Fe}\cdot lny_{Fe}+y_{Mn}\cdot lny_{Mn}+y_{Cr}\cdot lny_{Cr}+y_{Si}\cdot lny_{Si}+y_{Nb}\cdot lny_{Nb}+y_{Al}\cdot lny_{Al})+$$

$$y_{Fe}\cdot y_{Mn}\cdot L_{Fe,Mn:C}^{0,\varphi}+y_{Fe}\cdot y_{Mn}\cdot(y_{Fe}-y_{Mn})\cdot L_{Fe,Mn:C}^{1,\varphi}+$$

$$y_{Fe}\cdot y_{Cr}\cdot L_{Fe,Cr:C}^{0,\varphi}+y_{Fe}\cdot y_{Cr}\cdot(y_{Fe}-y_{Cr})\cdot L_{Fe,Cr:C}^{1,\varphi}+$$

$$y_{Fe}\cdot y_{Si}\cdot L_{Fe,Si:C}^{0,\varphi}+y_{Fe}\cdot y_{Si}\cdot(y_{Fe}-y_{Si})\cdot L_{Fe,Si:C}^{1,\varphi}+$$

$$y_{Fe}\cdot y_{Nb}\cdot L_{Fe,Nb:C}^{0,\varphi}+y_{Fe}\cdot y_{Nb}\cdot(y_{Fe}-y_{Nb})\cdot L_{Fe,Nb:C}^{1,\varphi}+$$

$$y_{Fe}\cdot y_{Al}\cdot L_{Fe,Al:C}^{0,\varphi}+y_{Fe}\cdot y_{Al}\cdot(y_{Fe}-y_{Al})\cdot L_{Fe,Al:C}^{1,\varphi}+$$

$$y_{Mn}\cdot y_{Cr}\cdot L_{Mn,Cr:C}^{0,\varphi}+y_{Mn}\cdot y_{Cr}\cdot(y_{Mn}-y_{Cr})\cdot L_{Mn,Cr:C}^{1,\varphi}+$$

$$y_{Mn}\cdot y_{Si}\cdot L_{Mn,Si:C}^{0,\varphi}+y_{Mn}\cdot y_{Si}\cdot(y_{Mn}-y_{Si})\cdot L_{Mn,Si:C}^{1,\varphi}+$$

$$y_{Mn}\cdot y_{Nb}\cdot L_{Mn,Nb:C}^{0,\varphi}+y_{Mn}\cdot y_{Nb}\cdot(y_{Mn}-y_{Nb})\cdot L_{Mn,Nb:C}^{1,\varphi}+$$

$$y_{Mn}\cdot y_{Al}\cdot L_{Mn,Al:C}^{0,\varphi}+y_{Mn}\cdot y_{Al}\cdot(y_{Mn}-y_{Al})\cdot L_{Mn,Al:C}^{1,\varphi}+$$

$$y_{Cr}\cdot y_{Si}\cdot L_{Cr,Si:C}^{0,\varphi}+y_{Cr}\cdot y_{Si}\cdot(y_{Cr}-y_{Si})\cdot L_{Cr,Si:C}^{1,\varphi}+$$

$$y_{Cr}\cdot y_{Nb}\cdot L_{Cr,Nb:C}^{0,\varphi}+y_{Cr}\cdot y_{Nb}\cdot(y_{Cr}-y_{Nb})\cdot L_{Cr,Nb:C}^{1,\varphi}+$$

$$y_{Cr} \cdot y_{Al} \cdot L^{0,\varphi}_{Cr,Al:C} + y_{Cr} \cdot y_{Al} \cdot (y_{Cr} - y_{Al}) \cdot L^{1,\varphi}_{Cr,Al:C} +$$

$$y_{Si} \cdot y_{Nb} \cdot L^{0,\varphi}_{Si,Nb:C} + y_{Si} \cdot y_{Nb} \cdot (y_{Si} - y_{Nb}) \cdot L^{1,\varphi}_{Si,Nb:C} +$$

$$y_{Si} \cdot y_{Al} \cdot L^{0,\varphi}_{Si,Al:C} + y_{Si} \cdot y_{Al} \cdot (y_{Si} - y_{Al}) \cdot L^{1,\varphi}_{Si,Al:C} +$$

$$y_{Nb} \cdot y_{Al} \cdot L^{0,\varphi}_{Nb,Al:C} + y_{Nb} \cdot y_{Al} \cdot (y_{Nb} - y_{Al}) \cdot L^{1,\varphi}_{Nb,Al:C} +$$

$$y_{Fe} \cdot y_{Mn} \cdot y_{Cr} \cdot L^{0,\varphi}_{Fe,Mn,Cr:C} + y_{Fe} \cdot y_{Mn} \cdot y_{Si} \cdot L^{0,\varphi}_{Fe,Mn,Si:C} + y_{Fe} \cdot y_{Mn} \cdot y_{Nb} \cdot L^{0,\varphi}_{Fe,Mn,Nb:C}$$

$$+ y_{Fe} \cdot y_{Mn} \cdot y_{Al} \cdot L^{0,\varphi}_{Fe,Mn,Al:C} + y_{Fe} \cdot y_{Cr} \cdot y_{Si} \cdot L^{0,\varphi}_{Fe,Cr,Si:C} + y_{Fe} \cdot y_{Cr} \cdot y_{Nb} \cdot L^{0,\varphi}_{Fe,Cr,Nb:C}$$

$$+ y_{Fe} \cdot y_{Cr} \cdot y_{Al} \cdot L^{0,\varphi}_{Fe,Cr,Al:C} + y_{Fe} \cdot y_{Si} \cdot y_{Nb} \cdot L^{0,\varphi}_{Fe,Si,Nb:C} + y_{Fe} \cdot y_{Si} \cdot y_{Al} \cdot L^{0,\varphi}_{Fe,Si,Al:C}$$

$$+ y_{Fe} \cdot y_{Nb} \cdot y_{Al} \cdot L^{0,\varphi}_{Fe,Nb,Al:C} + y_{Mn} \cdot y_{Cr} \cdot y_{Si} \cdot L^{0,\varphi}_{Mn,Cr,Si:C} + y_{Mn} \cdot y_{Cr} \cdot y_{Nb} \cdot L^{0,\varphi}_{Mn,Cr,Nb:C}$$

$$+ y_{Mn} \cdot y_{Cr} \cdot y_{Al} \cdot L^{0,\varphi}_{Mn,Cr,Al:C} + y_{Mn} \cdot y_{Si} \cdot y_{Nb} \cdot L^{0,\varphi}_{Mn,Si,Nb:C} + y_{Mn} \cdot y_{Si} \cdot y_{Al} \cdot L^{0,\varphi}_{Mn,Si,Al:C}$$

$$+ y_{Mn} \cdot y_{Nb} \cdot y_{Al} \cdot L^{0,\varphi}_{Mn,Nb,Al:C} + y_{Cr} \cdot y_{Si} \cdot y_{Nb} \cdot L^{0,\varphi}_{Cr,Si,Nb:C} + y_{Cr} \cdot y_{Si} \cdot y_{Al} \cdot L^{0,\varphi}_{Cr,Si,Al:C}$$

$$+ y_{Si} \cdot y_{Nb} \cdot y_{Al} \cdot L^{0,\varphi}_{Si,Nb,Al:C}$$

DEFINITION OF PARAMETER: G(PHASE,Z:VA;0)

(40)

$$G^{0,\Phi}_{Z:Va} = y_{Fe} \cdot G^{0,\Phi}_{Fe:Va} + y_{Mn} \cdot G^{0,\Phi}_{Mn:Va} + y_{Cr} \cdot G^{0,\Phi}_{Cr:Va} + y_{Si} \cdot G^{0,\Phi}_{Si:Va} + y_{Nb} \cdot G^{0,\Phi}_{Nb:Va} + y_{Al} \cdot G^{0,\Phi}_{Al:Va}$$

$$+ R \cdot T(y_{Fe} \cdot lny_{Fe} + y_{Mn} \cdot lny_{Mn} + y_{Cr} \cdot lny_{Cr} + y_{Si} \cdot lny_{Si} + y_{Nb} \cdot lny_{Nb} + y_{Al} \cdot lny_{Al}) +$$

$$y_{Fe} \cdot y_{Mn} \cdot L^{0,\varphi}_{Fe,Mn:Va} + y_{Fe} \cdot y_{Mn} \cdot (y_{Fe} - y_{Mn}) \cdot L^{1,\varphi}_{Fe,Mn:Va} +$$

$$y_{Fe} \cdot y_{Cr} \cdot L^{0,\varphi}_{Fe,Cr:Va} + y_{Fe} \cdot y_{Cr} \cdot (y_{Fe} - y_{Cr}) \cdot L^{1,\varphi}_{Fe,Cr:Va} +$$

$$y_{Fe} \cdot y_{Si} \cdot L^{0,\varphi}_{Fe,Si:Va} + y_{Fe} \cdot y_{Si} \cdot (y_{Fe} - y_{Si}) \cdot L^{1,\varphi}_{Fe,Si:Va} + y_{Fe} \cdot y_{Si} \cdot (y_{Fe} - y_{Si})^2 \cdot L^{2,\varphi}_{Fe,Si:Va}$$

$$y_{Fe} \cdot y_{Nb} \cdot L^{0,\varphi}_{Fe,Nb:Va} + y_{Fe} \cdot y_{Nb} \cdot (y_{Fe} - y_{Nb}) \cdot L^{1,\varphi}_{Fe,Nb:Va} +$$

$$y_{Fe} \cdot y_{Al} \cdot L^{0,\varphi}_{Fe,Al:Va} + y_{Fe} \cdot y_{Al} \cdot (y_{Fe} - y_{Al}) \cdot L^{1,\varphi}_{Fe,Al:Va} +$$

$$y_{Mn} \cdot y_{Cr} \cdot L^{0,\varphi}_{Mn,Cr:Va} + y_{Mn} \cdot y_{Cr} \cdot (y_{Mn} - y_{Cr}) \cdot L^{1,\varphi}_{Mn,Cr:Va} +$$

$$y_{Mn} \cdot y_{Si} \cdot L^{0,\varphi}_{Mn,Si:Va} + y_{Mn} \cdot y_{Si} \cdot (y_{Mn} - y_{Si}) \cdot L^{1,\varphi}_{Mn,Si:Va} +$$

$$y_{Mn} \cdot y_{Nb} \cdot L^{0,\varphi}_{Mn,Nb:Va} + y_{Mn} \cdot y_{Nb} \cdot (y_{Mn} - y_{Nb}) \cdot L^{1,\varphi}_{Mn,Nb:Va} +$$

$$y_{Mn} \cdot y_{Al} \cdot L^{0,\varphi}_{Mn,Al:Va} + y_{Mn} \cdot y_{Al} \cdot (y_{Mn} - y_{Al}) \cdot L^{1,\varphi}_{Mn,Al:Va} +$$

$$y_{Cr} \cdot y_{Si} \cdot L^{0,\varphi}_{Cr,Si:Va} + y_{Cr} \cdot y_{Si} \cdot (y_{Cr} - y_{Si}) \cdot L^{1,\varphi}_{Cr,Si:Va} +$$

$$y_{Cr} \cdot y_{Nb} \cdot L^{0,\varphi}_{Cr,Nb:Va} + y_{Cr} \cdot y_{Nb} \cdot (y_{Cr} - y_{Nb}) \cdot L^{1,\varphi}_{Cr,Nb:Va} +$$

$$y_{Cr} \cdot y_{Al} \cdot L^{0,\varphi}_{Cr,Al:Va} + y_{Cr} \cdot y_{Al} \cdot (y_{Cr} - y_{Al}) \cdot L^{1,\varphi}_{Cr,Al:Va} + y_{Cr} \cdot y_{Al} \cdot (y_{Cr} - y_{Al})^2 \cdot L^{2,\varphi}_{Cr,Al:Va} +$$

$$y_{Si} \cdot y_{Nb} \cdot L^{0,\varphi}_{Si,Nb:Va} + y_{Si} \cdot y_{Nb} \cdot (y_{Si} - y_{Nb}) \cdot L^{1,\varphi}_{Si,Nb:Va} +$$

$$y_{Si} \cdot y_{Al} \cdot L^{0,\varphi}_{Si,Al:Va} + y_{Si} \cdot y_{Al} \cdot (y_{Si} - y_{Al}) \cdot L^{1,\varphi}_{Si,Al:Va} +$$

$$y_{Nb} \cdot y_{Al} \cdot L^{0,\varphi}_{Nb,Al:Va} + y_{Nb} \cdot y_{Al} \cdot (y_{Nb} - y_{Al}) \cdot L^{1,\varphi}_{Nb,Al:Va} +$$

$$y_{Fe} \cdot y_{Mn} \cdot y_{Cr} \cdot L^{0,\varphi}_{Fe,Mn,Cr:Va} + y_{Fe} \cdot y_{Mn} \cdot y_{Si} \cdot L^{0,\varphi}_{Fe,Mn,Si:Va} + y_{Fe} \cdot y_{Mn} \cdot y_{Nb} \cdot L^{0,\varphi}_{Fe,Mn,Nb:Va}$$

$$+ y_{Fe} \cdot y_{Mn} \cdot y_{Al} \cdot L^{0,\varphi}_{Fe,Mn,Al:Va} + y_{Fe} \cdot y_{Cr} \cdot y_{Si} \cdot L^{0,\varphi}_{Fe,Cr,Si:Va} + y_{Fe} \cdot y_{Cr} \cdot y_{Nb} \cdot L^{0,\varphi}_{Fe,Cr,Nb:Va}$$

$$+ y_{Fe} \cdot y_{Cr} \cdot y_{Al} \cdot L^{0,\varphi}_{Fe,Cr,Al:Va} + y_{Fe} \cdot y_{Si} \cdot y_{Nb} \cdot L^{0,\varphi}_{Fe,Si,Nb:Va} + y_{Fe} \cdot y_{Si} \cdot y_{Al} \cdot L^{0,\varphi}_{Fe,Si,Al:Va}$$

$$+ y_{Fe} \cdot y_{Nb} \cdot y_{Al} \cdot L^{0,\varphi}_{Fe,Nb,Al:C} + y_{Mn} \cdot y_{Cr} \cdot y_{Si} \cdot L^{0,\varphi}_{Mn,Cr,Si:Va} + y_{Mn} \cdot y_{Cr} \cdot y_{Nb} \cdot L^{0,\varphi}_{Mn,Cr,Nb:Va}$$

$$+ y_{Mn} \cdot y_{Cr} \cdot y_{Al} \cdot L^{0,\varphi}_{Mn,Cr,Al:Va} + y_{Mn} \cdot y_{Si} \cdot y_{Nb} \cdot L^{0,\varphi}_{Mn,Si,Nb:Va} + y_{Mn} \cdot y_{Si} \cdot y_{Al} \cdot L^{0,\varphi}_{Mn,Si,Al:Va}$$

$$+y_{Mn}\cdot y_{Nb}\cdot y_{Al}\cdot L^{0,\varphi}_{Mn,Nb,Al:Va}+y_{Cr}\cdot y_{Si}\cdot y_{Nb}\cdot L^{0,\varphi}_{Cr,Si,Nb:Va}+y_{Cr}\cdot y_{Si}\cdot y_{Al}\cdot L^{0,\varphi}_{Cr,Si,Al:Va}$$

$$+y_{Si}\cdot y_{Nb}\cdot y_{Al}\cdot L^{0,\varphi}_{Si,Nb,Al:Va}$$

DEFINITION OF PARAMETER: L(PHASE,Z:C,VA;0)

(41)

$$L^{0,\varphi}_{Z:C,Va}=$$

$$y_{Fe}L^{0,\varphi}_{Fe:C,Va}+y_{Mn}L^{0,\varphi}_{Mn:C,Va}+y_{Cr}L^{0,\varphi}_{Cr:C,Va}+y_{Si}L^{0,\varphi}_{Si:C,Va}+y_{Nb}L^{0,\varphi}_{Nb:C,Va}+y_{Al}L^{0,\varphi}_{Al:C,Va}+$$

$$y_{Fe}\cdot y_{Mn}\cdot L^{0,\varphi}_{Fe,Mn:C,Va}+y_{Fe}\cdot y_{Cr}\cdot L^{0,\varphi}_{Fe,Cr:C,Va}+y_{Fe}\cdot y_{Si}\cdot L^{0,\varphi}_{Fe,Si:C,Va}+y_{Fe}\cdot y_{Nb}\cdot L^{0,\varphi}_{Fe,Nb:C,Va}$$

$$+y_{Fe}\cdot y_{Al}\cdot L^{0,\varphi}_{Fe,Al:C,Va}+y_{Mn}\cdot y_{Cr}\cdot L^{0,\varphi}_{Mn,Cr:C,Va}+y_{Mn}\cdot y_{Si}\cdot L^{0,\varphi}_{Mn,Si:C,Va}+y_{Mn}\cdot y_{Nb}\cdot L^{0,\varphi}_{Mn,Nb:C,Va}$$

$$+y_{Mn}\cdot y_{Al}\cdot L^{0,\varphi}_{Mn,Al:C,Va}+y_{Cr}\cdot y_{Si}\cdot L^{0,\varphi}_{Cr,Si:C,Va}+y_{Cr}\cdot y_{Nb}\cdot L^{0,\varphi}_{Cr,Nb:C,Va}+y_{Cr}\cdot y_{Al}\cdot L^{0,\varphi}_{Cr,Al:C,Va}$$

$$+y_{Si}\cdot y_{Nb}\cdot L^{0,\varphi}_{Si,Nb:C,Va}+y_{Si}\cdot y_{Al}\cdot L^{0,\varphi}_{Si,Al:C,Va}+y_{Nb}\cdot y_{Al}\cdot L^{0,\varphi}_{Nb,Al:C,Va}$$

DEFINITION OF PARAMETER: L(PHASE,Z:C,VA;1)

(42)

$$L^{1,\varphi}_{Z:C,Va}=y_{Fe}L^{1,\varphi}_{Fe:C,Va}+y_{Mn}L^{1,\varphi}_{Mn:C,Va}+y_{Cr}L^{1,\varphi}_{Cr:C,Va}+y_{Si}L^{1,\varphi}_{Si:C,Va}+y_{Nb}L^{1,\varphi}_{Nb:C,Va}+y_{Al}L^{1,\varphi}_{Al:C,Va}$$

$$y_{Fe} \cdot y_{Mn}(y_{Fe} - y_{Mn})L^{1,\varphi}_{Fe,Mn:C,Va} + y_{Fe} \cdot y_{Cr} \cdot (y_{Fe} - y_{Cr}) \cdot L^{1,\varphi}_{Fe,Cr:C,Va} + y_{Fe} \cdot y_{Si} \cdot (y_{Fe} - y_{Si}) \cdot L^{1,\varphi}_{Fe,Si:C,Va} + y_{Fe} \cdot y_{Nb} \cdot (y_{Fe} - y_{Nb}) \cdot L^{1,\varphi}_{Fe,Nb:C,Va} + y_{Fe} \cdot y_{Al} \cdot (y_{Fe} - y_{Al}) \cdot L^{1,\varphi}_{Fe,Al:C,Va} + y_{Mn} \cdot y_{Cr} \cdot (y_{Mn} - y_{Cr}) \cdot L^{1,\varphi}_{Mn,Cr:C,Va} + y_{Mn} \cdot y_{Si} \cdot (y_{Mn} - y_{Si}) \cdot L^{1,\varphi}_{Mn,Si:C,Va} + y_{Mn} \cdot y_{Nb} \cdot (y_{Mn} - y_{Nb}) \cdot L^{1,\varphi}_{Mn,Nb:C,Va} + y_{Mn} \cdot y_{Al} \cdot (y_{Mn} - y_{Al}) \cdot L^{1,\varphi}_{Mn,Al:C,Va} + y_{Cr} \cdot y_{Si} \cdot (y_{Cr} - y_{Si}) \cdot L^{1,\varphi}_{Cr,Si:C,Va} + y_{Cr} \cdot y_{Nb} \cdot (y_{Cr} - y_{Nb}) \cdot L^{1,\varphi}_{Cr,Nb:C,Va} + y_{Cr} \cdot y_{Al} \cdot (y_{Cr} - y_{Al}) \cdot L^{1,\varphi}_{Cr,Al:C,Va} + y_{Si} \cdot y_{Nb} \cdot (y_{Si} - y_{Nb}) \cdot L^{1,\varphi}_{Si,Nb:C,Va} + y_{Si} \cdot y_{Al} \cdot (y_{Si} - y_{Al}) \cdot L^{1,\varphi}_{Si,Al:C,Va} + y_{Nb} \cdot y_{Al} \cdot (y_{Nb} - y_{Al}) \cdot L^{1,\varphi}_{Nb,Al:C,Va}$$

DEFINITION OF PARAMETER: <u>BMAGN(PHASE,Z:C;0)</u>

(43)

$$\beta^{0,\Phi}_{Z:C} = y_{Fe} \cdot \beta^{0,\Phi}_{Fe:C} + y_{Mn} \cdot \beta^{0,\Phi}_{Mn:C} + y_{Cr} \cdot \beta^{0,\Phi}_{Cr:C} + y_{Si} \cdot \beta^{0,\Phi}_{Si:C} + y_{Nb} \cdot \beta^{0,\Phi}_{Nb:C} + y_{Al} \cdot \beta^{0,\Phi}_{Al:C}$$

$$y_{Fe} \cdot y_{Mn} \cdot \beta^{0,\varphi}_{Fe,Mn:C} + y_{Fe} \cdot y_{Mn} \cdot (y_{Fe} - y_{Mn}) \cdot \beta^{1,\varphi}_{Fe,Mn:C} +$$

$$y_{Fe} \cdot y_{Cr} \cdot \beta^{0,\varphi}_{Fe,Cr:C} + y_{Fe} \cdot y_{Cr} \cdot (y_{Fe} - y_{Cr}) \cdot \beta^{1,\varphi}_{Fe,Cr:C} +$$

$$y_{Fe} \cdot y_{Si} \cdot \beta^{0,\varphi}_{Fe,Si:C} + y_{Fe} \cdot y_{Si} \cdot (y_{Fe} - y_{Si}) \cdot \beta^{1,\varphi}_{Fe,Si:C} +$$

$$y_{Fe} \cdot y_{Nb} \cdot \beta^{0,\varphi}_{Fe,Nb:C} + y_{Fe} \cdot y_{Nb} \cdot (y_{Fe} - y_{Nb}) \cdot \beta^{1,\varphi}_{Fe,Nb:C} +$$

$$y_{Fe} \cdot y_{Al} \cdot \beta^{0,\varphi}_{Fe,Al:C} + y_{Fe} \cdot y_{Al} \cdot (y_{Fe} - y_{Al}) \cdot \beta^{1,\varphi}_{Fe,Al:C} +$$

$$y_{Mn} \cdot y_{Cr} \cdot \beta^{0,\varphi}_{Mn,Cr:C} + y_{Mn} \cdot y_{Cr} \cdot (y_{Mn} - y_{Cr}) \cdot \beta^{1,\varphi}_{Mn,Cr:C} +$$

$$y_{Mn} \cdot y_{Si} \cdot \beta^{0,\varphi}_{Mn,Si:C} + y_{Mn} \cdot y_{Si} \cdot (y_{Mn} - y_{Si}) \cdot \beta^{1,\varphi}_{Mn,Si:C} +$$

$$y_{Mn} \cdot y_{Nb} \cdot \beta^{0,\varphi}_{Mn,Nb:C} + y_{Mn} \cdot y_{Nb} \cdot (y_{Mn} - y_{Nb}) \cdot \beta^{1,\varphi}_{Mn,Nb:C} +$$

$$y_{Mn} \cdot y_{Al} \cdot \beta^{0,\varphi}_{Mn,Al:C} + y_{Mn} \cdot y_{Al} \cdot (y_{Mn} - y_{Al}) \cdot \beta^{1,\varphi}_{Mn,Al:C} +$$

$$y_{Cr} \cdot y_{Si} \cdot \beta^{0,\varphi}_{Cr,Si:C} + y_{Cr} \cdot y_{Si} \cdot (y_{Cr} - y_{Si}) \cdot \beta^{1,\varphi}_{Cr,Si:C} +$$

$$y_{Cr} \cdot y_{Nb} \cdot \beta^{0,\varphi}_{Cr,Nb:C} + y_{Cr} \cdot y_{Nb} \cdot (y_{Cr} - y_{Nb}) \cdot \beta^{1,\varphi}_{Cr,Nb:C} +$$

$$y_{Cr} \cdot y_{Al} \cdot \beta^{0,\varphi}_{Cr,Al:C} + y_{Cr} \cdot y_{Al} \cdot (y_{Cr} - y_{Al}) \cdot \beta^{1,\varphi}_{Cr,Al:C} +$$

$$y_{Si} \cdot y_{Nb} \cdot \beta^{0,\varphi}_{Si,Nb:C} + y_{Si} \cdot y_{Nb} \cdot (y_{Si} - y_{Nb}) \cdot \beta^{1,\varphi}_{Si,Nb:C} +$$

$$y_{Si} \cdot y_{Al} \cdot \beta^{0,\varphi}_{Si,Al:C} + y_{Si} \cdot y_{Al} \cdot (y_{Si} - y_{Al}) \cdot \beta^{1,\varphi}_{Si,Al:C} +$$

$$y_{Nb} \cdot y_{Al} \cdot \beta^{0,\varphi}_{Nb,Al:C} + y_{Nb} \cdot y_{Al} \cdot (y_{Nb} - y_{Al}) \cdot \beta^{1,\varphi}_{Nb,Al:C} +$$

$$y_{Fe} \cdot y_{Mn} \cdot y_{Cr} \cdot \beta^{0,\varphi}_{Fe,Mn,Cr:C} + y_{Fe} \cdot y_{Mn} \cdot y_{Si} \cdot \beta^{0,\varphi}_{Fe,Mn,Si:C} + y_{Fe} \cdot y_{Mn} \cdot y_{Nb} \cdot \beta^{0,\varphi}_{Fe,Mn,Nb:C} +$$

$$y_{Fe} \cdot y_{Mn} \cdot y_{Al} \cdot \beta^{0,\varphi}_{Fe,Mn,Al:C} + y_{Fe} \cdot y_{Cr} \cdot y_{Si} \cdot \beta^{0,\varphi}_{Fe,Cr,Si:C} + y_{Fe} \cdot y_{Cr} \cdot y_{Nb} \cdot \beta^{0,\varphi}_{Fe,Cr,Nb:C}$$

$$+ y_{Fe} \cdot y_{Cr} \cdot y_{Al} \cdot \beta^{0,\varphi}_{Fe,Cr,Al:C} + y_{Fe} \cdot y_{Si} \cdot y_{Nb} \cdot \beta^{0,\varphi}_{Fe,Si,Nb:C} + y_{Fe} \cdot y_{Si} \cdot y_{Al} \cdot \beta^{0,\varphi}_{Fe,Si,Al:C}$$

$$+ y_{Fe} \cdot y_{Nb} \cdot y_{Al} \cdot L^{0,\varphi}_{Fe,Nb,Al:C} + y_{Mn} \cdot y_{Cr} \cdot y_{Si} \cdot \beta^{0,\varphi}_{Mn,Cr,Si:C} + y_{Mn} \cdot y_{Cr} \cdot y_{Nb} \cdot \beta^{0,\varphi}_{Mn,Cr,Nb:C}$$

$$+ y_{Mn} \cdot y_{Cr} \cdot y_{Al} \cdot \beta^{0,\varphi}_{Mn,Cr,Al:C} + y_{Mn} \cdot y_{Si} \cdot y_{Nb} \cdot \beta^{0,\varphi}_{Mn,Si,Nb:C} + y_{Mn} \cdot y_{Si} \cdot y_{Al} \cdot \beta^{0,\varphi}_{Mn,Si,Al:C}$$

$$+ y_{Mn} \cdot y_{Nb} \cdot y_{Al} \cdot \beta^{0,\varphi}_{Mn,Nb,Al:C} + y_{Cr} \cdot y_{Si} \cdot y_{Nb} \cdot \beta^{0,\varphi}_{Cr,Si,Nb:C} + y_{Cr} \cdot y_{Si} \cdot y_{Al} \cdot \beta^{0,\varphi}_{Cr,Si,Al:C}$$

$$+ y_{Si} \cdot y_{Nb} \cdot y_{Al} \cdot \beta^{0,\varphi}_{Si,Nb,Al:C}$$

DEFINITION OF PARAMETER: <u>BMAGN (PHASE,Z:VA;0)</u>

(44)

$$\beta^{0,\Phi}_{Z:Va} = y_{Fe} \cdot \beta^{0,\Phi}_{Fe:Va} + y_{Mn} \cdot \beta^{0,\Phi}_{Mn:Va} + y_{Cr} \cdot \beta^{0,\Phi}_{Cr:Va} + y_{Si} \cdot \beta^{0,\Phi}_{Si:Va} + y_{Nb} \cdot \beta^{0,\Phi}_{Nb:Va} + y_{Al} \cdot \beta^{0,\Phi}_{Al:Va}$$

$$y_{Fe} \cdot y_{Mn} \cdot \beta^{0,\varphi}_{Fe,Mn:Va} + y_{Fe} \cdot y_{Mn} \cdot (y_{Fe} - y_{Mn}) \cdot \beta^{1,\varphi}_{Fe,Mn:Va} +$$

$$y_{Fe} \cdot y_{Cr} \cdot \beta^{0,\varphi}_{Fe,Cr:Va} + y_{Fe} \cdot y_{Cr} \cdot (y_{Fe} - y_{Cr}) \cdot \beta^{1,\varphi}_{Fe,Cr:Va} +$$

$$y_{Fe} \cdot y_{Si} \cdot \beta^{0,\varphi}_{Fe,Si:Va} + y_{Fe} \cdot y_{Si} \cdot (y_{Fe} - y_{Si}) \cdot \beta^{1,\varphi}_{Fe,Si:Va} +$$

$$y_{Fe} \cdot y_{Nb} \cdot \beta^{0,\varphi}_{Fe,Nb:Va} + y_{Fe} \cdot y_{Nb} \cdot (y_{Fe} - y_{Nb}) \cdot \beta^{1,\varphi}_{Fe,Nb:Va} +$$

$$y_{Fe} \cdot y_{Al} \cdot \beta^{0,\varphi}_{Fe,Al:Va} + y_{Fe} \cdot y_{Al} \cdot (y_{Fe} - y_{Al}) \cdot \beta^{1,\varphi}_{Fe,Al:Va} +$$

$$y_{Mn} \cdot y_{Cr} \cdot \beta^{0,\varphi}_{Mn,Cr:Va} + y_{Mn} \cdot y_{Cr} \cdot (y_{Mn} - y_{Cr}) \cdot \beta^{1,\varphi}_{Mn,Cr:Va} + y_{Mn} \cdot y_{Cr} \cdot (y_{Mn} - y_{Cr})^2 \cdot \beta^{2,\varphi}_{Mn,Cr:Va}$$

$$y_{Mn} \cdot y_{Si} \cdot \beta^{0,\varphi}_{Mn,Si:Va} + y_{Mn} \cdot y_{Si} \cdot (y_{Mn} - y_{Si}) \cdot \beta^{1,\varphi}_{Mn,Si:Va} +$$

$$y_{Mn} \cdot y_{Nb} \cdot \beta^{0,\varphi}_{Mn,Nb:Va} + y_{Mn} \cdot y_{Nb} \cdot (y_{Mn} - y_{Nb}) \cdot \beta^{1,\varphi}_{Mn,Nb:Va} +$$

$$y_{Mn} \cdot y_{Al} \cdot \beta^{0,\varphi}_{Mn,Al:Va} + y_{Mn} \cdot y_{Al} \cdot (y_{Mn} - y_{Al}) \cdot \beta^{1,\varphi}_{Mn,Al:Va} +$$

$$y_{Cr} \cdot y_{Si} \cdot \beta^{0,\varphi}_{Cr,Si:Va} + y_{Cr} \cdot y_{Si} \cdot (y_{Cr} - y_{Si}) \cdot \beta^{1,\varphi}_{Cr,Si:Va} +$$

$$y_{Cr} \cdot y_{Nb} \cdot \beta^{0,\varphi}_{Cr,Nb:Va} + y_{Cr} \cdot y_{Nb} \cdot (y_{Cr} - y_{Nb}) \cdot \beta^{1,\varphi}_{Cr,Nb:Va} +$$

$$y_{Cr} \cdot y_{Al} \cdot \beta^{0,\varphi}_{Cr,Al:Va} + y_{Cr} \cdot y_{Al} \cdot (y_{Cr} - y_{Al}) \cdot \beta^{1,\varphi}_{Cr,Al:Va} +$$

$$y_{Si} \cdot y_{Nb} \cdot \beta^{0,\varphi}_{Si,Nb:Va} + y_{Si} \cdot y_{Nb} \cdot (y_{Si} - y_{Nb}) \cdot \beta^{1,\varphi}_{Si,Nb:Va} +$$

$$y_{Si} \cdot y_{Al} \cdot \beta^{0,\varphi}_{Si,Al:Va} + y_{Si} \cdot y_{Al} \cdot (y_{Si} - y_{Al}) \cdot \beta^{1,\varphi}_{Si,Al:Va} +$$

$$y_{Nb} \cdot y_{Al} \cdot \beta^{0,\varphi}_{Nb,Al:C} + y_{Nb} \cdot y_{Al} \cdot (y_{Nb} - y_{Al}) \cdot \beta^{1,\varphi}_{Nb,Al:C} +$$

$$y_{Fe} \cdot y_{Mn} \cdot y_{Cr} \cdot \beta^{0,\varphi}_{Fe,Mn,Cr:Va} + y_{Fe} \cdot y_{Mn} \cdot y_{Si} \cdot \beta^{0,\varphi}_{Fe,Mn,Si:Va} + y_{Fe} \cdot y_{Mn} \cdot y_{Nb} \cdot \beta^{0,\varphi}_{Fe,Mn,Nb:Va}$$

$$+ y_{Fe} \cdot y_{Mn} \cdot y_{Al} \cdot \beta^{0,\varphi}_{Fe,Mn,Al:Va} + y_{Fe} \cdot y_{Cr} \cdot y_{Si} \cdot \beta^{0,\varphi}_{Fe,Cr,Si:Va} + y_{Fe} \cdot y_{Cr} \cdot y_{Nb} \cdot \beta^{0,\varphi}_{Fe,Cr,Nb:Va}$$

$$+y_{Fe}\cdot y_{Cr}\cdot y_{Al}\cdot \beta^{0,\varphi}_{Fe,Cr,Al:Va}+y_{Fe}\cdot y_{Si}\cdot y_{Nb}\cdot \beta^{0,\varphi}_{Fe,Si,Nb:Va}+y_{Fe}\cdot y_{Si}\cdot y_{Al}\cdot \beta^{0,\varphi}_{Fe,Si,Al:Va}$$

$$+y_{Fe}\cdot y_{Nb}\cdot y_{Al}\cdot L^{0,\varphi}_{Fe,Nb,Al:C}+y_{Mn}\cdot y_{Cr}\cdot y_{Si}\cdot \beta^{0,\varphi}_{Mn,Cr,Si:Va}+y_{Mn}\cdot y_{Cr}\cdot y_{Nb}\cdot \beta^{0,\varphi}_{Mn,Cr,Nb:Va}$$

$$+y_{Mn}\cdot y_{Cr}\cdot y_{Al}\cdot \beta^{0,\varphi}_{Mn,Cr,Al:Va}+y_{Mn}\cdot y_{Si}\cdot y_{Nb}\cdot \beta^{0,\varphi}_{Mn,Si,Nb:Va}+y_{Mn}\cdot y_{Si}\cdot y_{Al}\cdot \beta^{0,\varphi}_{Mn,Si,Al:Va}$$

$$+y_{Mn}\cdot y_{Nb}\cdot y_{Al}\cdot \beta^{0,\varphi}_{Mn,Nb,Al:Va}+y_{Cr}\cdot y_{Si}\cdot y_{Nb}\cdot \beta^{0,\varphi}_{Cr,Si,Nb:Va}+y_{Cr}\cdot y_{Si}\cdot y_{Al}\cdot \beta^{0,\varphi}_{Cr,Si,Al:Va}$$

$$+y_{Si}\cdot y_{Nb}\cdot y_{Al}\cdot \beta^{0,\varphi}_{Si,Nb,Al:Va}$$

DEFINITION OF PARAMETER: BMAGN (PHASE,Z:C,VA;0) (45)

$$\beta^{0,\varphi}_{Z:C,Va}=y_{Fe}\beta^{0,\varphi}_{Fe:C,Va}+y_{Mn}\beta^{0,\varphi}_{Mn:C,Va}+y_{Cr}\beta^{0,\varphi}_{Cr:C,Va}+y_{Si}\beta^{0,\varphi}_{Si:C,Va}+y_{Nb}\beta^{0,\varphi}_{Nb:C,Va}+y_{Al}\beta^{0,\varphi}_{Al:C,Va}$$

$$y_{Fe}\cdot y_{Mn}\cdot \beta^{0,\varphi}_{Fe,Mn:C,Va}+y_{Fe}\cdot y_{Cr}\cdot \beta^{0,\varphi}_{Fe,Cr:C,Va}+y_{Fe}\cdot y_{Si}\cdot \beta^{0,\varphi}_{Fe,Si:C,Va}+y_{Fe}\cdot y_{Nb}\cdot \beta^{0,\varphi}_{Fe,Nb:C,Va}$$

$$+y_{Fe}\cdot y_{Al}\cdot \beta^{0,\varphi}_{Fe,Al:C,Va}+y_{Mn}\cdot y_{Cr}\cdot \beta^{0,\varphi}_{Mn,Cr:C,Va}+y_{Mn}\cdot y_{Si}\cdot \beta^{0,\varphi}_{Mn,Si:C,Va}$$

$$+y_{Mn}\cdot y_{Nb}\cdot \beta^{0,\varphi}_{Mn,Nb:C,Va}+y_{Mn}\cdot y_{Al}\cdot \beta^{0,\varphi}_{Mn,Al:C,Va}+y_{Cr}\cdot y_{Si}\cdot \beta^{0,\varphi}_{Cr,Si:C,Va}$$

$$+y_{Cr}\cdot y_{Nb}\cdot \beta^{0,\varphi}_{Cr,Nb:C,Va}+y_{Cr}\cdot y_{Al}\cdot \beta^{0,\varphi}_{Cr,Al:C,Va}+y_{Si}\cdot y_{Nb}\cdot \beta^{0,\varphi}_{Si,Nb:C,Va}$$

$$+y_{Si}\cdot y_{Al}\cdot \beta^{0,\varphi}_{Si,Al:C,Va}+y_{Nb}\cdot y_{Al}\cdot \beta^{0,\varphi}_{Nb,Al:C,Va}$$

DEFINITION OF PARAMETER: BMAGN (PHASE,Z:C,VA;1) (46)

$$\beta^{1,\varphi}_{Z:C,Va}=y_{Fe}\beta^{1,\varphi}_{Fe:C,Va}+y_{Mn}\beta^{1,\varphi}_{Mn:C,Va}+y_{Cr}\beta^{1,\varphi}_{Cr:C,Va}+y_{Si}\beta^{1,\varphi}_{Si:C,Va}+y_{Nb}\beta^{1,\varphi}_{Nb:C,Va}++y_{Al}\beta^{1,\varphi}_{Al:C,Va}$$

$$y_{Fe} \cdot y_{Mn}(y_{Fe} - y_{Mn})\beta^{1,\varphi}_{Fe,Mn:C,Va} + y_{Fe} \cdot y_{Cr} \cdot (y_{Fe} - y_{Cr}) \cdot \beta^{1,\varphi}_{Fe,Cr:C,Va} + y_{Fe} \cdot y_{Si} \cdot (y_{Fe}$$

$$- y_{Si}) \cdot \beta^{1,\varphi}_{Fe,Si:C,Va} + y_{Fe} \cdot y_{Nb} \cdot (y_{Fe} - y_{Nb}) \cdot \beta^{1,\varphi}_{Fe,Nb:C,Va} + y_{Fe}$$

$$\cdot y_{Al} \cdot (y_{Fe} - y_{Al}) \cdot \beta^{1,\varphi}_{Fe,Al:C,Va} + y_{Mn} \cdot y_{Cr} \cdot (y_{Mn} - y_{Cr}) \cdot \beta^{1,\varphi}_{Mn,Cr:C,Va}$$

$$+ y_{Mn} \cdot y_{Si} \cdot (y_{Mn} - y_{Si}) \cdot \beta^{1,\varphi}_{Mn,Si:C,Va} + y_{Mn} \cdot y_{Nb} \cdot (y_{Mn} - y_{Nb}) \cdot \beta^{1,\varphi}_{Mn,Nb:C,Va}$$

$$+ y_{Mn} \cdot y_{Al} \cdot (y_{Mn} - y_{Al}) \cdot \beta^{1,\varphi}_{Mn,Al:C,Va} + y_{Cr} \cdot y_{Si} \cdot (y_{Cr} - y_{Si}) \cdot \beta^{1,\varphi}_{Cr,Si:C,Va}$$

$$+ y_{Cr} \cdot y_{Nb} \cdot (y_{Cr} - y_{Nb}) \cdot \beta^{1,\varphi}_{Cr,Nb:C,Va} + y_{Cr} \cdot y_{Al} \cdot (y_{Cr} - y_{Al}) \cdot \beta^{1,\varphi}_{Cr,Al:C,Va}$$

$$+ y_{Si} \cdot y_{Nb} \cdot (y_{Si} - y_{Nb}) \cdot \beta^{1,\varphi}_{Si,Nb:C,Va} + y_{Si} \cdot y_{Al} \cdot (y_{Si} - y_{Al}) \cdot \beta^{1,\varphi}_{Si,Al:C,Va}$$

$$+ y_{Nb} \cdot y_{Al} \cdot (y_{Nb} - y_{Al}) \cdot \beta^{1,\varphi}_{Nb,Al:C,Va}$$

DEFINITION OF PARAMETER: TC(PHASE,Z:C;0)

(47)

$$T_{C^{0,\Phi}_{Z:C}} = y_{Fe} \cdot T_{C^{0,\Phi}_{Fe:C}} + y_{Mn} \cdot T_{C^{0,\Phi}_{Mn:C}} + y_{Cr} \cdot T_{C^{0,\Phi}_{Cr:C}} + y_{Si} \cdot T_{C^{0,\Phi}_{Si:C}} + y_{Nb} \cdot T_{C^{0,\Phi}_{Nb:C}} + y_{Al} \cdot T_{C^{0,\Phi}_{Al:C}}$$

$$y_{Fe} \cdot y_{Mn} \cdot T_{C^{0,\varphi}_{Fe,Mn:C}} + y_{Fe} \cdot y_{Mn} \cdot (y_{Fe} - y_{Mn}) \cdot T_{C^{1,\varphi}_{Fe,Mn:C}} +$$

$$y_{Fe} \cdot y_{Cr} \cdot T_{C^{0,\varphi}_{Fe,Cr:C}} + y_{Fe} \cdot y_{Cr} \cdot (y_{Fe} - y_{Cr}) \cdot T_{C^{1,\varphi}_{Fe,Cr:C}} +$$

$$y_{Fe} \cdot y_{Si} \cdot T_{C^{0,\varphi}_{Fe,Si:C}} + y_{Fe} \cdot y_{Si} \cdot (y_{Fe} - y_{Si}) \cdot T_{C^{1,\varphi}_{Fe,Si:C}} +$$

$$y_{Fe} \cdot y_{Nb} \cdot T_{C^{0,\varphi}_{Fe,Nb:C}} + y_{Fe} \cdot y_{Nb} \cdot (y_{Fe} - y_{Nb}) \cdot T_{C^{1,\varphi}_{Fe,Nb:C}} +$$

$$y_{Fe} \cdot y_{Al} \cdot T_{C^{0,\varphi}_{Fe,Al:C}} + y_{Fe} \cdot y_{Al} \cdot (y_{Fe} - y_{Al}) \cdot T_{C^{1,\varphi}_{Fe,Al:C}} +$$

$$y_{Mn} \cdot y_{Cr} \cdot T_{C^{0,\varphi}_{Mn,Cr:C}} + y_{Mn} \cdot y_{Cr} \cdot (y_{Mn} - y_{Cr}) \cdot T_{C^{1,\varphi}_{Mn,Cr:C}} +$$

$$y_{Mn} \cdot y_{Si} \cdot T_{C^{0,\varphi}_{Mn,Si:C}} + y_{Mn} \cdot y_{Si} \cdot (y_{Mn} - y_{Si}) \cdot T_{C^{1,\varphi}_{Mn,Si:C}} +$$

$$y_{Mn} \cdot y_{Nb} \cdot T_{C^{0,\varphi}_{Mn,Nb:C}} + y_{Mn} \cdot y_{Nb} \cdot (y_{Mn} - y_{Nb}) \cdot T_{C^{1,\varphi}_{Mn,Nb:C}} +$$

$$y_{Mn} \cdot y_{Al} \cdot T_{C\,Mn,Al:C}^{0,\varphi} + y_{Mn} \cdot y_{Al} \cdot (y_{Mn} - y_{Al}) \cdot T_{C\,Mn,Al:C}^{1,\varphi} +$$

$$y_{Cr} \cdot y_{Si} \cdot T_{C\,Cr,Si:C}^{0,\varphi} + y_{Cr} \cdot y_{Si} \cdot (y_{Cr} - y_{Si}) \cdot T_{C\,Cr,Si:C}^{1,\varphi} +$$

$$y_{Cr} \cdot y_{Nb} \cdot T_{C\,Cr,Nb:C}^{0,\varphi} + y_{Cr} \cdot y_{Nb} \cdot (y_{Cr} - y_{Nb}) \cdot T_{C\,Cr,Nb:C}^{1,\varphi} +$$

$$y_{Cr} \cdot y_{Al} \cdot T_{C\,Cr,Al:C}^{0,\varphi} + y_{Cr} \cdot y_{Al} \cdot (y_{Cr} - y_{Al}) \cdot T_{C\,Cr,Al:C}^{1,\varphi} +$$

$$y_{Si} \cdot y_{Nb} \cdot T_{C\,Si,Nb:C}^{0,\varphi} + y_{Si} \cdot y_{Nb} \cdot (y_{Si} - y_{Nb}) \cdot T_{C\,Si,Nb:C}^{1,\varphi} +$$

$$y_{Si} \cdot y_{Al} \cdot T_{C\,Si,Al:C}^{0,\varphi} + y_{Si} \cdot y_{Al} \cdot (y_{Si} - y_{Al}) \cdot T_{C\,Si,Al:C}^{1,\varphi} +$$

$$y_{Nb} \cdot y_{Al} \cdot L_{Nb,Al:C}^{0,\varphi} + y_{Nb} \cdot y_{Al} \cdot (y_{Nb} - y_{Al}) \cdot L_{Nb,Al:C}^{1,\varphi} +$$

$$y_{Fe} \cdot y_{Mn} \cdot y_{Cr} \cdot T_{C\,Fe,Mn,Cr:C}^{0,\varphi} + y_{Fe} \cdot y_{Mn} \cdot y_{Si} \cdot T_{C\,Fe,Mn,Si:C}^{0,\varphi} + y_{Fe} \cdot y_{Mn} \cdot y_{Nb} \cdot T_{C\,Fe,Mn,Nb:C}^{0,\varphi} + y_{Fe}$$

$$\cdot y_{Mn} \cdot y_{Al} \cdot T_{C\,Fe,Mn,Al:C}^{0,\varphi} + y_{Fe} \cdot y_{Cr} \cdot y_{Si} \cdot T_{C\,Fe,Cr,Si:C}^{0,\varphi} + y_{Fe} \cdot y_{Cr} \cdot y_{Nb}$$

$$\cdot T_{C\,Fe,Cr,Nb:C}^{0,\varphi} + y_{Fe} \cdot y_{Cr} \cdot y_{Al} \cdot T_{C\,Fe,Cr,Al:C}^{0,\varphi} + y_{Fe} \cdot y_{Si} \cdot y_{Nb} \cdot T_{C\,Fe,Si,Nb:C}^{0,\varphi} + y_{Fe}$$

$$\cdot y_{Si} \cdot y_{Al} \cdot T_{C\,Fe,Si,Al:C}^{0,\varphi} + y_{Mn} \cdot y_{Cr} \cdot y_{Si} \cdot T_{C\,Mn,Cr,Si:C}^{0,\varphi} + y_{Mn} \cdot y_{Cr} \cdot y_{Nb}$$

$$\cdot T_{C\,Mn,Cr,Nb:C}^{0,\varphi} + y_{Mn} \cdot y_{Cr} \cdot y_{Al} \cdot T_{C\,Mn,Cr,Al:C}^{0,\varphi} + y_{Mn} \cdot y_{Si} \cdot y_{Nb} \cdot T_{C\,Mn,Si,Nb:C}^{0,\varphi} + y_{Mn}$$

$$\cdot y_{Si} \cdot y_{Al} \cdot T_{C\,Mn,Si,Al:C}^{0,\varphi} + y_{Mn} \cdot y_{Nb} \cdot y_{Al} \cdot T_{C\,Mn,Nb,Al:C}^{0,\varphi} + y_{Cr} \cdot y_{Si} \cdot y_{Nb}$$

$$\cdot T_{C\,Cr,Si,Nb:C}^{0,\varphi} + y_{Cr} \cdot y_{Si} \cdot y_{Al} \cdot T_{C\,Cr,Si,Al:C}^{0,\varphi} + y_{Si} \cdot y_{Nb} \cdot y_{Al} \cdot T_{C\,Si,Nb,Al:C}^{0,\varphi}$$

DEFINITION OF PARAMETER: <u>TC(PHASE,Z:VA;0)</u>

(48)

$$T_{C\,Z:Va}^{0,\Phi} = y_{Fe} \cdot T_{C\,Fe:Va}^{0,\Phi} + y_{Mn} \cdot T_{C\,Mn:Va}^{0,\Phi} + y_{Cr} \cdot T_{C\,Cr:Va}^{0,\Phi} + y_{Si} \cdot T_{C\,Si:Va}^{0,\Phi} + y_{Nb} \cdot T_{C\,Nb:Va}^{0,\Phi} +$$

$$+ y_{Al} \cdot G_{Al:Va}^{0,\Phi} +$$

$$y_{Fe} \cdot y_{Mn} \cdot T_{C_{Fe,Mn:Va}}^{0,\varphi} + y_{Fe} \cdot y_{Mn} \cdot (y_{Fe} - y_{Mn}) \cdot T_{C_{Fe,Mn:Va}}^{1,\varphi} +$$

$$y_{Fe} \cdot y_{Cr} \cdot T_{C_{Fe,Cr:Va}}^{0,\varphi} + y_{Fe} \cdot y_{Cr} \cdot (y_{Fe} - y_{Cr}) \cdot T_{C_{Fe,Cr:Va}}^{1,\varphi} +$$

$$y_{Fe} \cdot y_{Si} \cdot T_{C_{Fe,Si:Va}}^{0,\varphi} + y_{Fe} \cdot y_{Si} \cdot (y_{Fe} - y_{Si}) \cdot T_{C_{Fe,Si:Va}}^{1,\varphi} +$$

$$y_{Fe} \cdot y_{Nb} \cdot T_{C_{Fe,Nb:Va}}^{0,\varphi} + y_{Fe} \cdot y_{Nb} \cdot (y_{Fe} - y_{Nb}) \cdot T_{C_{Fe,Nb:Va}}^{1,\varphi} +$$

$$y_{Fe} \cdot y_{Al} \cdot T_{C_{Fe,Al:Va}}^{0,\varphi} + y_{Fe} \cdot y_{Al} \cdot (y_{Fe} - y_{Al}) \cdot T_{C_{Fe,Al:Va}}^{1,\varphi} +$$

$$y_{Mn} \cdot y_{Cr} \cdot T_{C_{Mn,Cr:Va}}^{0,\varphi} + y_{Mn} \cdot y_{Cr} \cdot (y_{Mn} - y_{Cr}) \cdot T_{C_{Mn,Cr:Va}}^{1,\varphi} +$$

$$y_{Mn} \cdot y_{Si} \cdot L_{Mn,Si:Va}^{0,\varphi} + y_{Mn} \cdot y_{Si} \cdot (y_{Mn} - y_{Si}) \cdot L_{Mn,Si:Va}^{1,\varphi} +$$

$$y_{Mn} \cdot y_{Nb} \cdot T_{C_{Mn,Nb:Va}}^{0,\varphi} + y_{Mn} \cdot y_{Nb} \cdot (y_{Mn} - y_{Nb}) \cdot T_{C_{Mn,Nb:Va}}^{1,\varphi} +$$

$$y_{Mn} \cdot y_{Al} \cdot T_{C_{Mn,Al:Va}}^{0,\varphi} + y_{Mn} \cdot y_{Al} \cdot (y_{Mn} - y_{Al}) \cdot T_{C_{Mn,Al:Va}}^{1,\varphi} +$$

$$y_{Cr} \cdot y_{Si} \cdot T_{C_{Cr,Si:Va}}^{0,\varphi} + y_{Cr} \cdot y_{Si} \cdot (y_{Cr} - y_{Si}) \cdot T_{C_{Cr,Si:Va}}^{1,\varphi} +$$

$$y_{Cr} \cdot y_{Nb} \cdot T_{C_{Cr,Nb:Va}}^{0,\varphi} + y_{Cr} \cdot y_{Nb} \cdot (y_{Cr} - y_{Nb}) \cdot T_{C_{Cr,Nb:Va}}^{1,\varphi} +$$

$$y_{Cr} \cdot y_{Al} \cdot T_{C_{Cr,Al:Va}}^{0,\varphi} + y_{Cr} \cdot y_{Al} \cdot (y_{Cr} - y_{Al}) \cdot T_{C_{Cr,Al:Va}}^{1,\varphi} +$$

$$y_{Si} \cdot y_{Nb} \cdot T_{C_{Si,Nb:Va}}^{0,\varphi} + y_{Si} \cdot y_{Nb} \cdot (y_{Si} - y_{Nb}) \cdot T_{C_{Si,Nb:Va}}^{1,\varphi} +$$

$$y_{Si} \cdot y_{Al} \cdot T_{C_{Si,Al:Va}}^{0,\varphi} + y_{Si} \cdot y_{Al} \cdot (y_{Si} - y_{Al}) \cdot T_{C_{Si,Al:Va}}^{1,\varphi} +$$

$$y_{Fe} \cdot y_{Mn} \cdot y_{Cr} \cdot T_{C_{Fe,Mn,Cr:Va}}^{0,\varphi} + y_{Fe} \cdot y_{Mn} \cdot y_{Si} \cdot T_{C_{Fe,Mn,Si:Va}}^{0,\varphi} + y_{Fe} \cdot y_{Mn} \cdot y_{Nb} \cdot T_{C_{Fe,Mn,Nb:Va}}^{0,\varphi}$$

$$+ y_{Fe} \cdot y_{Mn} \cdot y_{Al} \cdot T_{C_{Fe,Mn,Al:Va}}^{0,\varphi} + y_{Fe} \cdot y_{Cr} \cdot y_{Si} \cdot T_{C_{Fe,Cr,Si:Va}}^{0,\varphi} + y_{Fe} \cdot y_{Cr} \cdot y_{Nb}$$

$$\cdot T_{C_{Fe,Cr,Nb:Va}}^{0,\varphi} + y_{Fe} \cdot y_{Cr} \cdot y_{Al} \cdot T_{C_{Fe,Cr,Al:Va}}^{0,\varphi} + y_{Fe} \cdot y_{Si} \cdot y_{Nb} \cdot T_{C_{Fe,Si,Nb:Va}}^{0,\varphi} + y_{Fe}$$

$$\cdot y_{Si} \cdot y_{Al} \cdot T_{C_{Fe,Si,Al:Va}}^{0,\varphi} + y_{Mn} \cdot y_{Cr} \cdot y_{Si} \cdot T_{C_{Mn,Cr,Si:Va}}^{0,\varphi} + y_{Mn} \cdot y_{Cr} \cdot y_{Nb}$$

$$\cdot T_{C_{Mn,Cr,Nb:Va}}^{0,\varphi} + y_{Mn} \cdot y_{Cr} \cdot y_{Al} \cdot T_{C_{Mn,Cr,Al:Va}}^{0,\varphi} + y_{Mn} \cdot y_{Si} \cdot y_{Nb} \cdot T_{C_{Mn,Si,Nb:Va}}^{0,\varphi}$$

$$+ y_{Mn} \cdot y_{Si} \cdot y_{Al} \cdot T_{C_{Mn,Si,Al:Va}}^{0,\varphi} + y_{Cr} \cdot y_{Si} \cdot y_{Nb} \cdot T_{C_{Cr,Si,Nb:Va}}^{0,\varphi} + y_{Cr} \cdot y_{Si} \cdot y_{Al}$$

$$\cdot T_{C_{Cr,Si,Al:Va}}^{0,\varphi} + y_{Si} \cdot y_{Nb} \cdot y_{Al} \cdot T_{C_{Si,Nb,Al:Va}}^{0,\varphi}$$

DEFINITION OF PARAMETER: TC(PHASE,Z:C,VA;0)

(49)

$$T_{C_{Z:C,Va}}^{0,\varphi} = y_{Fe} T_{C_{Fe:C,Va}}^{0,\varphi} + y_{Mn} T_{C_{Mn:C,Va}}^{0,\varphi} + y_{Cr} T_{C_{Cr:C,Va}}^{0,\varphi} + y_{Si} T_{C_{Si:C,Va}}^{0,\varphi} + y_{Nb} T_{C_{Nb:C,Va}}^{0,\varphi} + y_{Al} L_{Al:C,Va}^{0,\varphi}$$

$$y_{Fe} \cdot y_{Mn} \cdot T_{C_{Fe,Mn:C,Va}}^{0,\varphi} + y_{Fe} \cdot y_{Cr} \cdot T_{C_{Fe,Cr:C,Va}}^{0,\varphi} + y_{Fe} \cdot y_{Si} \cdot T_{C_{Fe,Si:C,Va}}^{0,\varphi} + y_{Fe} \cdot y_{Nb} \cdot$$

$$T_{C_{Fe,Nb:C,Va}}^{0,\varphi} + y_{Fe} \cdot y_{Al} \cdot T_{C_{Fe,Al:C,Va}}^{0,\varphi} + y_{Mn} \cdot y_{Cr} \cdot T_{C_{Mn,Cr:C,Va}}^{0,\varphi} + y_{Mn} \cdot y_{Si} \cdot T_{C_{Mn,Si:C,Va}}^{0,\varphi} +$$

$$y_{Mn} \cdot y_{Nb} \cdot T_{C_{Mn,Nb:C,Va}}^{0,\varphi} + y_{Mn} \cdot y_{Al} \cdot T_{C_{Mn,Al:C,Va}}^{0,\varphi} + y_{Cr} \cdot y_{Si} \cdot T_{C_{Cr,Si:C,Va}}^{0,\varphi} + y_{Cr} \cdot y_{Nb} \cdot$$

$$T_{C_{Cr,Nb:C,Va}}^{0,\varphi} + y_{Cr} \cdot y_{Al} \cdot T_{C_{Cr,Al:C,Va}}^{0,\varphi} + y_{Si} \cdot y_{Nb} \cdot T_{C_{Si,Nb:C,Va}}^{0,\varphi} + y_{Si} \cdot y_{Al} \cdot T_{C_{Si,Al:C,Va}}^{0,\varphi} +$$

$$y_{Nb} \cdot y_{Al} \cdot T_{C_{Nb,Al:C,Va}}^{0,\varphi}$$

DEFINITION OF PARAMETER: TC(PHASE,Z:C,VA;1)

(50)

$$T_{C_{Z:C,Va}}^{1,\varphi} = y_{Fe} T_{C_{Fe:C,Va}}^{1,\varphi} + y_{Mn} T_{C_{Mn:C,Va}}^{1,\varphi} + y_{Cr} T_{C_{Cr:C,Va}}^{1,\varphi} + y_{Si} T_{C_{Si:C,Va}}^{1,\varphi} + y_{Nb} T_{C_{Nb:C,Va}}^{1,\varphi} + y_{Al} T_{C_{Al:C,Va}}^{1,\varphi}$$

$$+$$

$$y_{Fe} \cdot y_{Mn}(y_{Fe} - y_{Mn}) T^{1,\varphi}_{C_{Fe,Mn:C,Va}} + y_{Fe} \cdot y_{Cr} \cdot (y_{Fe} - y_{Cr}) \cdot T^{1,\varphi}_{C_{Fe,Cr:C,Va}} + y_{Fe} \cdot y_{Si} \cdot (y_{Fe}$$

$$- y_{Si}) \cdot T^{1,\varphi}_{C_{Fe,Si:C,Va}} + y_{Fe} \cdot y_{Nb} \cdot (y_{Fe} - y_{Nb}) \cdot T^{1,\varphi}_{C_{Fe,Nb:C,Va}} + y_{Fe}$$

$$\cdot y_{Al} \cdot (y_{Fe} - y_{Al}) \cdot T^{1,\varphi}_{C_{Fe,Al:C,Va}} + y_{Mn} \cdot y_{Cr} \cdot (y_{Mn} - y_{Cr}) \cdot T^{1,\varphi}_{C_{Mn,Cr:C,Va}}$$

$$+ y_{Mn} \cdot y_{Si} \cdot (y_{Mn} - y_{Si}) \cdot T^{1,\varphi}_{C_{Mn,Si:C,Va}} + y_{Mn} \cdot y_{Nb} \cdot (y_{Mn} - y_{Nb}) \cdot T^{1,\varphi}_{C_{Mn,Nb:C,Va}}$$

$$+ y_{Mn} \cdot y_{Al} \cdot (y_{Mn} - y_{Al}) \cdot T^{1,\varphi}_{C_{Mn,Al:C,Va}} + y_{Cr} \cdot y_{Si} \cdot (y_{Cr} - y_{Si}) \cdot T^{1,\varphi}_{C_{Cr,Si:C,Va}}$$

$$+ y_{Cr} \cdot y_{Nb} \cdot (y_{Cr} - y_{Nb}) \cdot T^{1,\varphi}_{C_{Cr,Nb:C,Va}} + y_{Cr} \cdot y_{Al} \cdot (y_{Cr} - y_{Al}) \cdot T^{1,\varphi}_{C_{Cr,Al:C,Va}}$$

$$+ y_{Si} \cdot y_{Nb} \cdot (y_{Si} - y_{Nb}) \cdot T^{1,\varphi}_{C_{Si,Nb:C,Va}} + y_{Si} \cdot y_{Al} \cdot (y_{Si} - y_{Al}) \cdot T^{1,\varphi}_{C_{Si,Al:C,Va}}$$

$$+ y_{Nb} \cdot y_{Al} \cdot (y_{Nb} - y_{Al}) \cdot T^{1,\varphi}_{C_{Nb,Al:C,Va}}$$

9.2 2nd STEP: Acquisition of GES phase description for THERMOCALC

Below is the list of the REDLICH-KISTER_MUGGIANU equations participating in austenite are described.

FCC_A1

```
 EXCESS MODEL IS REDLICH-KISTER_MUGGIANU
 ADDITIONAL CONTRIBUTION FROM MAGNETIC ORDERING
    Magnetic function below Curie Temperature
    +1-.860338755*TAO**(-1)-.17449124*TAO**3-.00775516624*TAO**9
    -.0017449124*TAO**15
    Magnetic function above Curie Temperature
     -.0426902268*TAO**(-5)-.0013552453*TAO**(-15)
    -2.84601512E-04*TAO**(-25)
 2 SUBLATTICES, SITES  1:  1
  CONSTITUENTS: AL,CR,FE,MN,NB,SI,Z : C,VA

    G(FCC_A1,AL:C;0)-H298(FCC_A1,AL;0)-H298(GRAPHITE,C;0) *** UNASSESSED ***
    G(FCC_A1,CR:C;0)-H298(GRAPHITE,C;0)-H298(BCC_A2,CR;0) = +GHSERCR
       +GHSERCC+1200-1.94*T
    G(FCC_A1,FE:C;0)-H298(GRAPHITE,C;0)-H298(BCC_A2,FE;0) = +77207
       -15.877*T+GFEFCC+GHSERCC+GPCFCC
    TC(FCC_A1,FE:C;0) = -201
    BMAGN(FCC_A1,FE:C;0) = -2.1
    G(FCC_A1,MN:C;0)-H298(GRAPHITE,C;0)-H298(CBCC_A12,MN;0) = +502
       +15.261*T+GHSERMN+GHSERCC
    G(FCC_A1,NB:C;0)-H298(GRAPHITE,C;0)-H298(BCC_A2,NB;0) = -136399
       +43.8135*T-5.497*T*LN(T)+.00173994*T**2+GHEXTNB+GHSERCC
    G(FCC_A1,SI:C;0)-H298(GRAPHITE,C;0)-H298(DIAMOND_A4,SI;0) = +GHSERSI
```

+GHSERCC-20510+38.7*T

G(FCC_A1,Z:C;0)-H298(GRAPHITE,C;0)-H298(BCC_A2,Z;0) = +LAE1+LAE2

BMAGN(FCC_A1,Z:C;0) = +Y1*BA1

TC(FCC_A1,Z:C;0) = +Y1*TA1

G(FCC_A1,AL:VA;0)-H298(FCC_A1,AL;0) = 298.15<T< 2900.00: +GHSERAL

G(FCC_A1,CR:VA;0)-H298(BCC_A2,CR;0) = +GCRFCC+GPCRBCC

TC(FCC_A1,CR:VA;0) = -1109

BMAGN(FCC_A1,CR:VA;0) = -2.46

G(FCC_A1,FE:VA;0)-H298(BCC_A2,FE;0) = +GFEFCC+GPFEFCC

TC(FCC_A1,FE:VA;0) = -201

BMAGN(FCC_A1,FE:VA;0) = -2.1

G(FCC_A1,MN:VA;0)-H298(CBCC_A12,MN;0) = +GMNFCC

TC(FCC_A1,MN:VA;0) = 298.15<T< 2000.00: -1620

BMAGN(FCC_A1,MN:VA;0) = 298.15<T< 2000.00: -1.86

G(FCC_A1,NB:VA;0)-H298(BCC_A2,NB;0) = +13500+1.7*T+GHEXTNB

G(FCC_A1,SI:VA;0)-H298(DIAMOND_A4,SI;0) =

298.15<T< 3600.00: +51000-21.8*T+GHSERSI

G(FCC_A1,Z:VA;0)-H298(BCC_A2,Z;0) = +GAZVA1+GAZVA2+GAZVA3+GAZVA4

BMAGN(FCC_A1,Z:VA;0) = +Y1*BA2+Y2*BA3+Y3*BA4+Y4*BA5+Y5*BA6

TC(FCC_A1,Z:VA;0) = +Y1*TA2+Y2*TA3+Y3*TA4+Y7*TA5+Y8*TA6+Y38*TA7

L(FCC_A1,CR,FE:C;0) = -74319+3.2353*T

L(FCC_A1,CR,MN:C;0) = 56000

L(FCC_A1,CR:C,VA;0) = -11977+6.8194*T

L(FCC_A1,FE,MN:C;0) = +34052-23.467*T

L(FCC_A1,FE,NB:C,VA;0) = -40000

L(FCC_A1,FE,SI:C;0) = +143220+39.31*T

L(FCC_A1,FE,SI:C;1) = -216321

L(FCC_A1,FE:C,VA;0) = -34671

L(FCC_A1,MN:C,VA;0) = -43433

L(FCC_A1,NB:C,VA;0) = -98823+11.525*T

L(FCC_A1,Z:C,VA;0) = +Y1*LA29+Y2*LA30+Y3*LA31+Y5*LA32+Y13*LA33

L(FCC_A1,AL,CR:VA;0) = -63800-5*T

L(FCC_A1,AL,CR:VA;1) = 8000

L(FCC_A1,AL,CR:VA;2) = -4000

L(FCC_A1,AL,FE:VA;0) = -76066.1+18.6758*T

L(FCC_A1,AL,FE:VA;1) = +21167.4+1.3398*T

L(FCC_A1,AL,MN:VA;0) = -83829+37.6788*T

L(FCC_A1,AL,MN:VA;1) = +18378-5.07*T

L(FCC_A1,AL,SI:VA;0) = 298.15<T< 2000.00: -3749.9-2.58962*T

L(FCC_A1,CR,FE:VA;0) = +10833-7.477*T

L(FCC_A1,CR,FE:VA;1) = 1410

L(FCC_A1,CR,FE,MN:VA;0) = -6815

L(FCC_A1,CR,MN:VA;0) = -19088+17.5423*T

L(FCC_A1,CR,SI:VA;0) = -122850+9.85457*T

L(FCC_A1,CR,SI:VA;1) = -49502+13.76967*T

L(FCC_A1,FE,MN:VA;0) = -7762+3.865*T

L(FCC_A1,FE,MN:VA;1) = -259

TC(FCC_A1,FE,MN:VA;0) = -2282

TC(FCC_A1,FE,MN:VA;1) = -2068

L(FCC_A1,FE,MN,SI:VA;0) = -56655-55.613*T

TC(FCC_A1,FE,MN,SI:VA;0) = 13854

L(FCC_A1,FE,NB:VA;0) = -4784

L(FCC_A1,FE,SI:VA;0) = -125248+41.116*T

L(FCC_A1,FE,SI:VA;1) = -142708

L(FCC_A1,FE,SI:VA;2) = 89907

L(FCC_A1,MN,SI:VA;0) = -95600+2.94097*T

L(FCC_A1,MN,SI:VA;1) = -7500

GES:

Following is the list of the REDLICH-KISTER_MUGGIANU equation participating in ferrite are described.

BCC_A2

EXCESS MODEL IS REDLICH-KISTER_MUGGIANU

ADDITIONAL CONTRIBUTION FROM MAGNETIC ORDERING

Magnetic function below Curie Temperature

+1-.905299383*TAO**(-1)-.153008346*TAO**3-.00680037095*TAO**9

-.00153008346*TAO**15

Magnetic function above Curie Temperature

-.0641731208*TAO**(-5)-.00203724193*TAO**(-15)

-4.27820805E-04*TAO**(-25)

2 SUBLATTICES, SITES 1: 3

CONSTITUENTS: AL,CR,FE,MN,NB,SI,Z : C,VA

G(BCC_A2,AL:C;0)-H298(FCC_A1,AL;0)- 3 H298(GRAPHITE,C;0) ***

UNASSESSED ***

G(BCC_A2,CR:C;0)- 3 H298(GRAPHITE,C;0)-H298(BCC_A2,CR;0) = +GHSERCR

+3*GHSERCC+GPCRBCC+3*GPCGRA+416000

TC(BCC_A2,CR:C;0) = -311.5

BMAGN(BCC_A2,CR:C;0) = -.008

G(BCC_A2,FE:C;0)- 3 H298(GRAPHITE,C;0)-H298(BCC_A2,FE;0) = +322050

+75.667*T+GHSERFE+GPFEBCC+3*GHSERCC+3*GPCGRA

TC(BCC_A2,FE:C;0) = 1043

BMAGN(BCC_A2,FE:C;0) = 2.22

G(BCC_A2,MN:C;0)- 3 H298(GRAPHITE,C;0)-H298(CBCC_A12,MN;0) = +10000

+30*T+GHSERMN+3*GHSERCC

G(BCC_A2,NB:C;0)- 3 H298(GRAPHITE,C;0)-H298(BCC_A2,NB;0) = +313790

-50*T+GHSERNB+3*GHSERCC

G(BCC_A2,SI:C;0)- 3 H298(GRAPHITE,C;0)-H298(DIAMOND_A4,SI;0) = +322050

-75.667*T+GSIBCC+3*GHSERCC+3*GPCGRA

G(BCC_A2,Z:C;0)- 3 H298(GRAPHITE,C;0)-H298(BCC_A2,Z;0) = +Y1*GF1

+Y2*GF2+Y3*GF3+Y4*GF4+Y5*GF5+R*T*SYLNY+Y7*LF1+Y9*LF3+Y11*LF5

BMAGN(BCC_A2,Z:C;0) = +Y1*BF1+Y3*BF3+Y9*BF9

TC(BCC_A2,Z:C;0) = +Y1*TF1+Y3*TF3+Y9*TF4+Y10*TF5

G(BCC_A2,AL:VA;0)-H298(FCC_A1,AL;0) = 298.15<T< 2900.00: +GALBCC

G(BCC_A2,CR:VA;0)-H298(BCC_A2,CR;0) = +GHSERCR+GPCRBCC

TC(BCC_A2,CR:VA;0) = -311.5

BMAGN(BCC_A2,CR:VA;0) = -.01

G(BCC_A2,FE:VA;0)-H298(BCC_A2,FE;0) = +GHSERFE+GPFEBCC

TC(BCC_A2,FE:VA;0) = 1043

BMAGN(BCC_A2,FE:VA;0) = 2.22

G(BCC_A2,MN:VA;0)-H298(CBCC_A12,MN;0) = +GMNBCC

TC(BCC_A2,MN:VA;0) = 298.15<T< 2000.00: -580

BMAGN(BCC_A2,MN:VA;0) = 298.15<T< 2000.00: -.27

G(BCC_A2,NB:VA;0)-H298(BCC_A2,NB;0) = +GHSERNB

G(BCC_A2,SI:VA;0)-H298(DIAMOND_A4,SI;0) = 298.15<T< 3600.00: +GSIBCC

G(BCC_A2,Z:VA;0)-H298(BCC_A2,Z;0) = +GFZVA1+GFZVA2+GFZVA3

BMAGN(BCC_A2,Z:VA;0) = +Y1*BF37+Y2*BF38+Y3*BF39+Y9*BF45+Y17*BF53

TC(BCC_A2,Z:VA;0)=+Y1*TF6+Y2*TF7+Y3*TF8+Y7*TF9+Y9*TF10+Y10*TF11
  +Y12*TF12+Y16*TF13+Y17*TF14

L(BCC_A2,CR,FE:C;0) = -1250000+667.7*T

TC(BCC_A2,CR,FE:C;0) = 1650

TC(BCC_A2,CR,FE:C;1) = 550

BMAGN(BCC_A2,CR,FE:C;0) = -.85

L(BCC_A2,CR:C,VA;0) = -190*T

L(BCC_A2,FE,MN:C;0) = +34052-23.467*T

L(BCC_A2,FE,SI:C;0) = 78866

L(BCC_A2,FE:C,VA;0) = -190*T

L(BCC_A2,NB:C,VA;0) = -452303

L(BCC_A2,Z:C,VA;0) = +Y1*LF80+Y3*LF82+Y5*LF84

L(BCC_A2,AL,CR:VA;0) = -55370-10*T

L(BCC_A2,AL,CR:VA;1) = +1830-10*T

L(BCC_A2,AL,CR:VA;2) = -8800

L(BCC_A2,AL,FE:VA;0) = +4*LALFEB0-4*ALFEW1

L(BCC_A2,AL,FE:VA;1) = +8*LALFEB1

TC(BCC_A2,AL,FE:VA;1) = +8*ETCALFE

L(BCC_A2,AL,MN:VA;0) = -120077+52.851*T

L(BCC_A2,AL,MN:VA;1) = -40652+29.2764*T

L(BCC_A2,CR,FE:VA;0) = +20500-9.68*T

TC(BCC_A2,CR,FE:VA;0) = 1650

TC(BCC_A2,CR,FE:VA;1) = 550

BMAGN(BCC_A2,CR,FE:VA;0) = -.85

L(BCC_A2,CR,FE,MN:VA;0) = -8374

L(BCC_A2,CR,MN:VA;0) = -20328+18.7339*T

L(BCC_A2,CR,MN:VA;1) = -9162+4.4183*T

TC(BCC_A2,CR,MN:VA;0) = -1325

TC(BCC_A2,CR,MN:VA;2) = -1133

TC(BCC_A2,CR,MN:VA;4) = -10294

TC(BCC_A2,CR,MN:VA;6) = 26706

TC(BCC_A2,CR,MN:VA;8) = -28117

BMAGN(BCC_A2,CR,MN:VA;0) = .48643

BMAGN(BCC_A2,CR,MN:VA;2) = -.72035

BMAGN(BCC_A2,CR,MN:VA;4) = -1.93265

L(BCC_A2,CR,SI:VA;0) = -102850.19+9.85457*T

L(BCC_A2,CR,SI:VA;1) = -49502.35+13.76967*T

L(BCC_A2,FE,MN:VA;0) = -2759+1.237*T

TC(BCC_A2,FE,MN:VA;0) = 123

L(BCC_A2,FE,MN,SI:VA;0) = -97474

L(BCC_A2,FE,NB:VA;0) = -4400+6.333*T

L(BCC_A2,FE,SI:VA;0) = +4*L0BCC-4*FESIW1

L(BCC_A2,FE,SI:VA;1) = +8*L1BCC

L(BCC_A2,FE,SI:VA;2) = +16*L2BCC

TC(BCC_A2,FE,SI:VA;1) = +8*ETCFESI

L(BCC_A2,MN,SI:VA;0) = -89620.7+2.94097*T

L(BCC_A2,MN,SI:VA;1) = -7500

GES:

Following is the list of the REDLICH-KISTER_MUGGIANU equations participating in cementite are described.

CEMENTITE

EXCESS MODEL IS REDLICH-KISTER_MUGGIANU

2 SUBLATTICES, SITES 3: 1

CONSTITUENTS: AL,CR,FE,MN,NB,SI,Z : C

G(CEMENTITE,AL:C;0)- 3 H298(FCC_A1,AL;0)-H298(GRAPHITE,C;0) = 97800

G(CEMENTITE,CR:C;0)-H298(GRAPHITE,C;0)- 3 H298(BCC_A2,CR;0) =

+3*GHSERCR+GHSERCC-48000-9.2888*T

G(CEMENTITE,FE:C;0)-H298(GRAPHITE,C;0)- 3 H298(BCC_A2,FE;0) = +GFECEM

G(CEMENTITE,MN:C;0)-H298(GRAPHITE,C;0)- 3 H298(CBCC_A12,MN;0) = -40379

+3.524*T+3*GHSERMN+GHSERCC

G(CEMENTITE,NB:C;0)-H298(GRAPHITE,C;0)- 3 H298(BCC_A2,NB;0) = -86000

+3*GHSERNB+GHSERCC

G(CEMENTITE,SI:C;0)-H298(GRAPHITE,C;0)- 3 H298(DIAMOND_A4,SI;0) = 250000

G(CEMENTITE,Z:C;0)-H298(GRAPHITE,C;0)- 3 H298(BCC_A2,Z;0) = +GCA1+GCA2+GCA3

L(CEMENTITE,CR,FE:C;0) = +25278-17.5*T

L(CEMENTITE,FE,MN:C;0) = +10434-14.281*T

GES:

9.3 3rd STEP: Para-equilibrium composition of the alloy

Following is the code inserted into the Thermocalc software:

go d

def-sys

c mn cr si nb fe al

rej p*

rest ph fcc-a1 bcc-a2 cem

get

go p-3

s-c t=1500 p=1e5 n=1

s-c x(C)= x(C)of initial alloy

s-c x(Al)= x(Al)of initial alloy

s-c x(Cr)= x(cr)of initial alloy

s-c x(Mn)= x(Mn)of initial alloy

s-c x(Nb)= x(Nb)of initial alloy

s-c x(Si)= x(Si)of initial alloy

l-c

c-e -

l-e

,,,,

ch-st

pha

cem fcc-a1#2 fcc-a1#1

su

c-e -

l-e

The result of the calculation is the alloy's composition X_{Fe}, X_{Mn}, X_{Cr}, X_{Si}, X_{Nb}, X_{Al} and X_{C} valuesunder paraequilibrium conditions..

9.4 4th STEP: Calculation of site fractions

From Eq. (14) the y_j (element site fractions) values are calculated. The required site fractions are listed in Table 10: Site Fraction where x_j are the mole fractions of the elements participating in the alloy calculated under paraequilibrium conditions in the previous step. Also all the y_j combinations required in the expanded form of the molar Gibbs free energy of the three phases under paraequilibrium are calculated (**Σφάλμα! Το αρχείο προέλευσης της αναφοράς δεν βρέθηκε.**)

Element	x_j	$y_{j(fcc)}$	$y_j^{(bcc)}$	$y_j^{(M_3C)}$	
Fe	x_{Fe}	$y_{Fe}^{(fcc)}$	$y_{Fe}^{(bcc)}$	$y_{Fe}^{(M_3C)}$	Y1
Mn	x_{Mn}	$y_{Mn}^{(fcc)}$	$y_{Mn}^{(bcc)}$	$y_{Mn}^{(M_3C)}$	Y2
Cr	x_{Cr}	$y_{Cr}^{(fcc)}$	$y_{Cr}{}^{*(bcc)}$	$y_{Cr}{}^{*(M_3C)}$	Y3
Si	x_{Si}	$y_{Si}^{(fcc)}$	$y_{Si}^{(bcc)}$	$y_{Si}^{(M_3C)}$	Y4
Nb	x_{Nb}	$y_{Nb}^{(fcc)}$	$y_{Nb}^{(bcc)}$	$y_{Nb}^{(M_3C)}$	Y5
Al	$^*x_{Al}$	$y_{Al}^{(fcc)}$	$y_{Al}^{(bcc)}$	$y_{Al}^{(M_3C)}$	Y6
C	$^*x_{Cl}$	$y_C^{(fcc)}$	$y_C^{(bcc)}$	$y_C^{(M_3C)}$	

$y_{Fe}*y_{Al}$ (Y15)	$y_{Mn}*y_{Al}$ (Y23)	$y_{Si}*y_{Nb}$ (Y31)	
$y_{Mn}*y_{Cr}$ (Y17)	$y_{Cr}*y_{Si}$ (Y25)	$y_{Si}*y_{Al}$ (Y33)	
$y_{Mn}*y_{Si}$ (Y19)	$y_{Cr}*y_{Nb}$ (Y27)	$y_{Nb}*y_{Al}$ (Y35)	
$y_{Mn}*y_{Nb}$ (Y21)	$y_{Cr}*y_{Al}$ (Y29)		

$y_{Fe}*y_{Mn}*y_{Cr}$ (Y37)	$y_{Fe}*y_{Cr}*y_{Nb}$ (Y42)	$y_{Mn}*y_{Cr}*y_{Si}$ (Y47)	$y_{Mn}*y_{Nb}*y_{Al}$ (Y52)
$y_{Fe}*y_{Mn}*y_{Si}$ (Y38)	$y_{Fe}*y_{Cr}*y_{Al}$(Y43)	$y_{Mn}*y_{Cr}*y_{Nb}$ (Y48)	$y_{Cr}*y_{Si}*y_{Nb}$ (Y53)
$y_{Fe}*y_{Mn}*y_{Nb}$ (Y39)	$y_{Fe}*y_{Si}*y_{Nb}$ (Y44)	$y_{Mn}*y_{Cr}*y_{Al}$(Y49)	$y_{Cr}*y_{Si}*y_{Nb}$ (Y54)
$y_{Fe}*y_{Mn}*y_{Al}$ (Y40)	$y_{Fe}*y_{Si}*y_{Al}$ (Y45)	$y_{Mn}*y_{Si}*y_{Nb}$ (Y50)	$y_{Si}*y_{Nb}*y_{Al}{}^*$ (Y55)
$y_{Fe}*y_{Cr}*y_{Si}$ (Y41)	$y_{Fe}*y_{Nb}*y_{Al}$ (Y46)	$y_{Mn}*y_{Si}*y_{Al}$ (Y51)	

$y_{Fe}*y_{Mn}*(y_{Fe}-y_{Mn})$ Y8	$y_{Fe}*y_{Al}*(y_{Fe}-y_{Al})$Y16	$y_{Mn}*y_{Al}*(y_{Mn}-y_{Al})$Y24	$y_{Si}*y_{Nb}*(y_{Si}-y_{Nb})$Y32
$y_{Fe}*y_{Cr}*(y_{Fe}-y_{Cr})$Y10	$y_{Mn}*y_{Cr}*(y_{Mn}-y_{Cr})$Y18	$y_{Cr}*y_{Si}*(y_{Cr}-y_{Si})$ Y26	$y_{Si}*y_{Al}*(y_{Si}-y_{Al})$ Y34

$y_{Fe}*y_{Si}*(y_{Fe}-y_{Si})$ Y12	$y_{Mn}*y_{Si}*(y_{Mn}-y_{Si})$ Y20	$y_{Cr}*y_{Nb}*(y_{Cr}-y_{Nb})$ Y28	$y_{Nb}*y_{Al}*(y_{Nb}-y_{Al})$ Y36
$y_{Fe}*y_{Nb}*(y_{Fe}-y_{Nb})$ Y14	$y_{Mn}*y_{Nb}*(y_{Mn}-y_{Nb})$ Y22	$y_{Cr}*y_{Al}*(y_{Cr}-y_{Al})$ Y30	

Table 10: Site Fractions

9.5 5th STEP: DEFINITION OF PHASE PARAMETER IN SSOL

Following are the resulting functions, where PHASE or φ stand, for either austenite, ferrite and cementite:

DEFINITION OF PARAMETER: G(PHASE,Z:C;0)

Y1	y_{Fe}
Y2	y_{Mn}
Y3	y_{Cr}
Y4	y_{Si}
Y5	y_{Nb}
Y6	y_{Al}

SYLNY$(y_{Fe} \cdot lny_{Fe} + y_{Mn} \cdot lny_{Mn} + y_{Cr} \cdot lny_{Cr} + y_{Si} \cdot lny_{Si} + y_{Nb} \cdot lny_{Nb} + y_{Al} \cdot lny_{Al})$

$G_{Z:C}^{0,\Phi}$=

GF1	$G_{Fe:C}^{0,\Phi}$	+322050+75.667*T+GHSERFE+GPFEBCC+3*GHSERCC+3*GPCGRA
GF2	$G_{Mn:C}^{0,\Phi}$	+10000+30*T+GHSERMN+3*GHSERCC
GF3	$G_{Cr:C}^{0,\Phi}$	+GHSERCR+3*GHSERCC+GPCRBCC+3*GPCGRA+416000
GF4	$G_{Si:C}^{0,\Phi}$	+322050-75.667*T+GSIBCC+3*GHSERCC+3*GPCGRA
GF5	$G_{Nb:C}^{0,\Phi}$	+313790-50*T+GHSERNB+3*GHSERCC
GF6	$G_{Al:C}^{0,\Phi}$	***UNASSESSED***

LF1	$L_{Fe,Mn:C}^{0,\varphi}$	L(BCC_A2,FE,MN:C;0) = +34052-23.467*T
LF2	$L_{Fe,Mn:C}^{1,\varphi}$	
LF3	$L_{Fe,Cr:C}^{0,\varphi}$	L(BCC_A2,CR,FE:C;0) = -1250000+667.7*T

LF4 $L^{1,\varphi}_{Fe,Cr:C}$

LF5 $L^{0,\varphi}_{Fe,Si:C}$ L(BCC_A2,FE,SI:C;0) = 78866

LF6 $L^{1,\varphi}_{Fe,Si:C}$

LF7 $L^{0,\varphi}_{Fe,Nb:C}$

LF8 $L^{1,\varphi}_{Fe,Nb:C}$

LF9 $L^{0,\varphi}_{Fe,Al:C}$

LF10 $L^{1,\varphi}_{Fe,Al:C}$

LF11 $L^{0,\varphi}_{Mn,Cr:C}$

LF12 $L^{1,\varphi}_{Mn,Cr:C}$

LF13 $L^{0,\varphi}_{Mn,Si:C}$

LF14 $L^{1,\varphi}_{Mn,Si:C}$

LF15 $L^{0,\varphi}_{Mn,Nb:C}$

LF16 $L^{1,\varphi}_{Mn,Nb:C}$

LF17 $L^{0,\varphi}_{Mn,Al:C}$

LF18 $L^{1,\varphi}_{Mn,Al:C}$

LF19 $L^{0,\varphi}_{Cr,Si:C}$

LF20 $L^{1,\varphi}_{Cr,Si:C}$

LF21 $L^{0,\varphi}_{Cr,Nb:C}$

LF22 $L^{1,\varphi}_{Cr,Nb:C}$

LF23 $L^{0,\varphi}_{Cr,Al:C}$

LF24 $L^{1,\varphi}_{Cr,Al:C}$

LF25 $L^{0,\varphi}_{Si,Nb:C}$

LF26 $L^{1,\varphi}_{Si,Nb:C}$

LF27 $L^{0,\varphi}_{Si,Al:C}$

LF28 $L^{1,\varphi}_{Si,Al:C}$

LF29 $L^{0,\varphi}_{Nb,Al:C}$

LF30 $L^{1,\varphi}_{Nb,Al:C}$

DEFINITION OF PARAMETER: G(PHASE,Z:VA;0)

$G^{0,\Phi}_{Z:Va}$

GF7	$G^{0,\Phi}_{Fe:Va}$	+GHSERFE+GPFEBCC
GF8	$G^{0,\Phi}_{Mn:Va}$	+GMNBCC
GF9	$G^{0,\Phi}_{Cr:Va}$	+GHSERCR+GPCRBCC
GF10	$G^{0,\Phi}_{Si:Va}$	+GSIBCC
GF11	$G^{0,\Phi}_{Nb:Va}$	+GHSERNB
GF12	$G^{0,\Phi}_{Al:Va}$	+GALBCC

LF31	$L^{0,\varphi}_{Fe,Mn:Va}$	-2759+1.237*T
LF32	$L^{1,\varphi}_{Fe,Mn:Va}$	
LF33	$L^{0,\varphi}_{Fe,Cr:Va}$	+20500-9.68*T
LF34	$L^{1,\varphi}_{Fe,Cr:Va}$	
LF35	$L^{0,\varphi}_{Fe,Si:Va}$	+4*L0BCC-4*FESIW1
LF36	$L^{1,\varphi}_{Fe,Si:Va}$	+8*L1BCC
LF37	$L^{2,\varphi}_{Fe,Si:Va}$	+16*L2BCC
LF38	$L^{0,\varphi}_{Fe,Nb:Va}$	-4400+6.333*T
LF39	$L^{1,\varphi}_{Fe,Nb:Va}$	
LF40	$L^{0,\varphi}_{Fe,Al:Va}$	+4*LALFEB0-4*ALFEW1
LF41	$L^{1,\varphi}_{Fe,Al:Va}$	+8*LALFEB1
LF42	$L^{0,\varphi}_{Mn,Cr:Va}$	-20328+18.7339*T
LF43	$L^{1,\varphi}_{Mn,Cr:Va}$	-9162+4.4183*T
LF44	$L^{0,\varphi}_{Mn,Si:Va}$	-89620.7+2.94097*T
LF45	$L^{1,\varphi}_{Mn,Si:Va}$	-7500
LF46	$L^{0,\varphi}_{Mn,Nb:Va}$	
LF47	$L^{1,\varphi}_{Mn,Nb:Va}$	
LF48	$L^{0,\varphi}_{Mn,Al:Va}$	-120077+52.851*T
LF49	$L^{1,\varphi}_{Mn,Al:Va}$	-40652+29.2764*T
LF50	$L^{0,\varphi}_{Cr,Si:Va}$	-102850.19+9.85457*T
LF51	$L^{1,\varphi}_{Cr,Si:Va}$	-49502.35+13.76967*T
LF52	$L^{0,\varphi}_{Cr,Nb:Va}$	
LF53	$L^{1,\varphi}_{Cr,Nb:Va}$	
LF54	$L^{0,\varphi}_{Cr,Al:Va}$	-55370-10*T

LF55 $L^{1,\varphi}_{Cr,Al:Va}$ +1830-10*T

LF56 $L^{2,\varphi}_{Cr,Al:Va}$ -8800

LF57 $L^{0,\varphi}_{Si,Nb:Va}$

LF58 $L^{1,\varphi}_{Si,Nb:Va}$

LF59 $L^{0,\varphi}_{Si,Al:Va}$

LF60 $L^{1,\varphi}_{Si,Al:Va}$

LF61 $L^{0,\varphi}_{Fe,Mn,Cr:Va}$ -8374

LF62 $L^{0,\varphi}_{Fe,Mn,Si:Va}$ -97474

LF63

DEFINITION OF PARAMETER: L(PHASE,Z:C,VA;0)

$L^{0,\varphi}_{Z:C,Va} = y_{Fe}$

LF80 $L^{0,\varphi}_{Fe:C,Va}$ -190*T

LF81 $L^{0,\varphi}_{Mn:C,Va}$

LF82 $L^{0,\varphi}_{Cr:C,Va}$ -190*T

LF83 $L^{0,\varphi}_{Si:C,Va}$

LF84 $L^{0,\varphi}_{Nb:C,Va}$

LF85 $L^{0,\varphi}_{Al:C,Va}$